

Review

# Reviews Based on the Reconfigurable Intelligent Surface Technical Issues

Ic-Pyo Hong 

Department of Smart Information and Technology Engineering, Kongju National University, Cheonan 31080, Republic of Korea; iphong@kongju.ac.kr; Tel.: +82-41-521-9199

**Abstract:** Reconfigurable intelligent surfaces (RISs) are programmable metasurface structures that can control the propagation of electromagnetic waves by changing the electrical and magnetic properties of the surface. They can be used to intelligently reconfigure the wireless environment to improve the capacity and coverage of wireless networks. In recent years, numerous theoretical innovations and prototype tests have demonstrated that the RIS has the advantages of low cost, low power consumption, and easy deployment, and creates many potential opportunities and broad application prospects in 5G and future 6G networks. In this paper, starting from the technological development of RISs, we discussed the technical issues of RISs. The standardization of RISs, types of RISs according to operation modes, channel modeling, considerations for hardware implementation, differences from existing communication modules and the need for active RIS implementation, noise and power characteristics to ensure the efficiency of RISs, and performance parameters of RISs and field test results of RISs in indoor and outdoor environments were reviewed. By resolving the current technical issues of RISs, it is expected that RISs will be successfully used for B5G/6G communication through commercialization.

**Keywords:** reconfigurable intelligent surfaces; metasurface; B5G/6G communication



**Citation:** Hong, I.-P. Reviews Based on the Reconfigurable Intelligent Surface Technical Issues. *Electronics* **2023**, *12*, 4489. <https://doi.org/10.3390/electronics12214489>

Academic Editors: Dimitra I. Kaklamani, Ikmo Park and Djuradj Budimir

Received: 28 August 2023

Revised: 27 September 2023

Accepted: 9 October 2023

Published: 1 November 2023



**Copyright:** © 2023 by the author. Licensee MDPI, Basel, Switzerland. This article is an open access article distributed under the terms and conditions of the Creative Commons Attribution (CC BY) license (<https://creativecommons.org/licenses/by/4.0/>).

## 1. Introduction

Recently, there has been increasing interest in reconfigurable intelligent surfaces (RISs), which plays an essential role in realizing the smart radio environment (SRE) as one of the key technologies for enabling communications beyond 5G(B5G)/6G [1], as shown in Figure 1. An RIS, also known as intelligent reflecting surfaces (IRS) [2], software-controlled metasurfaces (SCM) [3], or large intelligent surfaces (LIS) [4], are an extension of reconfigurable metasurface structures to surface structures that can modulate electromagnetic waves by controlling the phase, amplitude, and polarization of incident waves, which can improve the capacity and coverage of wireless networks by smartly reconfiguring the radio propagation environment.

### 1.1. RIS History

Metasurfaces [5], the two-dimensional equivalent surface of metamaterials, are artificial structures designed using very small (subwavelength) meta-atoms, typically arranged periodically or aperiodically in a plane [6,7]. Over the past decade, metasurfaces have developed rapidly and have been used extensively in the design of numerous new devices and applications in the microwave, terahertz, and visible light regions. The refraction and reflection of radio waves at the interface of two homogeneous and isotropic media is governed by Snell's law, and in 2011, a generalized version of Snell's law was proposed [8], which states that anomalous reflection or anomalous refraction occurs if there is a phase gradient at the metasurface, the interface of two media, as shown in Figure 2.

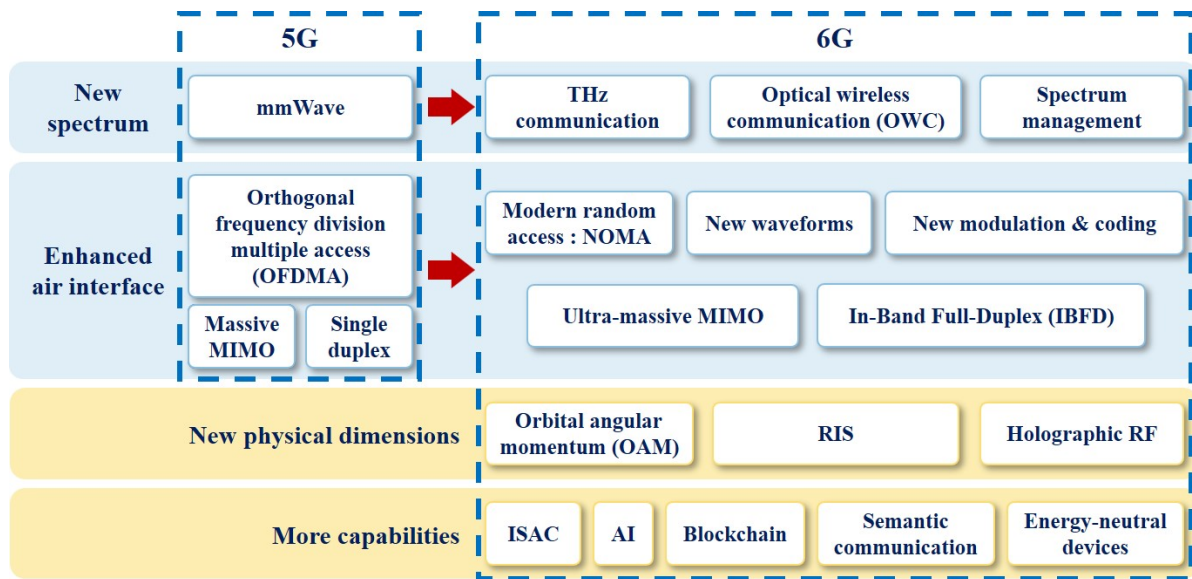


Figure 1. Expected 6G technologies.

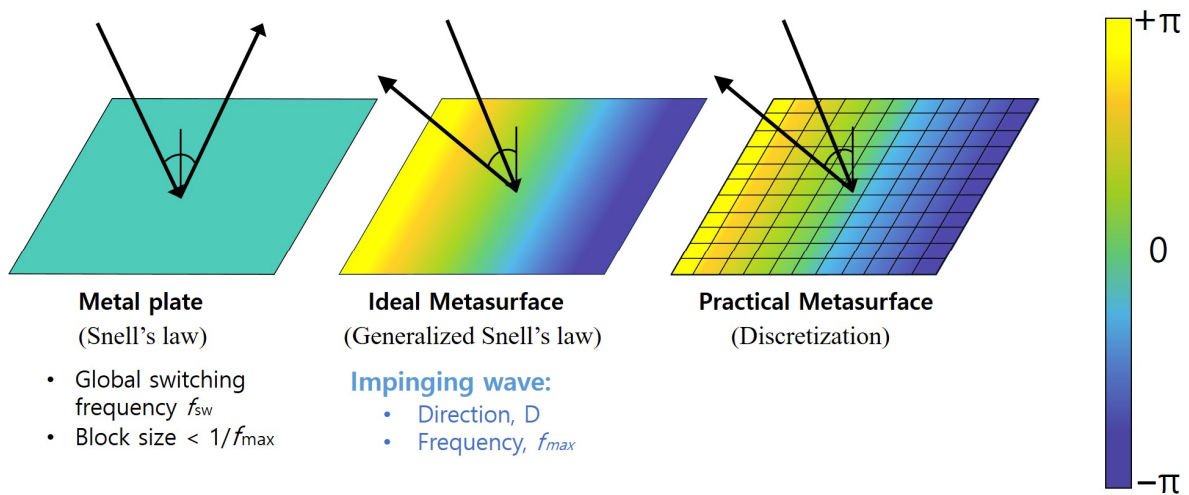


Figure 2. Metasurface structure—a generalized application of Snell's law.

One of the largest applications of phase-gradient metasurface structures is beam steering, where the phase shift of each unit cell in a metasurface is used to control the direction of transmitted or reflected radio waves. This phase change can be accomplished in the following two ways: passively, by designing each unit cell in the metasurface to have a different phase, and actively, by controlling the same unit cell electrically or mechanically to control its phase, amplitude, polarization, etc. [9]. In 2011, H. Kamoda et al. [10] designed and fabricated a  $160 \times 160$  reflectarray antenna with beam steering characteristics for millimeter-wave imaging at 60 GHz using PIN diode switching, as shown in Figure 3, suggesting that beam steering is possible due to the phase change caused by PIN diode switching. In 2014, Tie Jun Cui et al. [11] proposed the concepts of coding metamaterials, digital metamaterials, and programmable metamaterials, and showed that it is possible to control the incoming electromagnetic waves by turning on/off (phase change) each unit structure comprising the metamaterial, as shown in Figure 4. Attempts have been made to apply electromagnetic surface structures such as these metamaterials to communications, as shown in Table 1.

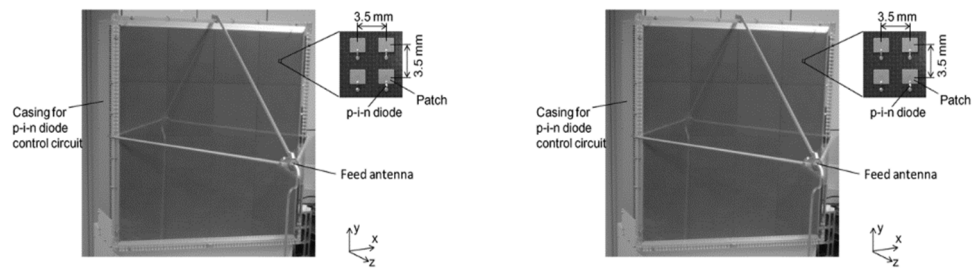


Figure 3. Reconfigurable array antenna using PIN diodes. Adapted with permission from [10]. Copyright 2011 IEEE.

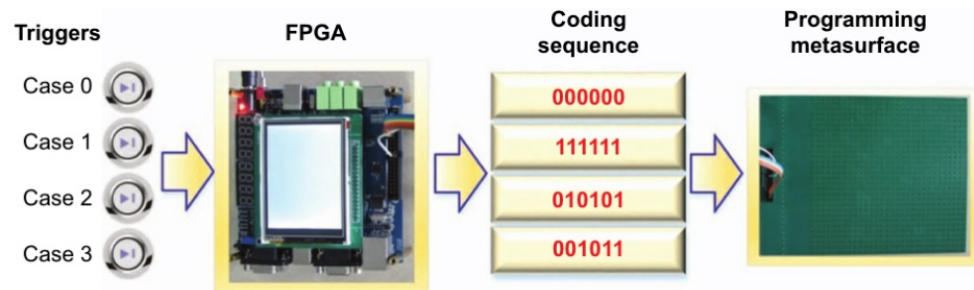


Figure 4. Programmable metamaterials [11].

Table 1. Communication applications of electromagnetic surface structures.

Year	Ref.	Structure	Technologies	Function
2012	[12]	Intelligent wall	PIN diode, active FSS	Perfect transmission/reflection surface
2014	[13]	Spatial microwave modulator	Binary phase control metasurface	Microwave field forming
2014	[11]	Coding metamaterial	Binary phase control metasurface	Reconfigurable scattering pattern
2016	[14]	Programmable metamaterial	PIN diode, metasurface	Reconfigurable phase, polarization, scattering
2016	[15]	Reconfigurable reflectarray	Varactor, reflectarray	Adaptive reflection phase
2018	[4]	Large intelligent surface	Radiation/sensing array, electromagnetic active material	Massive MIMO substitute
2018	[3]	Software controlled hypersurface	IoT gateway, metasurface	Radio absorption, polarization, beam steering

In 2019, M. Di Renzo et al. [16] presented the concept of a reconfigurable intelligent metasurface to realize a smart wireless environment by solving the following two major problems of wireless communication: meeting user requirements for radio waves by controlling the reconfigurable metastructure that can control the scattering, reflection, and refraction characteristics of radio waves, and by solving the problem of increasing power consumption due to the transmission of new signals, as shown in Figure 5.

### 1.2. RIS Introduction

In conventional wireless communications, the radio channel is defined passively, as shown in Figure 6a, as defined by Shannon and Wiener in 1948. As described earlier, an RIS is a planar surface composed of a large number of passive reflective elements, each of which can independently induce controllable amplitude and/or phase changes in the incident signal; thus, densely deploying RISs in wireless networks and smartly adjusting their reflections can flexibly reconfigure the signal propagation/radio channel between the transmitter and receiver, providing a new means to fundamentally solve the wireless channel fading

impairment and interference problems, and to dramatically improve wireless communication capacity and reliability. In other words, RIS-using phase-shifted metasurface structures can control the channel by controlling the reflection or transmission properties of the radio waves in the channel, thus making it an active characteristic to reconfigure the wireless channel as needed, as shown in Figure 6b. Therefore, a lot of research has been performed recently as a new paradigm to realize a smart and reconfigurable radio channel/radio propagation environment for B5G/6G wireless communication systems using RISs [17].

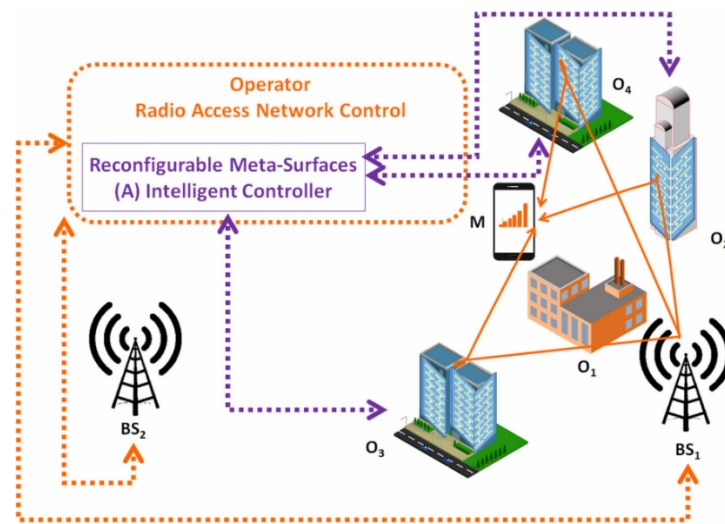


Figure 5. Concept of a smart wireless environment using reconfigurable metasurfaces [16].

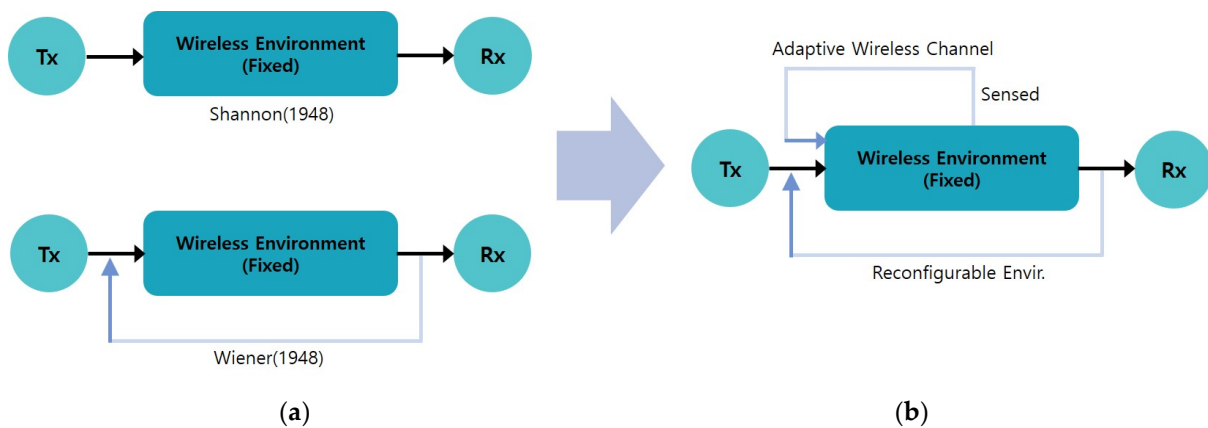
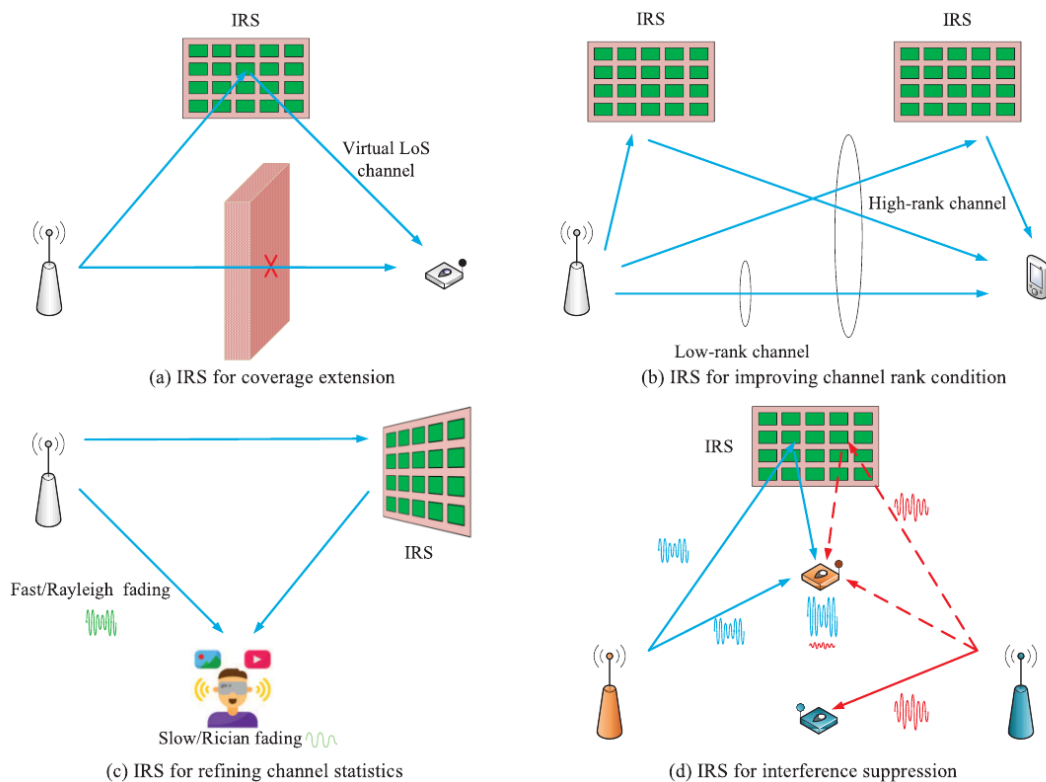


Figure 6. Wireless channel modeling: (a) passive wireless channel and (b) active wireless channel.

In particular, in the case of 5G and 6G communications, the importance of technologies utilizing RISs is increasing, as higher frequencies are used, as well as the density of the network, requiring technologies to realize high spatial resolution, i.e., an increase in channel capacity, with low hardware cost and low power consumption [18]. Currently, the frequency bands for 5G communication set by 3GPP are divided into FR1, from 410 to 7125 MHz, and FR2, from 24.25 to 52.6 GHz [19]; FR1 is generally referred to as ‘sub6G’ and FR2 as ‘mmWave’. In 5G communication, sub6G is known to cause severe shaded areas indoors due to the lack of spatial rank, but if an RIS is used, the rank can be increased by increasing the multipath component in space, and thus the throughput can be increased indoors. In the case of mmWave communication, due to the straightness of the radio waves, the radio waves are blocked by obstacles such as trees and buildings, reducing the communication coverage. However, if an RIS is used, the shaded areas are covered through the reflection of the signal, and the overall coverage can be increased [17]. As shown in Figure 7, the RIS can realize several functions in wireless channel reconfiguration,

such as creating a virtual line-of-sight (LOS) link to bypass obstacles between base stations and terminals through smart reflection and thus improving channel ranking conditions by adding signal paths in the desired direction; improving channel statistics/distribution by converting Rayleigh/fast fading to Rician/slow fading for ultra-high reliability; and suppressing/nullifying co-channel/inter-cell interference. In addition to the functional advantages of improving communication performance, the RIS has various practical advantages. First of all, a passive RIS consisting of a reflective element, such as a low-cost printed dipole, can be implemented and operated at a much lower hardware/energy cost than a conventional active array antenna because it can only passively reflect the incident radio waves without RF circuits at the transmitting radio frequency. RISs also operate in full-duplex (FD) mode and are free of antenna noise amplification and self-interference, which is an advantage over traditional active relays such as half-duplex (HD) relays, which have lower spectral efficiency, and FD relays, which require sophisticated techniques to eliminate self-interference. RISs are typically low-profile, lightweight, and conformal in shape, making them easy to mount/remove and deploy/replace on environmental objects. Finally, RISs act as auxiliary devices in wireless networks and can be transparently integrated, offering great flexibility and compatibility with existing wireless systems such as cellular or WiFi [20].



**Figure 7.** Application of wireless communication system using RIS. Adapted with permission from [20]. Copyright 2021 IEEE.

Since 2018–2019, when the concept of the RIS was first introduced, several considerations and critical perspectives have been presented on the advantages of the RIS as well as its practical implementation in wireless communication systems [21]. The first is the accurate electromagnetic modeling of the RIS, and most RIS-related studies assume that the metasurface comprising the RIS is an ideal reflector, but the hardware design for phase control, i.e., phase control resolution, RIS substrate characteristics, transmission/reflection/polarization characteristics of the incident radio waves, and the size of the RIS, should be considered. For example, modeling the size of the RIS is a very important issue because if the RIS does not reach a certain size, it is not possible to obtain excellent

SNR characteristics even with currently used relays. The second is channel modeling, which includes channel sensing and estimation, and most RIS-related studies assume that Channel State Information (CSI) can be perfectly obtained from base stations, RISs, and user terminals. However, currently, neither the base station nor the user terminal can recognize the RIS, and in the case of a wireless communication channel containing an RIS, the path loss between the base station–RIS and the RIS–user terminal must be considered; therefore, a real-time channel sensing and estimation method that considers multiplicative fading is required, unlike conventional channels. The third is the design of an RIS with excellent efficiency, which requires a large size and many array elements to operate over long distances, and a design that considers energy efficiency to solve this problem, and a design that considers the reflection efficiency depending on the direction and location of the RIS. Fourth, as for the performance parameters of the RIS, in the case of communication modules in general, radio frequency compatibility, signal compatibility, and resource management are tested for commercialization; however, in the case of the RIS, it is necessary to study which performance parameters should be tested because various combinations of the direction of incident radio waves and the direction of transmission/reflection are possible, as well as reflection performance. Finally, as an operational scenario for the RIS, it is necessary to consider the location of the RIS in the wireless network, the size of the RIS, the function of the RIS, the use of multiple RISs, the possibility of real-time control from the machine learning server, and the maintenance and robustness in the real environment. In real-world wireless networks, base stations from multiple operators may be located in the same area or location, and the installation of an RIS by one operator may inadvertently affect the performance of other operators' networks.

These are just a few of the practical issues that need to be addressed if an RIS is to be commercially successful as an innovative technology. Although there is a large body of literature on research topics related to RISs, very few studies have focused on the engineering aspects of RIS-enabled wireless communication systems that need to consider practical constraints for real-world applications. Therefore, this paper examines the technical issues that need to be considered for the practical implementation of RISs. As illustrated in Figure 8, this paper is structured as follows. In Section 2, we reviewed technical issues and related research on RIS standardization, types of RISs according to operation mode, channel modeling, considerations for hardware implementation, differences from existing communication modules and the need for active RIS implementation, and noise and power characteristics to ensure the efficiency of RISs. In Section 3, we reviewed the field test results of RISs in indoor and outdoor environments and the current level of commercialization.

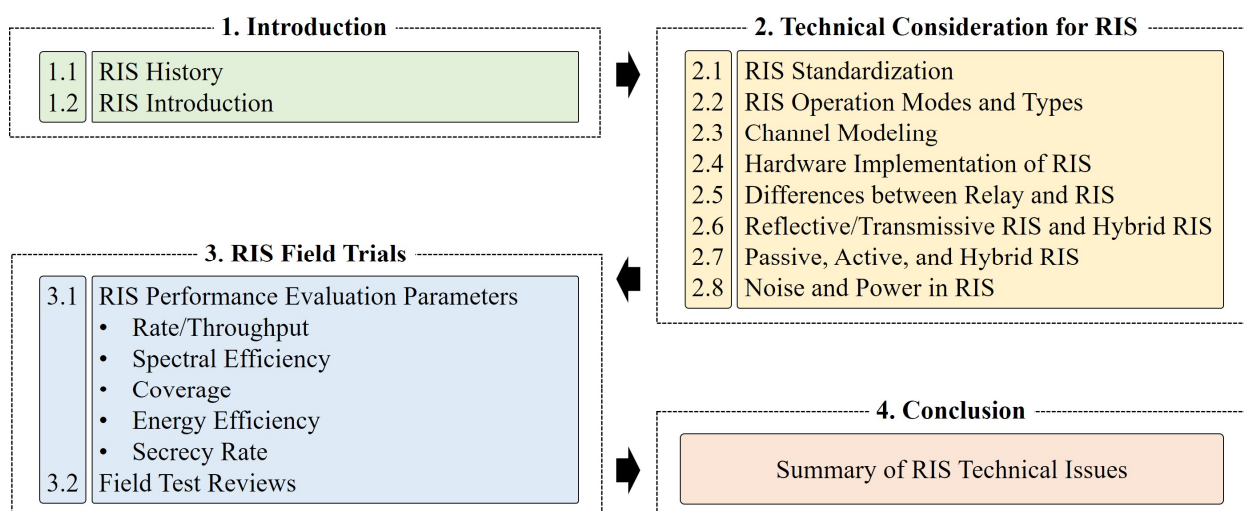


Figure 8. Organization of this paper.

## 2. Technical Considerations for RIS

### 2.1. RIS Standardization

Some of the pain points for the industry, especially network operators, in current 5G networks are scarce spectrum, high power consumption, and high deployment and maintenance costs. The overall goal of 3GPP and several other Standards Development Organizations (SDOs) is to support new paradigms and capabilities that can meet the needs of 5G networks and beyond by using limited spectrum, power, and hardware costs [22]. The RIS has recently emerged as a promising technology for next-generation wireless networks such as B5G and 6G, and there is a broad consensus in academia and industry that the RIS, which uses modulation and coding techniques to artificially configure the channel for optimized performance, can revolutionize the current communication paradigm of adapting to the channel [23]. The standardization process typically starts with Study Items (SIs) in one or several SDOs or industry forums, and then expands to international SDOs such as 3GPP, where Work Items (WIs) are established, technical specifications are comprehensively defined, and then are published and finalized as global standards.

RIS-related SDO activities are centered in the United States, Europe, and China. In the U.S., two Special Interest Groups (SIGs) and one Emerging Technology Initiative (ETI) [24] have been established within the IEEE Communication Society, Reconfigurable Intelligent Surfaces for Smart Radio Environment (RISE) [25] and REconFigurable Intelligent Surfaces for Signal Processing and CommunicatiONS (REFLECTIONS) [26], to foster collaboration among researchers in various fields such as wireless communications, signal processing, and metamaterials. In addition, industries, such as carriers and network infrastructure providers, are being engaged to provide understanding from an industrial perspective and to discuss the costs and potential applications of RISs.

In Europe, the European Telecommunications Standards Institute (ETSI) proposed and approved an Industry Specification Group (ISG) on the RIS in June 2021, with participation from chipset vendors, network infrastructure providers, telecommunication companies, research organizations, and universities. The ISG defined the use of the RIS, developed key performance indicators (KPIs), published deliverables such as technical reports on RIS deployment scenarios, communication models, and channel models, and proposed 11 core use cases of RISs in May 2023 [27,28]. Figure 9 shows ETSI’s plans for RIS standardization by year [28].

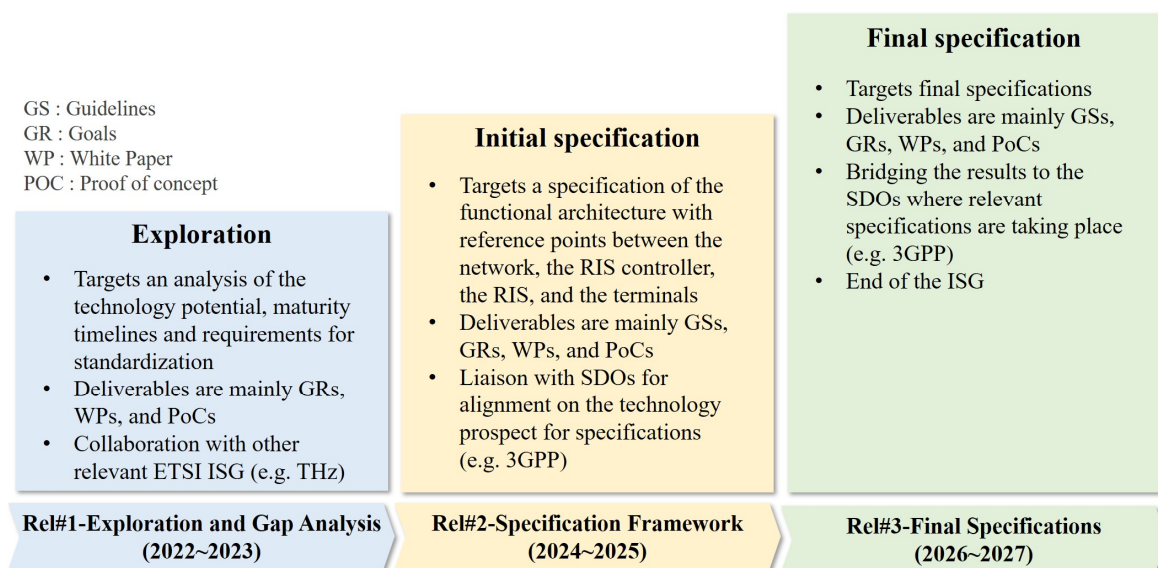
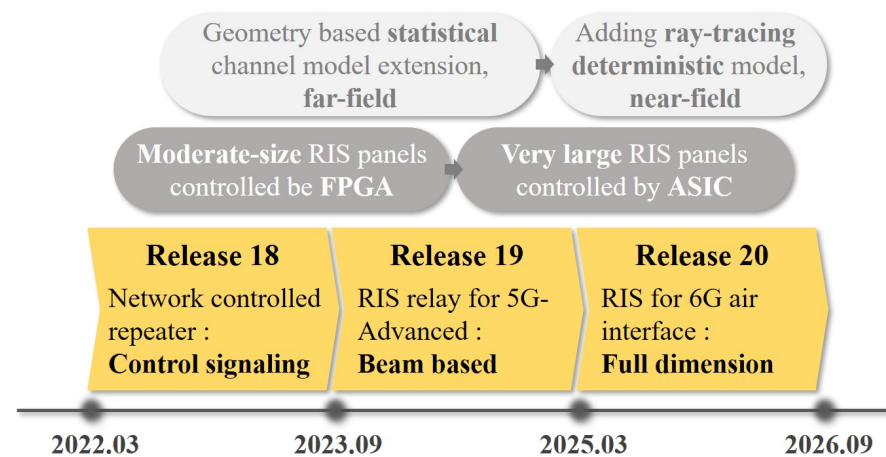


Figure 9. RIS standardization of ETSI.

In China, two standards organizations, China Communications Standards Association (CCSA) and FuTURE Forum, which is a non-profitable international organization jointly initiated by famous mobile telecommunication operators, mobile communication device manufactures, research institutes, and universities from both home and abroad in 2005, have started RIS-related standardization work. CCSA is an official standards organization established by enterprises and institutions in China to conduct standardization activities in the ICT field, and a proposal to create an SI for RISs was approved at the 55th meeting of TC5-WG6 in 2020 [29]. CCSA conducts research on realizing RIS-enabled wireless communication systems, including channel modeling, channel estimation and feedback, beamforming using RIS, RIS, and AI, and networking protocols for RIS-enabled networks, while FuTURE Forum conducts research on integrating RIS into next-generation wireless communication [30].

In addition to these regional RIS standardization activities, as a global standardization, during the ITU-R Working Party (WP) 5D meeting in October 2020, each country submitted candidate proposals for next-generation wireless technologies to be included in the IMT Future Technology Trends Report, and a report including an RIS was submitted, led by Chinese companies. According to the report, RIS is a key post-IMT-2020 wireless technology that can dynamically control the wireless environment and is mentioned as an important element for the physical layer of next-generation networks [31]. For 3GPP, the focus is currently on launching 5G Phase 2 with Release 18, as shown in Figure 10, and it is expected that RIS-related standardization after 2023 will start with SI on use cases, deployment scenarios, and channel models in Release 19, followed by WI after that SI is completed [32]. Since the first proposal was submitted by ZTE Corp. in March 2021 [33], many companies (mainly network operators) are interested in the RIS as it will be a key component in 5G-Advanced networks. As a completely new technology, one of the most important tasks to standardize RIS will be channel modeling.



**Figure 10.** RIS standardization schedule in 3GPP. Adapted with permission from [32]. Copyright 2022 IEEE.

## 2.2. RIS Operation Modes and Types

An RIS is a new network node consisting of a surface with reflective and/or transmissive capabilities that can be controlled by the RIS controller, passively and/or actively, as shown in Figure 11, to transform the wireless environment from a passive actor to an intelligent actor that can program the channel. Accordingly, the RIS can be categorized into the following six modes of operation in the network (Table 2): reflection mode, refraction mode, absorption mode, backscattering mode, transmitting mode, and receiving mode. Their respective characteristics are shown in [34].

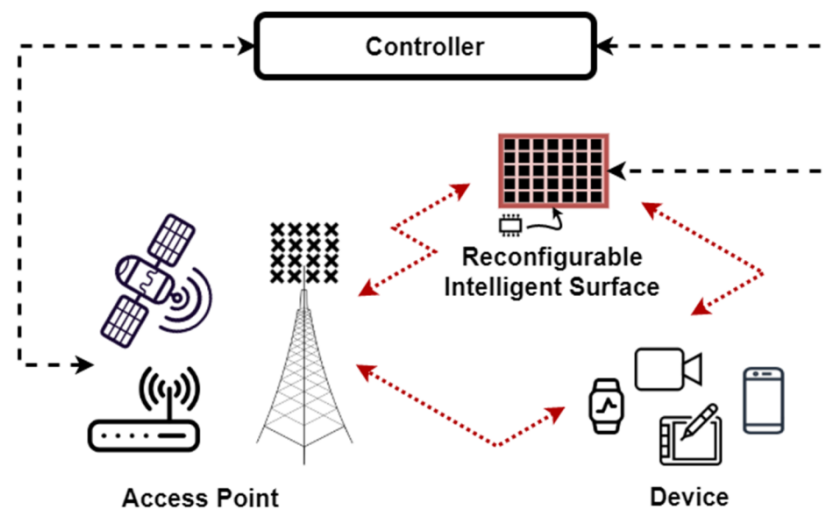


Figure 11. RIS aided wireless communication network example.

Table 2. RIS Operation Modes.

Operation Mode	Characteristics and Functions
Reflection	<ul style="list-style-type: none"> <li>Can act as a reflector in a wireless environment; used to improve coverage, mitigate interference, and increase capacity.</li> </ul>
Refraction	<ul style="list-style-type: none"> <li>Refracting incident electromagnetic waves in different directions by adjusting their phase as they pass through the RIS.</li> <li>Electromagnetic waves pass through the panel because there is no shielding layer inside the RIS panel.</li> <li>Outdoor to indoor scenario: To improve coverage of some specific areas inside a building, the RIS is used as a glass window to focus the incident electromagnetic waves on different target areas.</li> </ul>
Absorption	<ul style="list-style-type: none"> <li>Colliding radio waves with a specific center frequency and a specific bandwidth are ideally absorbed completely, eliminating reflected waves.</li> <li>Interference mitigation, privacy, and information security—implementing RIS on a building’s exterior to shield electromagnetic waves, isolating electromagnetic waves from each other indoors and outdoors or from different indoor spaces.</li> </ul>
Backscattering	<ul style="list-style-type: none"> <li>Reflected waves cover large areas rather than precise locations.</li> <li>A balance between gain and effective area is required to achieve wide-angle blind spot coverage.</li> <li>Backscatter mode is used for passive RISs manufactured to reflect incident EM signals in a specific direction.</li> </ul>
Transmitting	<ul style="list-style-type: none"> <li>Integrated into wireless transmitters to help form and steer transmitted radio waves.</li> <li>Dynamic Metasurface Antenna (DMA).</li> </ul>
Receiving	<ul style="list-style-type: none"> <li>RIS receives and processes radio signals.</li> <li>Embeds waveguides in each RIS element or group of elements to pass incident radio signals to the receiving hardware.</li> </ul>

### 2.3. Channel Modeling

As with other communication technologies, channel modeling (combined with interference analysis and RIS modeling) provides a communication model for performance evaluation of wireless networks and is an essential part of RIS research to understand RIS use cases in future wireless networks. Furthermore, one of the most important aspects of implementing next-generation wireless communication technologies is to develop accurate and consistent channel models that can be effectively validated by real-world measurements. From this perspective, it is important to consider not only the physical propagation effects in different environments, such as the varying path loss and scattering behavior in a large indoor office or street environment, but also the effects of RIS on the end-to-end channel model, such as the near-field effects and potential spatial correlation of an adjacent RIS, and the mutual coupling between RIS elements. In addition, the different frequency ranges, bandwidths, and RIS architectures, such as reflective array-based or metasurface-

based, play an important role in the underlying channel model. Furthermore, modified LOS probabilities and path loss indices can be derived by considering the potential locations of RISs in a real wireless environment [35]. Channel modeling typically requires a tradeoff between complexity and accuracy. For example, in most ray tracing-based channel modeling approaches, considering only a single reflection makes the model simpler but not perfectly accurate, while higher-order reflections, which can characterize more accurate channel models, are time-consuming to compute and simulate. To consider the RIS in channel modeling, the 3GPP's channel model is shown in Table 3. In urban scenarios, the base station (BS) to an RIS channel model can generally be modeled using the Uma/Umi model, i.e., depending on the height of the BS–RIS. The RIS–UE (user equipment) channel can be modeled as InH/InF if the link is indoors; otherwise, it can be modeled as Uma/Umi. If the distance between the RIS and UE or between the BS and RIS is very small, a pure LOS channel model can be applied. RIS–RIS channels can be cascaded by multiple RISs on the same link. In Outdoor-to-Indoor (O2I) use cases, the RIS–RIS channel can be outdoors or indoors, and for coverage extension, the RIS–RIS channel should be modeled as an Uma/Umi channel model [34,36].

**Table 3.** 3GPP channel models that are applicable to RIS use cases.

Scenarios	BS–UE Channel Model	BS–RIS Channel Model	RIS–UE Channel Model	RIS–RIS Channel Model
Urban deployment: avoiding indoor UE's penetration loss	Uma/Umi	Uma/Umi	InH/InF	Uma/Umi/InH/InF
Urban deployment: UE-controlled RIS	Uma/Umi	Uma/Umi	LoS	N/A
Urban deployment: RIS close to BS	Uma/Umi	LoS	Uma/Umi	Umi
Urban deployment: coverage extension	Uma/Umi	Uma/Umi	Uma/Umi	Uma/Umi
Indoor scenario	InH/InF	InH/InF/LoS	InH/InF/LoS	InH/InF

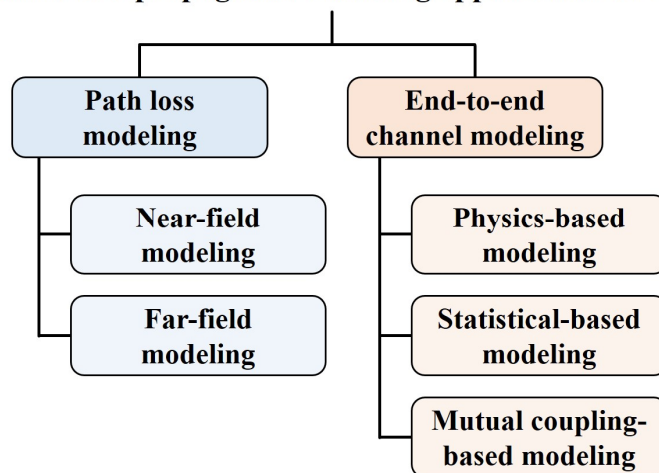
Uma: Urban Macro, Umi: Urban Micro, InF: Indoor Factory, InH: Indoor Hotspot.

Recently, research has been performed on propagation channel modeling to modify the radio propagation environment by including an RIS [37]. While many studies in the literature have modeled the path loss of RIS-enabled communication systems, end-to-end channel modeling has recently received significant attention. When modeling the total path loss of an RIS-enabled system, the near-field and far-field effects of the RIS should also be considered. Another important point is the methodology followed in modeling the end-to-end channel, while many researchers follow a physics-based channel modeling strategy, is that there are also statistical channel modeling strategies that consider the physical characteristics of reflection and scattering effects, statistical channel modeling strategies, scattering in the environment, and statistical characteristics of clusters. An electromagnetic (EM) compatible channel model has also been proposed. Channel models that consider EM characteristics such as mutual coupling between subwavelength unit cells have also been proposed. Considering the existing RIS-enabled channel modeling research, channel and propagation modeling approaches can be broadly classified (Figure 12a). Since there is no clear distinction between specific approaches in this classification, channel modeling studies where more than one approach is used can provide a broader perspective. One method of RIS channel modeling is based on the 3GPP standardized channel model, which has a modeling framework consisting of three parts (Figure 12b): general parameters, small-scale parameters (SSP), and channel impulse response (CIR). The model generates large scale parameters (LSPs) and SSPs for both Tx-RIS and RIS-Rx subchannels. Table 4 summarizes the research related to RIS channel modeling.

**Table 4.** RIS channel modeling research trends.

Ref.	Abstract
[38]	<ul style="list-style-type: none"> <li>• Path loss in near and far fields based on Huygens–Fresnel principle and Physical Optics (PO) method.</li> <li>• Modeling RIS as an EM sheet with negligible thickness.</li> </ul>
[39]	<ul style="list-style-type: none"> <li>• Calculate path loss with a physics-based approach.</li> <li>• Compute the electric field of a finite-size RIS in the near and far fields.</li> </ul>
[40]	<ul style="list-style-type: none"> <li>• Calculate path loss for a passive reflectarray RIS.</li> <li>• Calculate path loss as a function of the RIS size, link shape, and actual gain of RIS unit cells.</li> </ul>
[41]	<ul style="list-style-type: none"> <li>• Provide a realistic power scaling law for the far-field region of an array with the PO method.</li> </ul>
[42]	<ul style="list-style-type: none"> <li>• Calculate free-space path loss with physics/EM-based approach considering near-field and far-field regions of an RIS.</li> <li>• Validate with experiments/measurements using the fabricated RIS.</li> </ul>
[43]	<ul style="list-style-type: none"> <li>• Calculate path loss as a function of RIS size and transmission distance using the PO method and the Huygens–Fresnel principle.</li> <li>• Consider 2D homogeneous metasurfaces behaving in reflection/refraction mode in near and far fields.</li> </ul>
[44]	<ul style="list-style-type: none"> <li>• Analysis of the power scaling law for large RIS using a determined propagation model.</li> <li>• Show that an asymptotic limit can be obtained in the near field.</li> </ul>
[45]	<ul style="list-style-type: none"> <li>• Represents end-to-end channel model including physical parameters of RIS.</li> <li>• PO-based analysis using radar concept.</li> <li>• Each tile of RIS is modeled as an anomalous reflector.</li> </ul>
[46]	<ul style="list-style-type: none"> <li>• EM-compliant communication model that considers mutual coupling between RIS unit cells.</li> <li>• Full system representation with circuit-based models for all terminals.</li> <li>• Investigate inter-coupling between impedance-controlled thin dipoles and the effects of tuning elements.</li> </ul>
[47,48]	<ul style="list-style-type: none"> <li>• Statistical geometry-based non-stationary channel model for MIMO systems supporting RIS.</li> <li>• Considers various physical characteristics of the RIS, such as number and size of unit cells, Tx, RIS, and relative positions between them.</li> </ul>
[49–51]	<ul style="list-style-type: none"> <li>• Three-dimensional channel models for physical RIS characteristics and real-world deployment.</li> <li>• Introduction to the open-source, SimRIS channel simulator.</li> <li>• Consider technical specifications for sub-6 GHz and millimeter wave bands.</li> </ul>
[52]	<ul style="list-style-type: none"> <li>• Physics-based end-to-end model of RIS-parameterized radio channels with adjustable fading (open source PhysFad).</li> </ul>
[53]	<ul style="list-style-type: none"> <li>• Utilize the physics of electromagnetic (EM) fields and a modified Saleh–Valenzuela model.</li> <li>• Derive theoretical results for path loss, channel parameters, and received distortion power.</li> </ul>

**Channel and propagation modeling approaches for RISs**



(a)

**Figure 12.** Cont.

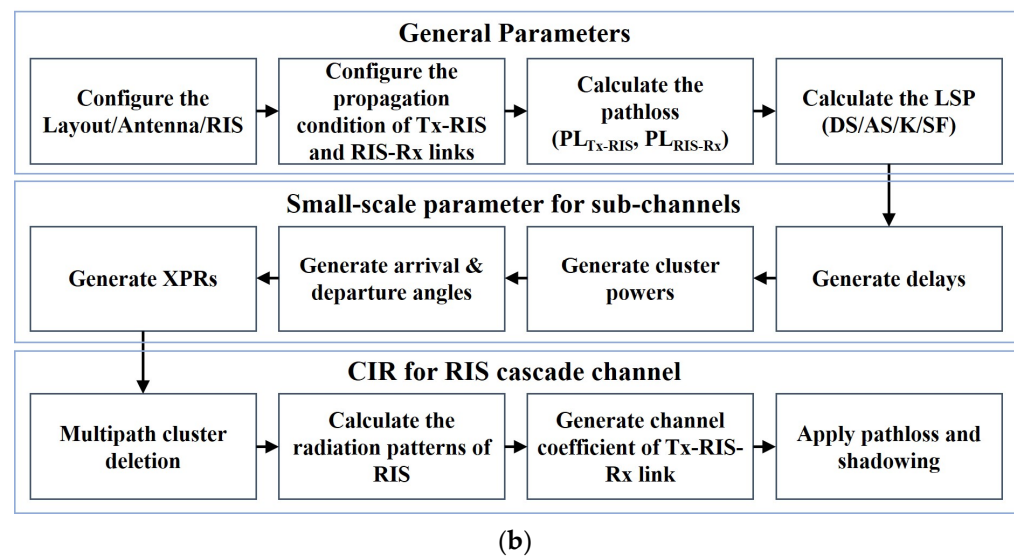


**Figure 12.** RIS channel modeling. (a) Classification of approaches. (b) How to model channels with RIS cascade [54].

#### 2.4. Hardware Implementation of RIS

In this section, we present the State-of-the-Art RIS hardware architecture and some representative implementations [55]. Compared to the transceiver technology currently used in wireless networks, the main feature of the RIS concept is that it is an extension of the reconfigurable metasurface concept, which provides the possibility to make and control the EM response to the incoming radio waves, thus controlling the wireless environment.

Traditionally, reconfigurable reflectarray antennas are similar in structure to an RIS, and several studies on reconfigurable metasurfaces have provided a way to dynamically control the unit cell reflection characteristics [56]. Two common ways to control the reflection response in reconfigurable reflectarray antennas are through the use of tunable delay lines and tunable resonant elements: the former technique involves coupling the radiating element to a section of transmission line whose electrical length is varied to provide different phase-shift characteristics before the coupling and re-radiation of the incident wave, and the latter technique involves changing the resonant frequency of the radiating element itself through reactive loading or switching structures [57]. Currently, the latter technique is mainly used in RISs.

There are a wide variety of electromagnetic conversion and sensing functions that can be achieved with the RIS and related technologies, including absorption, reflection, polarization, focusing, and phase shifting, as shown in Figure 13. Achieving this level of functionality requires careful design of the RIS unit cell and associated processing, bias, and control circuitry. As described earlier, the RIS structure is an extension of the metasurface structure, where the metasurface structure consists of a two-sided structure of a unit cell structure with a ground (Figure 14a), the reconfigurable metasurface structure adds a bias layer to the reconfigurable element, and the RIS consists of the following three substrate layers (Figure 14c): a metasurface layer, a circuit network layer, and a control layer.

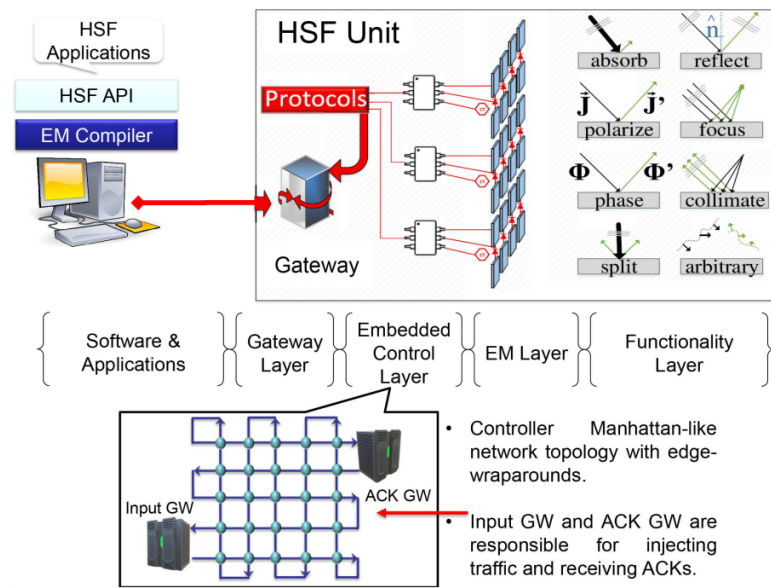


Figure 13. Hardware architecture of RIS. Adapted with permission from [58]. Copyright 2010 IEEE.

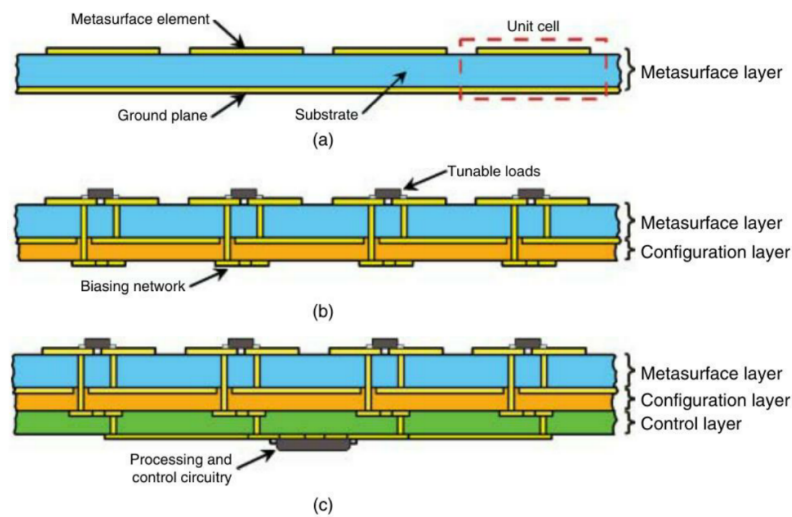


Figure 14. Comparison of the cross-sectional structure of metasurface and RIS. (a) Metasurface. (b) Reconfigurable metasurface. (c) Reconfigurable intelligent surface. Adapted with permission from [59]. Copyright 2023 John Wiley and Sons.

The metasurface layer of an RIS typically takes two forms. One approach is a semi-array-like structure with array elements placed in a region of  $\lambda/2$ , and the other approach is a reconfigurable metasurface structure using elements with periodicity much smaller than  $\lambda/2$  [60]. Reconfigurable metasurfaces employ reconfiguration mechanisms that can be divided into the following three categories: circuit reconfiguration, geometric reconfiguration, and material reconfiguration. Circuit reconfiguration is achieved through impedance changes within unit cell elements such as switches and variable capacitances. The main advantages of RISs are low fabrication cost, low latency, and low power consumption; at microwave frequencies, most RIS designs are based on integration with other voltage-driven circuit elements such as PIN diodes, varactors, or MEMS as circuit reconfiguration, which is the most popular approach in practice [61]. For example, the ON and OFF states of a PIN diode acting as a switch in the unit cell of an RIS can provide different resonant modes, providing one, two, or more phase states. Unlike PIN diodes, which can only provide discrete phases, varactors can be used to implement continuous phase changes in RIS designs. Geometric reconfiguration involves changing the electrical shape of the device, such as

rotating and deforming the resonator, while material reconfiguration involves changing the material property parameters and conductivity of the substrate using reconfigurable materials such as liquid crystals (LC), graphene, and ferroelectric thin films [62]. Thermal control materials, such as light-induced plasma, carbon nanotubes, and vanadium dioxide (VO<sub>2</sub>), are also being investigated for reconfigurable metasurface behavior [63–65]. A comparison of methods and features for RIS reconfiguration is shown in Table 5.

**Table 5.** Comparison of reconfigurable techniques (+: good, o: normal, -: poor, M: microwave, T: THz). Adapted with permission from [56]. Copyright 2014 IEEE.

Type	Technology	Stability	Integration	D/A Control	Cost	Loss (M/T)	Bias Power Consumption	Linearity	Switching Time
Circuit	PIN diode	+	–	D	+	–/–	–	o	+
	Varactor	+	–	D	+	–/–	+	–	+
	MEMS	o	+	D	+	+/o	+	+	o
Material	Ferroelectric thin film	o	+	A	o	–/–	+	o	+
	LC	o	o	A	o	–/+	o	o	–
	Graphene	–	+	A	o	–/+	+	–	+
	Photoconductive	o	–	A	o	–/–	–	–	+
Mechanical	Fluidic	o	–	A	o	o/+	+	o	–
	Micromotors	–	–	A	–	+	o	+	–

RISs can be divided into digital and analog (continuous) RISs according to the phase control scheme. Digital RISs are implemented with MEMS and PIN diodes and are widely studied due to their simple control circuitry and fast response; however, the phase quantization error introduced by digital phase control devices cannot be ignored [66]. For example, in the case of 1-bit phase control, the gain loss due to phase error is more than 3 dB, and the phase quantization error causes unacceptable gain loss [67]. Therefore, to eliminate the gain loss due to quantization error in digital RISs, analog tunable devices, namely varactor diodes, are used in analog RIS design [68]. An analog RIS using varactors can reduce the quantization loss due to phase shift because it implements continuous phase shift by changing the capacitance of the varactor diode, but it has the disadvantage of the loss characteristics of the varactor itself and the complexity of the circuit. The digital and analog unit cell structure of a transmitarray with a transmissive function during an RIS is shown in Figure 15.

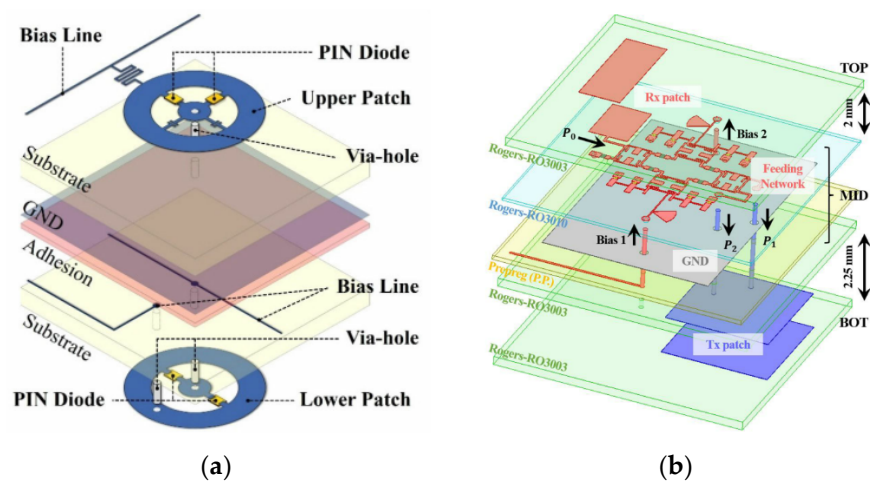


**Figure 15.** Unit cell structure of RIS. (a) Digital RIS [69]. (b) Analog RIS.

RISs can also be categorized into passive, nearly passive, and active RISs based on their power consumption as shown in Figure 16. Passive RISs, as shown in Figure 16a, have the disadvantage of having a fixed beam steering value that is initially designed by combining unit cells with phases of  $0^\circ$  and  $180^\circ$ , but they have the advantage of low fabrication cost and simplicity [70]. A nearly passive RIS, as shown in Figure 16b, is a term for a reconfigurable RIS using PIN diodes, which actually includes an active circuit with a bias, but it is classified as a nearly passive RIS in that it only controls the phase without amplifying the signal. In the case of an active RIS, a power amplifier is included to amplify the signal to overcome the disadvantage of double path loss of a passive RIS; however, due to problems such as high cost, complexity, and power consumption, a hybrid RIS has been recently proposed [71], as shown in Figure 16c.

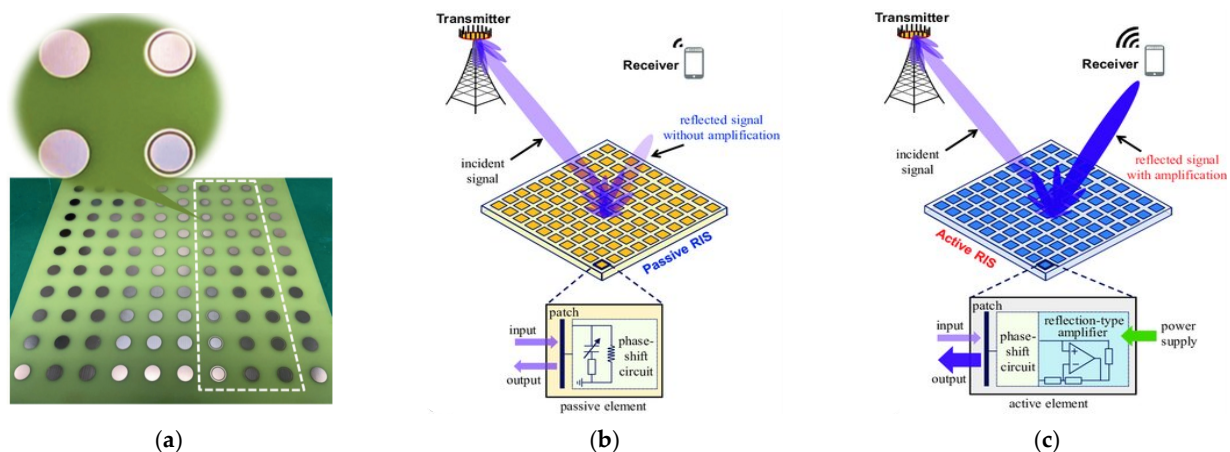


**Figure 16.** RIS classification based on power. (a) Passive RIS [70]. (b) Nearly passive RIS. (c) Active RIS. Adapted with permission from [71]. Copyright 2023 IEEE.

A bias network is required to control the unit cell reflection characteristics of the RIS. The structure of this network depends on the reconfiguration mechanism and the desired degrees of freedom of control of the propagating signal. For example, for a 1-bit RIS structure with a PIN diode reconfiguration unit cell, the bias network can consist of columns driven by a voltage such that each PIN diode in a single column is biased either in a reverse or forward direction with respect to  $0^\circ$  and  $180^\circ$ , respectively. This type of network is typically designed to be driven by an FPGA. The complexity of the bias circuit for RIS depends on factors such as the reconfiguration scheme, number of unit cells, and periodicity. Continuous tuning with a varactor, which requires a variable DC voltage between 0 and 30 V, typically relies on a digital-to-analog converter (DAC), which requires an analog-to-digital converter (ADC) channel for each unit cell to individually control the unit cell elements with an analog signal. DACs require digital control signals, such as in the form of the well-known serial communication protocols such as SPI and I2C, and associated circuitry and clock signals. The bias of a PIN diode, on the other hand, can be easily implemented to have a forward bias voltage of typically 0.7 to 1.5 volts and a typical operating current of about 1 to 10 mA. Of course, to reduce cost and size, digital circuits such as microcontroller IO ports are often used. For the bias circuit, if it is not electrically isolated from the RF emitters that make up the unit cell, it will not perform as designed. Therefore, an RF choke or optical bias circuit is required to electrically isolate it from the emitters in the unit cell. Zhang et al. [72] developed an optically controlled reconfigurable metasurface, which presents the concept of providing a bias voltage to a unit cell with varactor diodes through photodiodes controlled by light of varying intensity, as shown in Figure 17a.

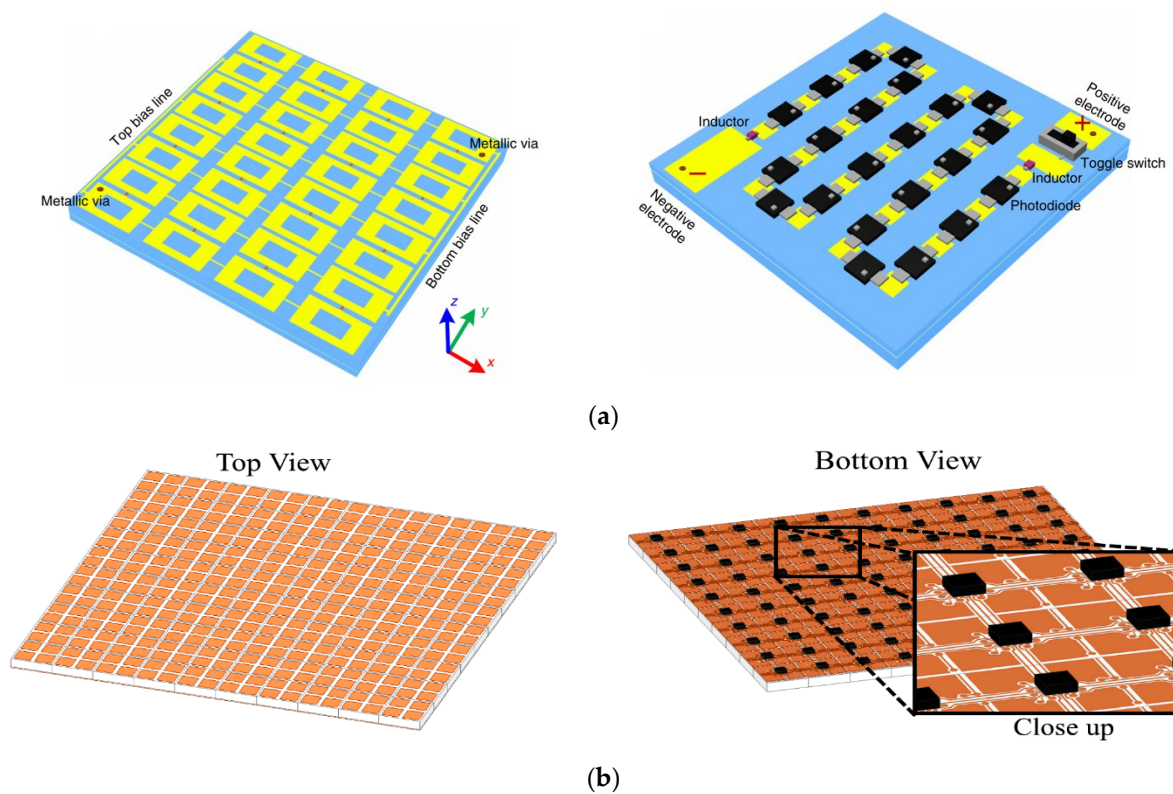


**Figure 17.** Bias circuits in the RIS. (a) Optical control bias circuit. Adapted with permission from [72]. Copyright 2023 IEEE. (b) Chip bias circuit. Adapted with permission from [73]. Copyright 2023 IEEE.

In addition, the complexity of the reconfiguration control circuit for beam steering in RIS can be problematic for large-area RISs [10]. Several methods have been proposed to simplify it, such as sequential loading [10] or unit cell gathering [73], as shown in Figure 17b. A method to reduce the bias network complexity through row/column control in reconfigurable reflectarray antennas was recently proposed by Artiga [74], in which the phase of each unit cell is controlled on a row-by-row basis such that additional phase shifts occur when rows and columns overlap. For an  $N \times M$  metasurface, this scheme requires only  $N + M$  analog control lines rather than  $N \times M$ . This study also proposed a 1-bit row/column control scheme that applies an XOR function to the digital unit cells, and showed that it can achieve similar gains to the individual control of 1-bit and 2-bit unit cells without increasing the sidelobe level. The complexity of the bias circuit becomes even more problematic at higher operating frequencies; to address this, the concept of a hypersurface has been proposed [73], where the impedance of each unit cell can be controlled to vary its size and phase using a very small ASIC. In this case, it is possible to realize the required unit cell periodicity at 60 GHz with about  $1 \text{ mm} \times 1 \text{ mm}$  [75].

The general architecture of the RIS consists of three layers and one RIS controller, as described earlier. The top layer acts as an antenna that directly controls the incoming electromagnetic waves. This layer consists of numerous reconfigurable conductive patches on a dielectric substrate. For practical implementation, this layer can also be equipped with a dedicated RF sensor to detect radio signals, which can directly sense the surrounding radio signals to support intelligent RIS configuration mechanisms. Then, an RF choke structure is placed in the middle layer to minimize RF signal leakage. Finally, control elements that reconfigure the reflective elements in real time are placed on the bottom layer. These control elements are typically implemented using commercial microcontrollers, SDR devices such as USRPs, or FPGAs, and interface with the entire network to receive and apply RIS control commands, as shown in Figure 18. A gateway interface is used to facilitate the transfer of information between the RIS and network equipment such as

base stations [76], and a wireless transceiver is used to provide the unit cell configuration information of the RIS through the gateway interface, which is usually coupled with a microcontroller. The microcontroller provides configuration signals to the bias network based on commands received from the network equipment and may also process data received from onboard error detection or sensing hardware before passing this information to the network controller.

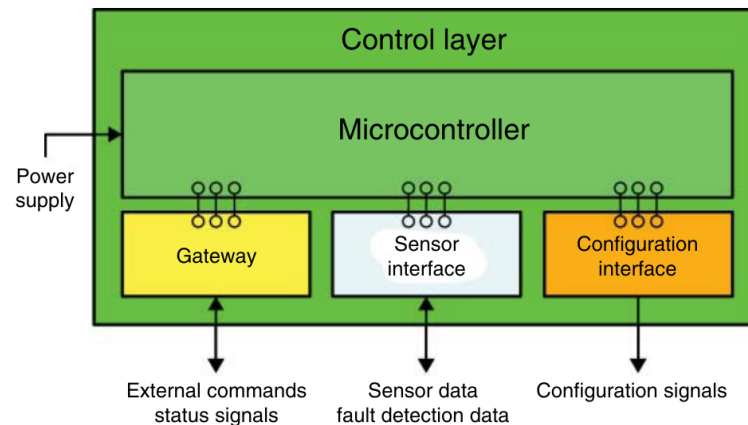


**Figure 18.** Example of control structure in RIS. Adapted with permission from [59]. Copyright 2023 John Wiley and Sons.

Most of the early RIS research was designed around the WiFi band. In 2020, Arun et al. [77] designed RFocus, a two-dimensional surface with 3200 rectangular arrays of passive antenna elements operating at 2.4 [GHz], as shown in Figure 19a. Each passive unit cell has a size of  $\lambda/4 \times \lambda/10$ , and electromagnetic waves are reflected or refracted. They showed that RFocus surfaces can be fabricated at low cost and can improve the average signal strength by a factor of 9.5. Dai. et al. [78] first designed a 2-bit  $16 \times 16$  RIS with a phase difference of  $90^\circ$  based on PIN diodes operating at 2.3 GHz and 28.5 GHz, as shown in Figure 19b. By using modular hardware and flexible software based on USRP, high antenna gains of 21.7 dBi at 2.3 GHz and 19.1 dBi at 28.5 GHz were achieved with low power characteristics. In 2021, Pei. et al. [79] designed a size  $55 \times 20$  1-bit RIS operating at 5.8 GHz based on a varactor diode, as shown in Figure 19c, and measured a power gain of 26 dB compared to the reference value of replacing the RIS with a copper plate in an indoor test where the transmitter and receiver were separated by a 30 cm thick concrete wall, and 27 dB in a short-range outdoor measurement. Long-range measurements also confirmed successful transmission of a 32 Mbps data stream over 500 m and low-power operation of 1 W. With the RIS utilizing the continuous control characteristics of varactor diodes, Fara. et al. [80] proposed the concept of using a  $14 \times 14$  RIS as ambient backscatter communications (AmBC) for IoT devices operating at 5.15–5.75 GHz (Figure 19d) and confirmed this with experimental measurements.

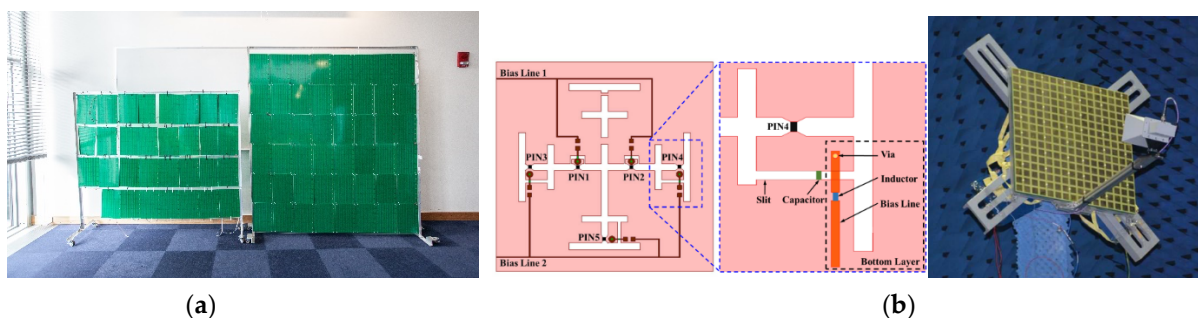


**Figure 19.** Cont.



**Figure 19.** Hardware implementation of RIS. (a) PIN diode—1 bit [76]. (b) PIN diode—2 bit. Adapted with permission from [78]. Copyright 2020 IEEE. (c) Varactor diode—1 bit. Adapted with permission from [79]. Copyright 2021 IEEE. (d) Varactor diode—analogue. Adapted with permission from [80]. Copyright 2022 IEEE.

Most of the published work on RISs focuses on idealized RISs and is limited to theoretical analysis and most of the experimental studies have been conducted in sub-6 GHz bands; there are not many studies related to practical RIS design and experimental characterization for millimeter-wave bands. In [81], a practical RIS design was proposed and near-field and far-field measurements for signal enhancement were performed. However, the operating bandwidth of the design [81] was 27.5 to 29.5 GHz (7% bandwidth), which cannot meet the wide bandwidth requirements of the 5G millimeter-wave band.

Shekhawat. et al. [82] designed a small unit cell and a  $25 \times 32$  element RIS prototype operating at 28.5 GHz, but did not provide the operating bandwidth. Similarly, Jeong et al. [83] presented a  $24 \times 24$  RIS consisting of a crossed dipole-shaped unit cell operating at 29 GHz to derive a path loss model, as shown in Figure 20. In particular, they presented an RIS phase control system consisting of an Arduino microcontroller and 144 shift registers connected in 6 series and 24 parallel to control 1152 PIN diodes. In 2023, ref. [84] proposed a  $20 \times 20$  RIS covering the entire millimeter-wave 5G n257 (26.5 to 29.5 GHz) and n258 (24.25–27.5 GHz) bands. The fabricated RIS exhibited a broadband characteristic of 22.5–29.5 GHz (26.9%) and a beam steering characteristic of  $50^\circ$ .

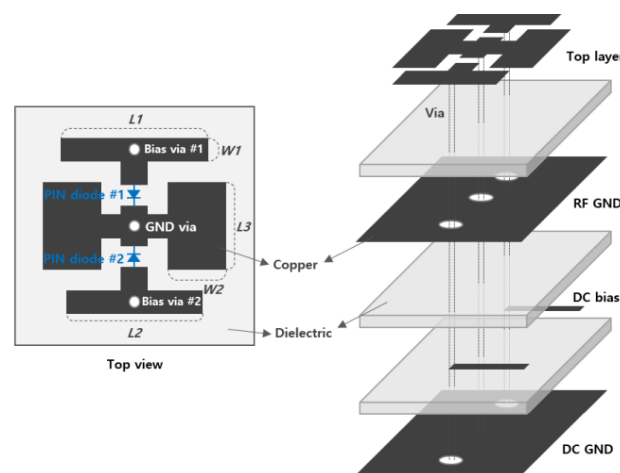


**Figure 20.** Millimeter-wave RIS unit cell. 29 GHz operating unit cell. Adapted with permission from [83]. Copyright 2022 IEEE.

PIN diodes or varactors typically have a large insertion loss characteristic, which further worsens overall efficiency. This can be mitigated by selecting diodes with low insertion loss, but at the cost of increased fabrication costs. Electrically controlled RISs can only realize a preset EM function, which is energy intensive in application scenarios where the EM function does not need to be reconfigured frequently. Therefore, elec-

Electromechanical RISs have been proposed as RISs for signal enhancement in static areas such as indoor telecommunication shaded areas. Recently, various electromechanically reconfigurable metasurfaces based on piezoelectric actuators [85], spring devices [86], and micromotors [87] have been proposed. These reconfigurable metasurfaces, which consist of a passive metasurface and a mechanical actuation module, have the general advantages of both high efficiency and reconfigurability. However, since most of the passive metasurfaces and mechanical actuators are complex and limited in installation and only support discrete phase states, there is a need for a practical electromechanical RIS design that is easy to fabricate and assemble, low-cost, and flexible in wavefront tuning. In 2023, Qu Kai et al. [88] designed an RIS operating at 2.55 GHz consisting of a passive metasurface and a stepper motor drive module as shown in Figure 21. By grouping  $16 \times 16$  unit cells into  $4 \times 4$  supercells and controlling the phase with a 12 V voltage, they demonstrated an improvement in received signal performance of about 5.2 dB through indoor measurements.

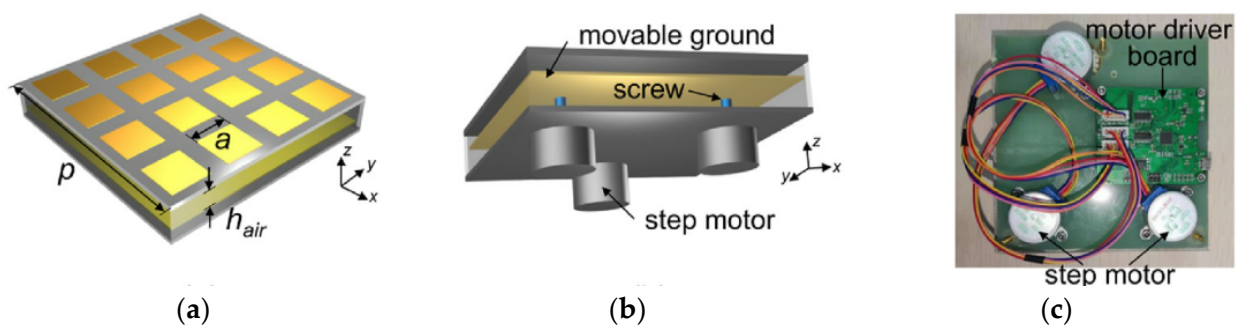


**Figure 21.** Unit cell of an electromechanical RIS [88]. (a) Schematic diagram. (b) Driver module of the RIS supercell. (c) Photograph of the driver module.

In order to realize the concept of a smart wireless environment, multiple RISs composed of reconfigurable metasurfaces are required to be installed in various environments that control the propagation channels, which requires high-quality communication services without visually affecting the RISs, if possible. Optically transparent RISs have potential applications in scenarios where high-quality communication services and good optical transparency must be provided simultaneously to a large number of mobile terminal devices. For example, optically transparent RIS can be used for glass curtain walls in urban buildings, glass walls in meeting rooms, aircraft, ships, trains, subways, shop windows and billboards in shopping malls, and showcase glass in museums, and solar panels can be installed on the back of the optically transparent RISs to achieve self-powered operation. In [89], an optically transparent 12 GHz-operating reconfigurable metasurface based on ITO film was proposed, as shown in Figure 22a. This structure has an optical transmittance characteristic of 80%, and a photovoltaic panel was attached to the back to realize an energy source. The disadvantage of ITO is that it has relatively large electromagnetic losses due to the physical properties of the material. In 2022, Liang et al. [90] designed a 2-bit photonic RIS operating at 3.5 GHz based on a metal mesh with high conductivity, which realized excellent beam steering characteristics from  $0^\circ$  to  $60^\circ$ , but had a low optical transmittance of 49.3%. When lumped elements such as an RLC are used to realize an optical transparent RIS, it is difficult to obtain a high optical transmittance due to the opacity of the device; therefore, vanadium dioxide ( $\text{VO}_2$ ), which can be actively controlled by current and temperature, is sometimes used. In [91], a transparent RIS with 88% optical transmittance and controllable loss characteristics from  $-1.27$  dB to  $-15.38$  dB at 10 GHz was designed and fabricated by combining a mesh-implemented LC resonator and a  $\text{VO}_2$  pattern. In [92], the bottom layer was realized with a metal mesh stripe pattern and the top layer with a metal mesh lattice pattern to improve the optical transparency of the RIS device to 79% without affecting its microwave properties in the operating band of 3.53–3.7 GHz. Existing optically transparent design technologies are immature and unreliable, posing challenges

in the processing of metal vias and multilayer structures, surface mounting of components, design of direct current (DC) supply networks, and other design and fabrication issues. Therefore, designing and fabricating optically transparent reconfigurable RISs with the same electromagnetic properties as conventional metasurfaces remains a great challenge.

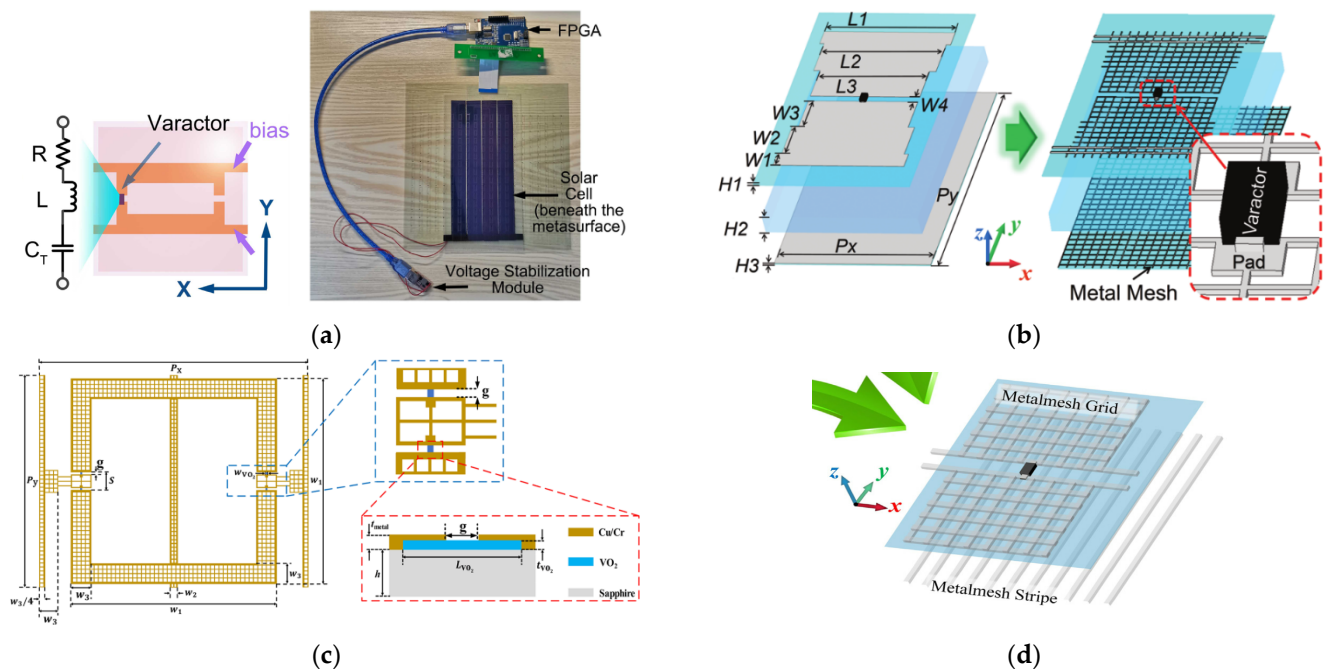


**Figure 22.** Optically transparent RIS unit cell. (a) ITO-based RIS. Adapted with permission from [89]. Copyright 2019 IOP Publishing Ltd. (b) Metal mesh-based RIS. Adapted with permission from [90]. Copyright 2022 John Wiley and Sons. (c) VO<sub>2</sub>-based RIS [91]. (d) Light transmittance-enhanced metal mesh RIS [92].

Regarding commercial RISs, NTT Docomo, together with Metawave, conducted a field test of a metamaterial reflector prototype operating in the 28 GHz band in 2018 [93]. During the test, the BS was installed on the roof of a building, making the road below the building a coverage blind spot, as shown in Figure 23a. By placing metamaterial reflectors to cover this area and adjusting the beam to reflect in this area, SNR improvements of over 15 dB and speed improvements of over 500 Mbit/s were observed [93]. In 2020, trials were conducted with AGC Inc. with a transparent dynamic metasurface [94]. The transparent dynamic metasurface consists of two transparent substrates, one of which has a pre-designed metamaterial pattern printed on it, and the distance between the two substrates can be adjusted to control the following three modes: full transmission, full reflection, and hybrid mode. In full transmission mode, the metasurface has a transmission loss of only about 1 dB, while in full reflection mode, it has a transmission loss of more than 10 dB. An improved version of the transparent dynamic metasurface was tested in 2021, which is capable of focusing millimeter waves [95]. At the focal point, the metasurface can improve the SNR by about 24 dB compared to ordinary glass. Placing a repeater at the focal point of the metasurface, as shown in Figure 23c, can be used as a solution to improve indoor coverage of millimeter waves, providing a reliable link between an outdoor mm wave BS and an indoor UE [96].

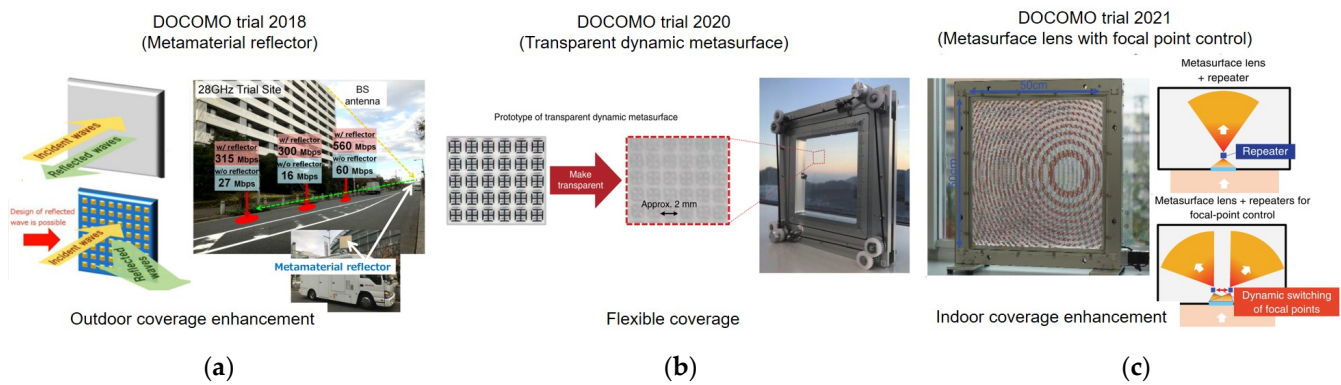


**Figure 23.** NTT Docomo RIS trials in (a) 2018. Adapted with permission from [93]. Copyright 2019 IEEE (b) 2020, and (c) 2021.

Also, in 2019, Lumotive (a U.S. startup) and TowerJazz (a global foundry) announced beam steering ICs based on liquid crystal metasurface technology for LiDAR systems in autonomous vehicles. In 2019, Pivotal Commware proposed a new technology called Holographic Beamforming (HBF) using Software Defined Antenna (SDA). The proposed holographic beamformer has the advantage of lower cost and power consumption compared to other transmission technologies such as massive MIMO and phased array [20]. In 2023, Greenerwave announced a commercialized active RIS packaged as an AP extender with a 500 MHz bandwidth in the frequency range of 27.5 to 29.5 GHz [96]. In addition, Japan Display of Japan announced an RIS that combines liquid crystal metasurface technology with TFT technology, operating at 28 GHz and capable of beam steering of  $\pm 60$  degrees, as shown in Figure 24 [97].

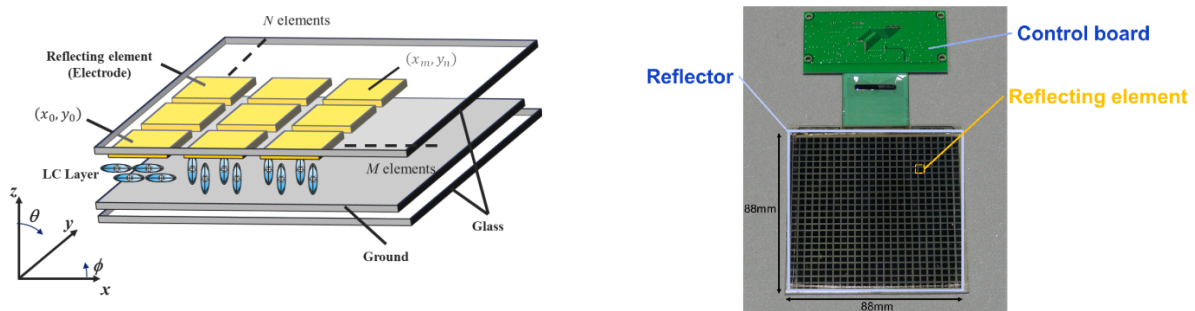


**Figure 24.** RIS using liquid crystal metasurfaces [97].

Implementing RIS hardware and applying it to real-world communications requires the following considerations. First, how to set up the experimental setup to measure the performance of an RIS. As it is already known, when the size of the array antenna is  $D$ , the near-field and far-field regions are determined by  $2D^2/\lambda$ . As the operating frequency increases and the size of the RIS increases, the RIS is more likely to be located in the near field. In the past, unit cell design has primarily focused on far-field scenarios. However, in indoor environments, near-field applications such as smart homes are becoming more prevalent. Studying the theory of electromagnetic field distribution in the near and far fields and analyzing the factors affecting the design of these components can effectively improve the efficiency of RIS systems in indoor scenarios.

The second is whether the phase control should be 1 bit or 2 bit, or whether finer resolution control is required. As discussed earlier, the phase resolution and phase shift range of each unit cell have an important impact on the RIS radiation performance. In addition, the single functional cell of the RIS prototype often induces discrete phase changes due to the limitations of the hardware structure. Since a 1-bit RIS can only provide two phase states, the antenna efficiency is low and the sidelobes are high, reducing the antenna

gain by more than 3 dB [66]. To mitigate the performance degradation caused by 1-bit phase quantization, some researchers have designed multibit RIS boards; however, multibit designs increase system complexity and hardware cost. Two-bit phase quantization is a compromise between system design complexity and component performance, with antenna gain loss of less than 1 dB and improved sidelobes [98]. Therefore, when designing RIS, researchers should consider the high precision gain brought by multiple bits and the complexity of system design. However, through block matching of different cells and controllable coupling design, “supercells” of continuous phase change can be realized in RIS prototypes; therefore, it is necessary to develop RIS prototypes that can arbitrarily adjust the phase resolution to meet high-precision requirements.

The third is how to realize hardware with broadband characteristics. According to Shannon’s theory, communication performance is limited by bandwidth; therefore, the design of an RIS with a wide operating bandwidth is essential for high-speed wireless communication systems. To increase the bandwidth, research is being conducted on unit cell design with double resonant elements and unit cell design using an air gap.

Fourth, it is necessary to determine the size of the RIS and the optimal number of unit cells for sufficient communication performance. As described earlier, it is important to determine the optimized RIS size according to the scenario; if the RIS does not reach a certain size, it is not possible to obtain excellent SNR characteristics by using the currently used relays [21]. As shown in Figure 25, the RIS is frequency-independent, but the number of unit cells per surface area increases with wavelength to the fourth power. A Decode and Forward (DF) relay can have a much smaller size than the RIS, except in cases where very high spectral efficiency is required.

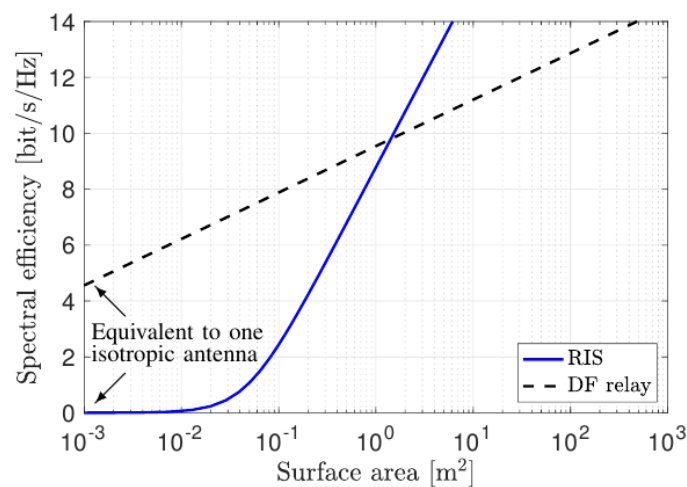


**Figure 25.** Spectral efficiency as a function of RIS and relay surface area. Adapted with permission from [21]. Copyright 2020 IEEE.

Finally, we need to consider the price of implementing the RIS hardware. The cost of manufacturing the hardware board for an RIS can be broken down into the following three parts: the PCB; the electronic components such as RF switches, MCUs, and resistor; and the cost of assembling all the components on the PCB. The costliest of these are low-loss substrates for use in the high-frequency band, high-frequency band components for reconfiguration such as PIN diodes or varactors, and additive PCB fabrication with a build-up process including vias. Therefore, engineers can reduce costs by using simplified reconfigurable elements such as FET switches, unit cell designs that do not use vias, etc. Figure 26a shows the RIS structure using FET switches [99] and Figure 26b shows the RIS unit cell realized with printing technology without using vias [100].

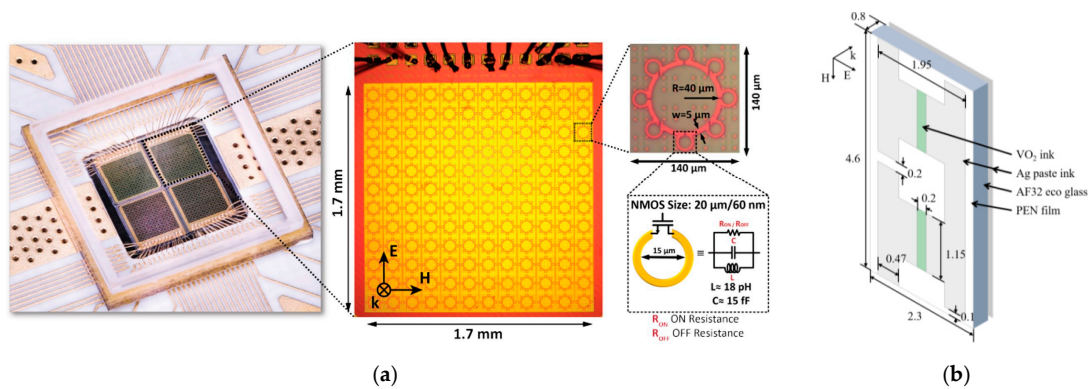


**Figure 26.** Cost effective RIS design. (a) RIS unit cell with FET switches. Adapted with permission from [99]. Copyright 2023 IEEE. (b) RIS unit cell without Vias. Adapted with permission from [100]. Copyright 2023 IEEE.

### 2.5. Differences between Relay and RIS [101]

Currently, relays are deployed in mobile communications to identify alternative propagation paths in real time that can receive signals carrying the same information as a way to avoid the channel instability [102]. Relays can be used to effectively turn a single non-line-of-sight (NLOS) link into multiple LOS links. This approach requires that each relay be equipped with a dedicated power source and the necessary front-end circuitry to receive, process, and retransmit. For this reason, using relays has the disadvantage of increasing network power consumption and cost. The network spectral efficiency provided by a relay-enabled system depends on the duplexing protocol used for transmission. When using a HD relay protocol, the transmitter and repeater cannot transmit simultaneously from the same physical resource. FD relay protocols can overcome this problem, but suffer from high loopback self-interference at the relay due to the simultaneous transmission and reception of signals, co-channel interference at the destination because the relay and transmitter emit different information from the same physical resource, and increased signal processing complexity and power consumption at the relay.

Relays are typically active devices that require power and consist of active electronic components such as DACs and ADCs, mixers, power amplifiers, and low-noise amplifiers for receiving. The implementation of decode-and-forward (DF) and amplify-and-forward (AF) relays, especially in millimeter-wave and submillimeter-wave frequency bands, typically requires multiple electronic components, resulting in high cost and power consumption [103]. In addition, as previously discussed, the use of FD relays further increases complexity because they require the use of custom antennas and analog/digital signal processing methods to eliminate loopback self-interference. Furthermore, the active electronics used in relays increase noise, which negatively impacts the performance of existing relay protocols. For example, in AF relays, noise is amplified at the relay. With DF relays, the effects of additive noise can be mitigated at the expense of increased signal processing complexity and power consumption because the signal is decoded and re-encoded (regenerated) at the relay. However, in FD relays, system performance is degraded by the effects of residual loopback self-interference. The spectral efficiency of a relay-assisted system depends on the duplexing protocol adopted. In a HD relay, the achievable rate is typically doubled because different physical resources are used for the data emitted by the transmitter and the repeater. On the other hand, the end-to-end signal-to-noise ratio can be increased by taking advantage of more favorable propagation conditions for the relayed signal and by optimally combining the direct and relayed signals. In an FD relay, the achievable speed is not doubled, but the relay is affected by residual loopback self-interference and the receiver is degraded by interference generated by the simultaneous transmission of the transmitter and relay.

The RIS is a technology that uses metasurfaces to reflect signals from the source node to the destination node with low energy consumption, as described earlier, and is not constrained by power supply. Considering the low-cost nature of RISs [104], implementing an RIS in practical applications is more favorable than relays. Therefore, it is meaningful to compare RISs and relays. In [105], it was shown that a multiple-input single-output (MISO) system using an RIS can achieve higher energy efficiency compared to an AF relay; in [101], an RIS-enabled single-input single-output (SISO) system was compared to a conventional DF relay. It has been shown that an RIS with large metasurfaces and massive devices can outperform active relays in terms of spectral efficiency and energy efficiency [21,101,106]. The differences between an RIS and relay are shown in Figure 27 and Table 6, respectively.

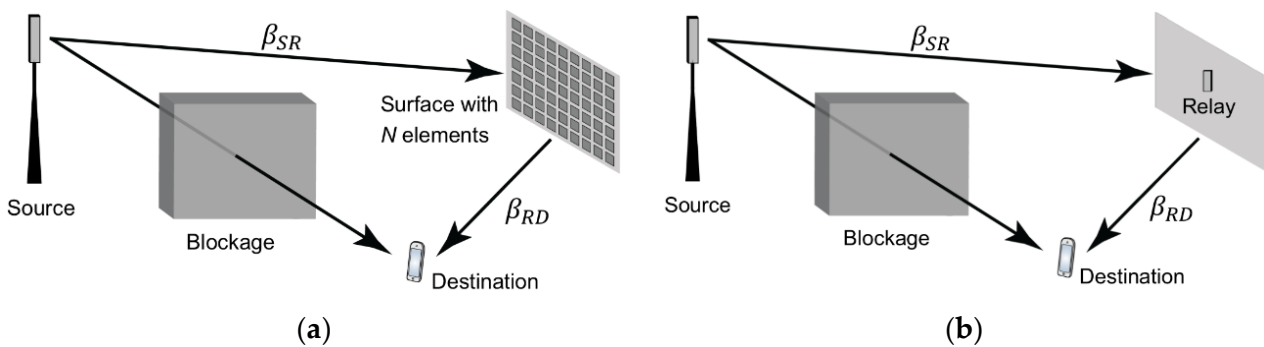


Figure 27. Comparison of RIS and relay. Adapted with permission from [101]. Copyright 2020 IEEE. (a) RIS. (b) Relay.

Table 6. Comparison of RIS and relay [101].

Parameters	RIS	Relay
Definition	The reflecting surface which scatters incoming EM waves with controllable delay/phase and polarization is known as an RIS.	The device which decodes incoming EM signal, amplifies and retransmit it back is known as a relay.
Operating mechanism	Passive/active reflection	Active reception and transmission
Duplex	Full	Half/full
Number of transmit RF Chains required	Zero	N
ADC/DAC and amplifier	Not required	Required
Energy consumption	Low	High
Spectral efficiency formula	<div style="border: 1px solid black; padding: 5px;"> <p>Spectral efficiency (IRS):</p> <math display="block">\log_2(1 + \rho N^2 \beta_{SR} \beta_{RD})</math> <p>Where,</p> <ul style="list-style-type: none"> <li><math>\rho</math> - Signal Transmit Power</li> <li><math>N</math> - IRS elements</li> <li><math>\beta_{SR}</math> -Path Loss between Source and Reflector</li> <li><math>\beta_{RD}</math> -Path Loss between Reflector and Destination</li> </ul> </div>	<div style="border: 1px solid black; padding: 5px;"> <p>Spectral efficiency of Relay :</p> <math display="block">\frac{1}{2} \log_2(1 + \rho \min(\beta_{SR}, \beta_{RD}))</math> <p>Where,</p> <ul style="list-style-type: none"> <li><math>\rho</math> - Signal Transmit Power</li> <li><math>\beta_{SR}</math> -Path Loss between Source and Relay</li> <li><math>\beta_{RD}</math> -Path Loss between Relay and Destination</li> </ul> </div>

RISs consist of a composite material multilayer structure with metal or dielectric patches printed on a grounded dielectric substrate, with reconfigurability implemented through low-power and low-complexity electronic circuits (switches or varactors). RISs typically do not require dedicated power amplifiers, mixers, and DACs/ADCs, making them less complex than relays if implemented using mass-produced and inexpensive large-area electronics. In addition, passive or nearly passive RISs are not affected by noise because they do not amplify or regenerate signals, but their performance can be degraded with phase noise [107,108]. RISs configured to act as reflectors are not affected by HD constraints and loopback self-interference, unlike relays. RISs are well suited for near-passive implementations because even metasurfaces without reconfigurability can be implemented with completely passive components, and low-power active components (switches or varactors) are only needed to ensure reconfigurability. The low-power nature of switches and varactors also lends itself to near-passive implementations using energy harvesting. In relay-assisted systems, it is typically assumed that the total RF power is allocated between the transmitter and relay to ensure total power constraint. In RISs, the total RF power is used by the transmitter; in addition, the power reflected and scattered by the RIS depends on the transmittance, which can be optimized through proper design of the metasurface [14]. In the ideal case, the total power reflected by the RIS is equal to the total power of the incident radio waves.

From a system model perspective, the RIS can be considered a full-duplex MIMO relay with no self-interference. In addition to the differences in system models, there are also differences in how performance is viewed in different cases. Finally, from an operator perspective, there are differences between the RIS and relay in how they are actually deployed and applied. RISs can be deployed in a more flexible way than relays because they can operate in a passive or nearly passive manner. Power and performance losses can be compensated for by increasing the number of reflective elements. The most important characteristic of RISs is that they can be independent of the power supply, which enables flexible, on-demand deployment of 6G networks. It not only complements coverage, but also provides on-demand services for users and traffic. To achieve the above goals, the network needs to control RISs in a wireless manner. A new design is required in terms of protocol architecture and control method. The designed solution must also ensure low power consumption and low complexity. Relays have no power limitations, which can make control and processing at the relay more complex.

On the other hand, a combined structure such as the one shown in Figure 28, which combines the advantages of relay and RIS, has also been proposed [109,110]. The key idea of the structure proposed in Figure 28a is that the power of the incident signal can be amplified through an FD relay without the need to place a power amplifier in the RIS. The proposed coupled structure consists of two RISs connected via an FD relay, which can split the required SNR gain into an array gain (using the focusing function of the RIS) and a power amplification gain. Thus, this structure can achieve spectral efficiency while significantly reducing the number of unit cells comprising the required RIS [110]. As a result, the proposed structure requires much less channel estimation/beam training overhead and offers improved robustness compared to conventional RIS solutions. Furthermore, by optimizing the position and orientation of the two surfaces, the proposed architecture can be deployed in a very flexible manner, which can provide much better coverage, which has been the subject of much recent research [111,112]. In Figure 28b, a MISO system is depicted in which a multi-antenna BS uses both a half-duplex DF relay and full-duplex RIS to transmit information to multiple single-antenna users [113]. The proposed hybrid relay-RIS system can achieve higher sum-rate and energy efficiency performance compared to the conventional relay-only system.

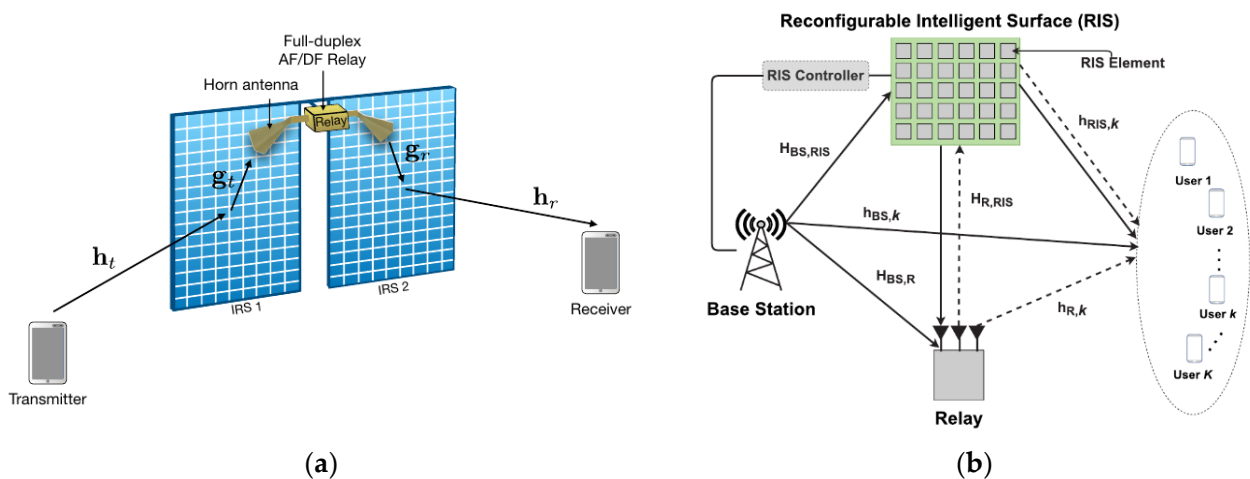


**Figure 28.** RIS with relays. (a) RIS with relays [109]. (b) MISO system with relays. Adapted with permission from [113]. Copyright 2023 IEEE.

2.6. Reflective/Transmissive RIS and Hybrid RIS

Most research on RISs has focused on reflective RISs. If each element of the RIS has a different hardware implementation (e.g., number of layers, size, thickness, number, and distribution of PIN diodes), the RIS can operate in the following three modes: transmissive [114], reflective, and hybrid transmissive and reflective [115], as shown in Figure 29, depending on the energy splitting for reflection and transmission [116–118]. A reflective RIS reflects the incident signal towards the user on the same side of the BS, while a transmissive RIS allows the signal to be transmitted towards the user on the opposite side. In the case of hybrid RIS, the RIS supports the dual functions of reflection and transmission [119].

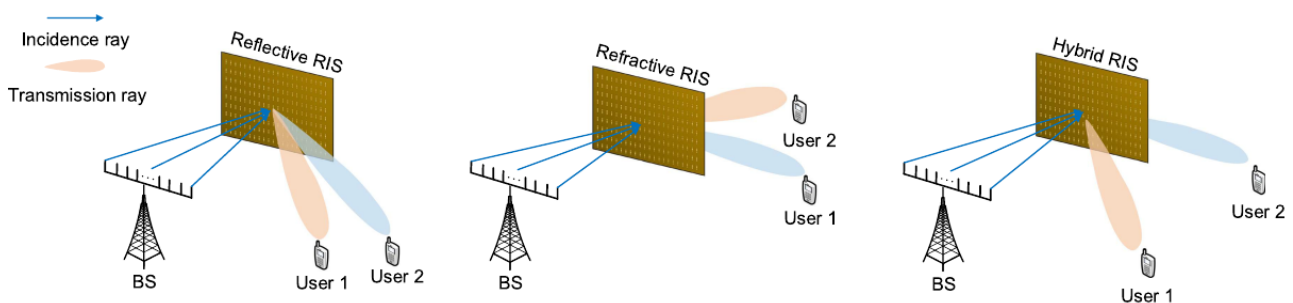


**Figure 29.** Types of RISs. Adapted with permission from [114]. Copyright 2022 IEEE.

A reflective RIS typically consists of three layers. The top layer is an array of 2D RIS unit cells that can directly interact with the incident signal, the middle layer is a conductor plate to reflect the incident propagating signal, and the bottom layer is a printed circuit connected to a controller, which can control the phase shift of the RIS unit cells. Two design schemes are widely used for transmissive RIS including the receiver–transmitter (Rx–Tx) structure and stacked FSS structure, as shown in Figure 30. In general, an Rx–Tx structure consists of three components: a receive (Rx) cell, a transmit (Tx) cell, and a phase shifter. A ground plane separates the Rx and Tx, allowing them to operate independently while avoiding mutual interference. The power transmission structure between them is usually implemented as a metal via or slot-coupling structure. When an incident wave arrives at the RIS, the Rx on one side of the RIS first receives the wave and converts it into an induced wave, which is then transmitted to the Tx placed on the other side of the RIS through a phase transition and re-radiated into free space. Therefore, the transmissive RIS structure can realize the MIMO function in practice because it can realize the beam steering characteristics for the incident wave. Stacked FSS structures are passive transmissive RIS

structures that consist of multiple FSS layers on metal and dielectric substrates. As the radio waves propagate through each FSS layer, a constant value of phase change occurs, and cascading multiple layers can generally realize a larger phase change. Unlike the Rx–Tx type, the stacked FSS structure has no ground plane, and the spacing between each layer is also an important design parameter.

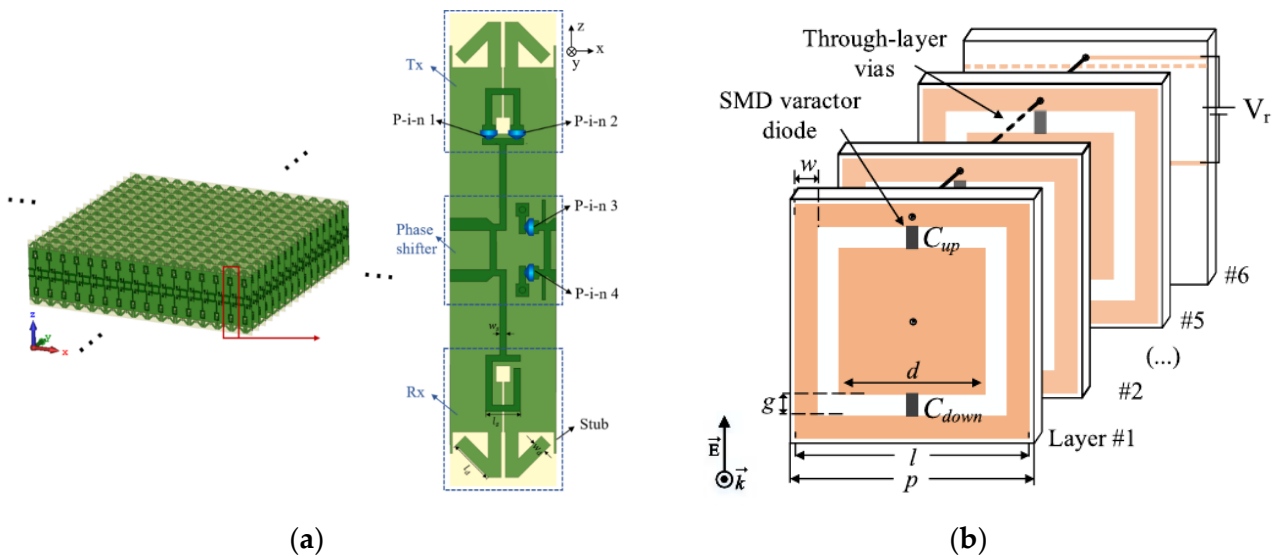


**Figure 30.** Types of transmissive RISs. (a) Receiver–transmitter structures. Adapted with permission from [120]. Copyright 2023 IEEE (b) Stacked FSS structures. Adapted with permission from [121]. Copyright 2017 IEEE.

The RIS ensures wireless connectivity over NLOS links in poor propagation conditions, such as when LOS links are blocked or shaded, and extends communication distance through controlled scattering and multipath components. However, reflective RISs only reflect signals within the front half space and blocks signals to users behind the RIS, resulting in poor performance for blocked users. This means that the service coverage is limited to  $180^\circ$  due to the location constraints of the nodes, which reduces the efficiency of RISs and can be a barrier to 6G small cell implementation. Therefore, a use case has been recently reported in [122] where users located on the sides of a surface not covered by transmitters can benefit from deploying RISs. Based on these considerations, an RIS design called hybrid RIS or Intelligent Omni Surface (IOS) has recently been introduced [123]. These RIS designs are also referred to as simultaneous transmit and reflect RIS (STAR-RIS) [124]. Unlike conventional RISs, hybrid RISs have dual functions of reflection and transmission, which can provide full spatial coverage to users located on either side of the surface to achieve omnidirectional wireless communication. Reflective RISs and STAR-RISs differ in terms of the components and substrates that make up the hardware; for example, in the case of reflective RISs, the substrate of reflective RISs uses conductors to prevent radio signals from penetrating the RIS at the operating frequency. On the other hand, the substrate of a STAR-RIS has a complex design structure because it must simultaneously transmit and reflect wireless signals at the operating frequency. However, when it comes to improving the efficiency of wireless networks, the STAR-RIS can provide more versatility for smart wireless environments, as shown in Figure 31, thanks to its ability to adjust the transmission and reflection coefficients [125].

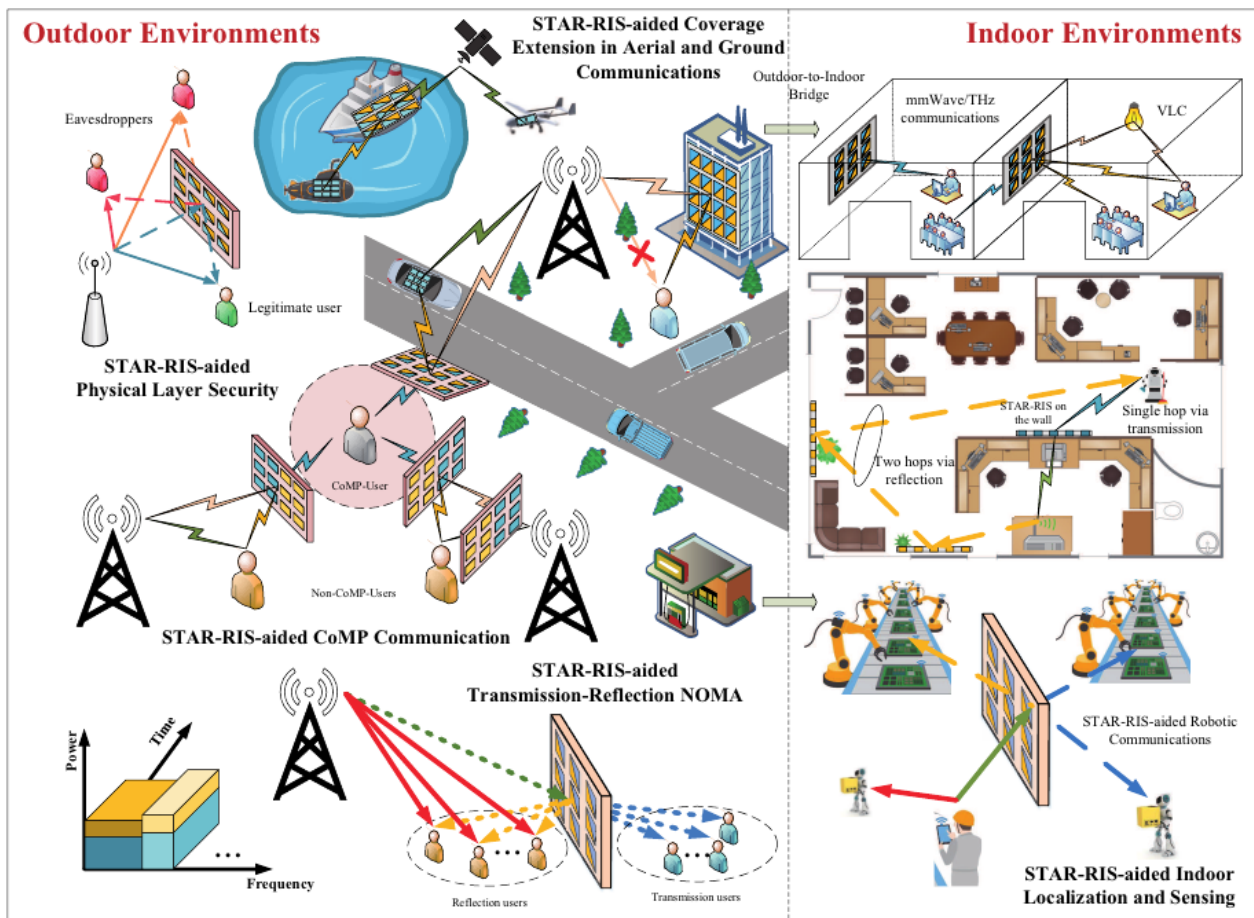


**Figure 31.** Application of STAR-RIS in wireless environment. Adapted with permission from [124]. Copyright 2021 IEEE.

2.7. Passive, Active, and Hybrid RIS

The RIS is an array structure consisting of a very large number of passive elements that reflect electromagnetic signals in a desired manner to reconstruct the propagation characteristics of the wireless environment. Thanks to its high array gain, low cost, low power, and negligible noise, the RIS is expected to improve channel capacity, expand coverage, and reduce power in future 6G networks.

The “RIS is passive” because it passively shifts the phase of a reflected signal without any active RF components. However, while the signal processing of the RIS is passive, the RIS itself is not completely passive as it uses active components to drive and reconfigure. For example, if a PIN diode is used to control the phase, current is required to keep the PIN diode ON, which is connected to some active components, and is called a nearly passive RIS.

An important advantage of the RIS is that the noise introduced by a passive RIS is negligible, resulting in a “square-law” array gain [126]. This means that the receiver SNR achieved by passive beamforming of the RIS is asymptotically proportional to  $N^2$  when the number  $N$  of the RIS unit cells is large. Thus, it can be seen that the desired signal power at the receiver is proportional to  $N^2$  due to the coherent superposition of the received signals, while the unwanted noise power at the receiver is invariant due to the negligible noise assumption [71]. Therefore, the RIS is expected to result in significant capacity gains in wireless systems by the square law, but in practice, these capacity gains are usually only observed in communication scenarios where the direct link between the transmitter and receiver is completely blocked or very weak [127]. On the other hand, in scenarios with strong direct links, the RIS can achieve very little visible gain,

and many RIS elements are needed to compensate for this loss [45]. This is due to the “multiplicative fading” or double path loss introduced by the RIS, i.e., the equivalent path loss of the transmitter–RIS–receiver link is the product (not the sum) of the path losses of the transmitter–RIS and RIS–receiver links, which is typically thousands of times larger than the direct link [45]. As a result, due to the “multiplicative fading” effect, a passive RIS is almost impossible to achieve a noticeable capacity gain in many wireless environments. Many existing studies on the RIS often ignore this effect by only considering scenarios where the direct link is severely impaired [128]. Therefore, addressing the fundamental performance bottleneck caused by the “multiplicative fading” effect is an important challenge for the RIS to improve its practicality in future 6G wireless networks. To solve these problems, the concept of an active RIS was proposed in [71,129]. The characteristic of an active RIS is that it cannot only adjust the phase shift, but can also amplify the attenuated received signal to the normal intensity level at the first hop. Therefore, an active RIS can effectively avoid the double path loss attenuation. The hardware architecture of an active RIS is fundamentally different from a passive RIS. To amplify the signal, active RISs are equipped with phase transition circuits and reflective amplifiers (e.g., current inverting converters) [71]. Unlike the low-power passive RIS, the amplifiers in active RISs and BSs can consume similar power, so the power consumption can no longer be ignored.

The SNR values of passive RISs and active RISs are plotted against the RIS unit cell number  $N$  in Figure 32. Here,  $N$  ranges from 10 to 1000 in Figure 32a and from  $10^4$  to  $3 \times 10^6$  in Figure 32b. From these figures, we can see that when  $N$  ranges from 10 to 1000, the SNR achievable by the user is about 40 dB higher for the active RIS-enabled system compared to the passive RIS-enabled system. Only when  $N = 2.5 \times 10^6$  does the performance gain achieved by the passive RIS become comparable to the performance gain achieved by the active RIS.

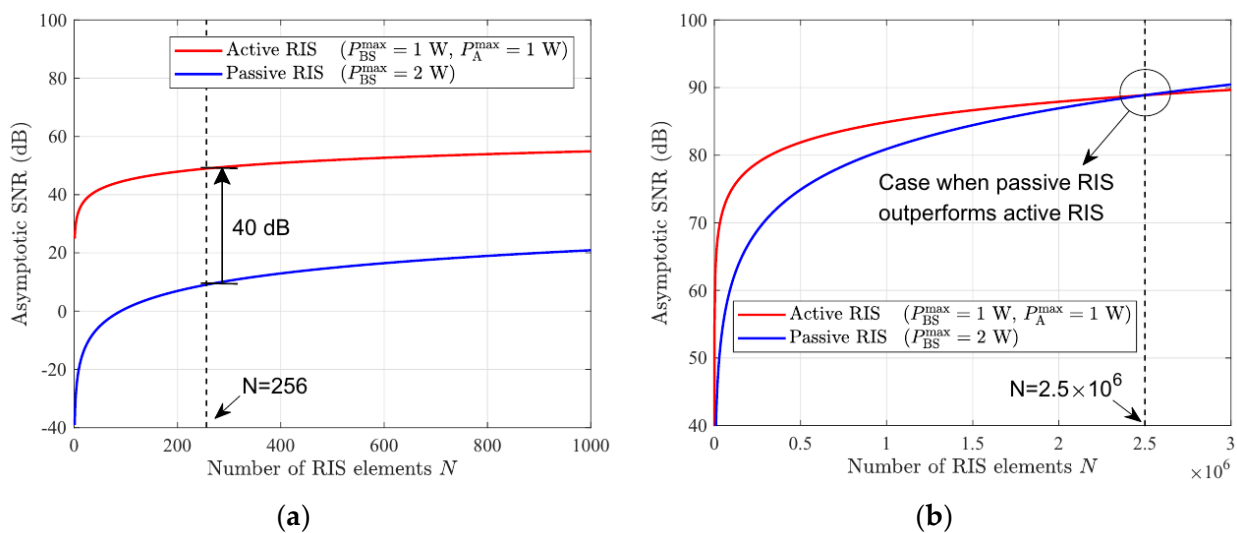


**Figure 32.** Passive vs. active RIS performance comparison. Adapted with permission from [71]. Copyright 2023 IEEE. (a)  $N$  ranges from 10 to 1000. (b)  $N$  ranges from  $10^4$  to  $3 \times 10^6$ .

Although the active RIS has been studied in many applications, most of the existing work has focused on narrowband scenarios operating on a single carrier. However, in a wideband scenario, the amplitude and phase shift of the reflected signal depend on the frequency of the incident signal [130]. To address this issue, new device designs have been proposed to achieve wider bandwidths, as shown in Figure 33 [131]. For the passive RIS, integrating multiple phase shifters operating at different frequencies in each unit cell can independently reconfigure the phase shift for incident waves of different bands to achieve broadband characteristics [132]. However, since the power amplifiers in the active RIS

cannot be tuned independently for different frequencies, broadband characteristics can be achieved by integrating multiple amplification and phase shifters operating at different frequencies in each unit cell, as shown in Figure 34 [133].

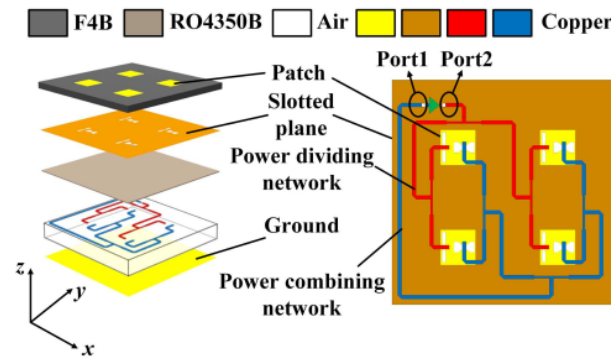


**Figure 33.** Broadband active RIS structure. Adapted with permission from [131]. Copyright 2022 IEEE.

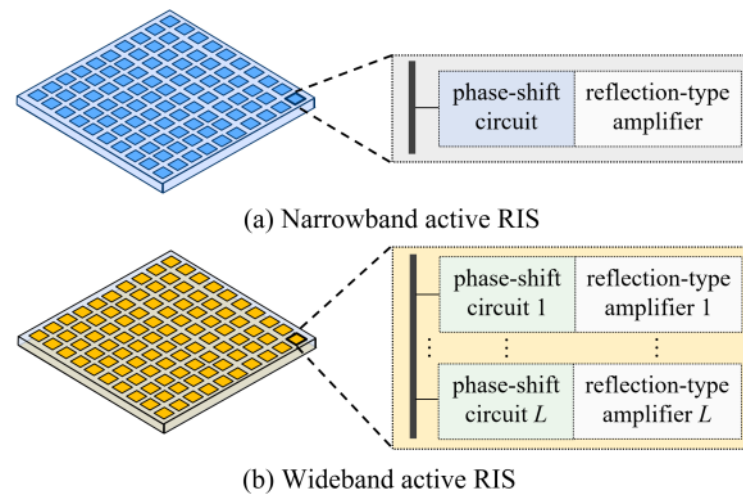


**Figure 34.** Narrowband vs. wideband active RIS structure comparison. Adapted with permission from [133]. Copyright 2023 IEEE.

Recently, hybrid RIS structures have been introduced to overcome the limitations of passive RISs, especially in poor transmission scenarios such as low signal-to-noise ratio (SNR) and/or severe path loss [134,135]. The core idea of hybrid RISs is to add a few active unit cells to the traditional passive RISs, which can simultaneously reflect and amplify the incident signal [136], as shown in Figure 35a. As a result, hybrid RISs can reduce the impact of redundant path loss and significantly improve the system performance in terms of spectral efficiency [137], secrecy rate [138], energy harvesting [139], and reliability [140], as shown in Figure 35b. Spectral efficiency and energy efficiency are key requirements for 6G networks, and the active RIS introduces a new feature called signal amplification, which helps to improve spectral efficiency at the cost of higher power consumption and hardware cost [141]. Therefore, hybrid RISs should flexibly determine the number of active and passive unit cells to maximize energy efficiency.

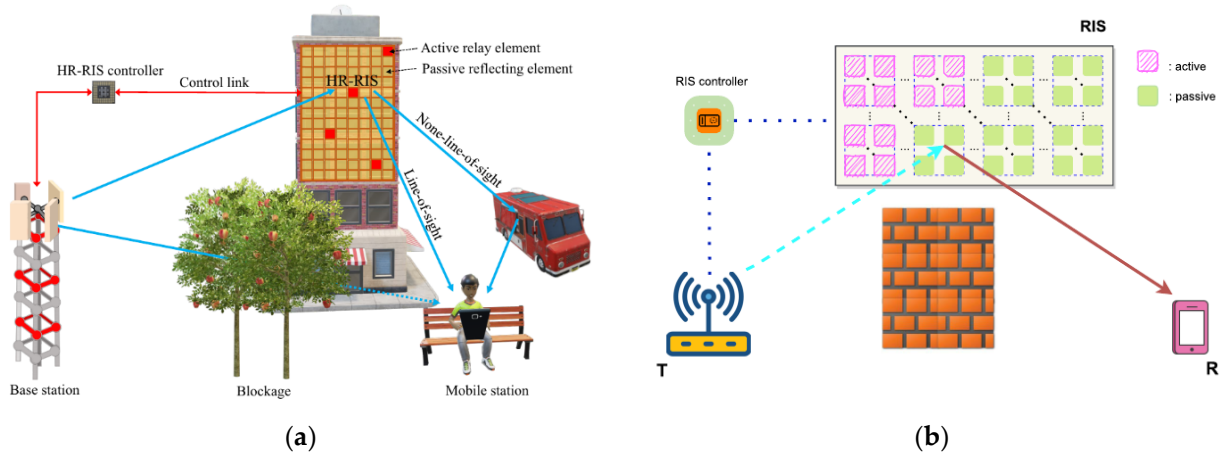


**Figure 35.** Hybrid RIS. (a) Hybrid relay–RIS structure [136]. (b) Hybrid RIS structure. Adapted with permission from [140]. Copyright 2022 IEEE.

### 2.8. Noise and Power in RIS

Due to the passive operation mechanism of the RIS, the noise power introduced by the RIS is very low, and many studies on RISs have assumed that the noise power of the RIS is negligible. However, since the radiating elements of the RIS unit cell are mostly patch antennas, the RIS actually generates noise [142]. Regardless of whether the RIS is passive or not, as long as the temperature is not absolute zero, the Brownian motion of the electrons is naturally present and thus noise is generated. The Johnson–Nyquist noise states that the noise power introduced into each device  $p_n$  is not lower than the theoretical limit of  $p_n = kT_pB$ , which is the product of the Boltzmann constant  $k = 1.3807 \times 10^{23} \text{ JK}^{-1}$ , the operating bandwidth  $B$ , and the thermal noise temperature  $T_p$ , with a standard value of 290 K [142]. The  $SNR_0$  input to the receiver through the antenna is given by Equation (1), where  $\eta_r$  is the radiation efficiency,  $\tau$  is the mismatch loss,  $S_i$  is the input signal,  $T_r$  is the noise temperature of the receiver, and  $T_a$  is the noise temperature of the antenna [143].

$$SNR_0 = \frac{\tau\eta_r S_i}{kB(\tau\eta_r T_a + \tau(1 - \eta_r)T_p + T_r)} \quad (1)$$

It can be seen from Equation (1) that if the RIS has sufficient directivity and gain, the signal power is sufficiently greater than the internal noise plus  $kT_pB$ . However, if the noise power due to low radiation efficiency, mismatch losses, etc. is greater than that, the output signal-to-noise ratio,  $SNR_0$ , through the RIS will decrease. In fact, the noise power introduced into each unit cell due to system noise is higher. For example, a passive reflector operating at an operating frequency of 915 MHz and a 250 kHz subcarrier has a noise power of about  $-107 \text{ dBm}$ , which is well above the natural lower bound [143]. If an RIS with a 100 MHz operating bandwidth has 10,000 unit cells, the noise power of the RIS can be estimated to be at least  $-54 \text{ dBm}$ . If the path loss of the RIS–receiver link is  $-30 \text{ dB}$ , the noise power at the receiver will be  $-84 \text{ dBm}$ , which is not small compared to the original noise power of the receiver [126]. In this case, when the number of RIS unit cells becomes large enough, the total noise at the receiver is gradually dominated by the noise introduced by the RIS, which becomes non-negligible and adversely affects the channel capacity [144].

As the RIS passively reflects the incident signal without high-power components such as power amplifiers and ADC/DACs, it consumes nearly zero power to realize phase shifting compared to conventional techniques such as massive MIMO and relays [144]. Therefore, the RIS is expected to significantly reduce the power consumption required for future 6G communications [105]. However, because hardware power is required to drive and reconfigure the RIS [105], the energy consumption may be higher than expected when the RIS is used in a real-world environment. For example, the power consumption

to drive an RIS with 1600 1-bit unit cells has been measured to be about 11.2 W [145]. In addition, reconfiguring the RIS requires additional power to support the RIS controller and transmit control signals, and realizing beamforming of the RIS requires additional power for channel estimation, channel feedback, and beamforming design. Therefore, the total power consumption generated by the RIS installation may not be low, and it is necessary to study the RIS with low-power structure and corresponding transmission methods to achieve energy efficiency in future 6G networks.

In 2019, in [105], the authors presented two computationally efficient energy efficiency (EE) maximization algorithms for BS transmit power allocation and RIS reflector values to show the total power consumption model of RIS-based MISO systems to help solve the EE maximization problem for active and passive beamforming designs. Based on the power consumption of conventional phase shifters, the authors in [105] argued that the RIS power consumption depends on the number of RIS unit cells and the resolution of individual unit cells. The power consumption of the RIS is then modeled as  $P_{RIS} = NP_N(b)$ , where  $N$  is the number of identical RIS unit cells and  $P_N(b)$  represents the power consumption of each RIS unit cell with a resolution of  $b$  bits [146]. However, both the power consumption of the control circuit and the impact of unit cell coding on power consumption are not considered, and the specific relationship between  $b$  and power consumption is not clearly presented. In [147], the authors developed a total power consumption model that further considers the process and power consumption of CSI estimation and feedback compared to [105]. Nevertheless, this study still mainly focuses on solving the optimization problems of phase-shifting design, system transmission, and reception, channel estimation, and feedback of the RIS, and does not address the power consumption model of the RIS in detail. Specific measurements of the RIS power consumption are mentioned in [42,79]. The authors of [42] show measurements of the RIS power consumption, indicating that different types of RISs have different power consumption characteristics. Varactor diode-based RISs have near-zero power consumption because they are driven by a reverse bias voltage; therefore, the varactor diode current in the unit cell during operation is negligible. The power consumption of a PIN diode-based RIS is related to the state of the unit cell, where the phase shift of each unit cell can be adjusted between 0 and  $\pi$  by electrically controlling the "ON" and "OFF" states of the PIN diodes. When all the diodes are in the "OFF" state, the current output from the DC voltage source is negligible; conversely, when a 0.7 V voltage signal is provided, all the diodes are in the "ON" state, which was measured to be 0.8 A for a size  $50 \times 34$  RIS in [42]. This indicates that the power consumption of each unit cell in the "ON" state is 0.33 mW. In practice, the controller providing control signals to the RIS also consumes energy, and the power consumption is related to the circuit design of the controller and the number of control signals output. The power consumption of a designed controller for a small RIS of size  $8 \times 32$  operating at 4.2 GHz was measured to be about 0.72 W, while the power consumption of a controller for a large RIS of size  $50 \times 34$  operating at 10.5 GHz was measured to be about 10 W [42]. The power consumption of a fabricated varactor diode-based RIS is discussed in [79]. Excluding the fabricated RIS board, the authors report that the FPGA control board using the Xilinx ZYNQ7100 consumes 1.5 W, and that the overall power consumption can be reduced to 1 W or less by using a low-power microcontroller rather than an FPGA. In the case of an FPGA control board with a built-in FPGA XC7K70T, which is often used as an RIS control board, the current is measured to be 0.2 A when the operating voltage is 24 V; therefore, the control board power consumption is  $P_c = 4.8$  W. This kind of RIS consumes very little power and shows the great potential of the RIS for future communication systems.

The power consumed by the RIS system can be divided into the dynamic power consumption  $P_d$ , which is consumed by the RIS unit cell, and the static power consumption  $P_s$ , which is the sum of the respective power consumption  $P_c$  and  $P_{td}$  of the control board and drive circuits that comprise the RIS controller, as shown in Figure 36a. Therefore, the total power consumed by the RIS system can be found as  $P_{total} = P_d + P_s = P_d + (P_c + P_{td})$ .

The power consumption classification for the PIN diode, varactor, and RF switch-based RIS is shown in Figure 36. Since different RISs use different types of drive circuits, the total drive circuitry is related to the type of reconfigurable components. For example, a PIN diode-based RIS unit cell can be driven by a shift register. A varactor diode-based RIS unit cell can be driven by a DAC and operational amplifier (OP Amp), PWM signal, and level regulator, or CMOS logic circuit, while an RF switch-based RIS unit cell can be driven by an FPGA and shift register. Furthermore, the drive circuit power consumption is related to the number of control signals. Specifically, it is related to the number of reconfigurable components  $N_c$  and the control degrees of freedom of the RIS (unit cell control, row control, column control, sub-array control). RIS unit cells divided into the same group can use the same control signal, and  $N_g$  represents the number of RIS unit cells in the same group with the same control signal.  $N_s$  is the number of control signals generated with each driving circuit. The static power consumption relationship for each reconfiguration scheme is shown in the equation below [148].

$$P_s = P_c + P_{td} = \begin{cases} P_c + \left[ \frac{\sum_{i=1}^N B_i}{N_g N_s} \right] P_d (PIN/Varactor) \\ P_c + \left[ \frac{N}{N_g N_s} \right] P_d (RF Switch) \end{cases} \quad (2)$$

Earlier, it was said that if the number of RIS unit cells grows infinitely, i.e., the area grows, the communication performance improvement effect of RIS increases; however, as the area grows, the overall power consumption of RIS increases, which eventually leads to higher RIS hardware power consumption. Therefore, it is necessary to optimize the relationship between the number of RIS unit cells, performance, and power consumption. Table 7 shows a comparison of the power consumption of the control circuit according to the reconfiguration method.

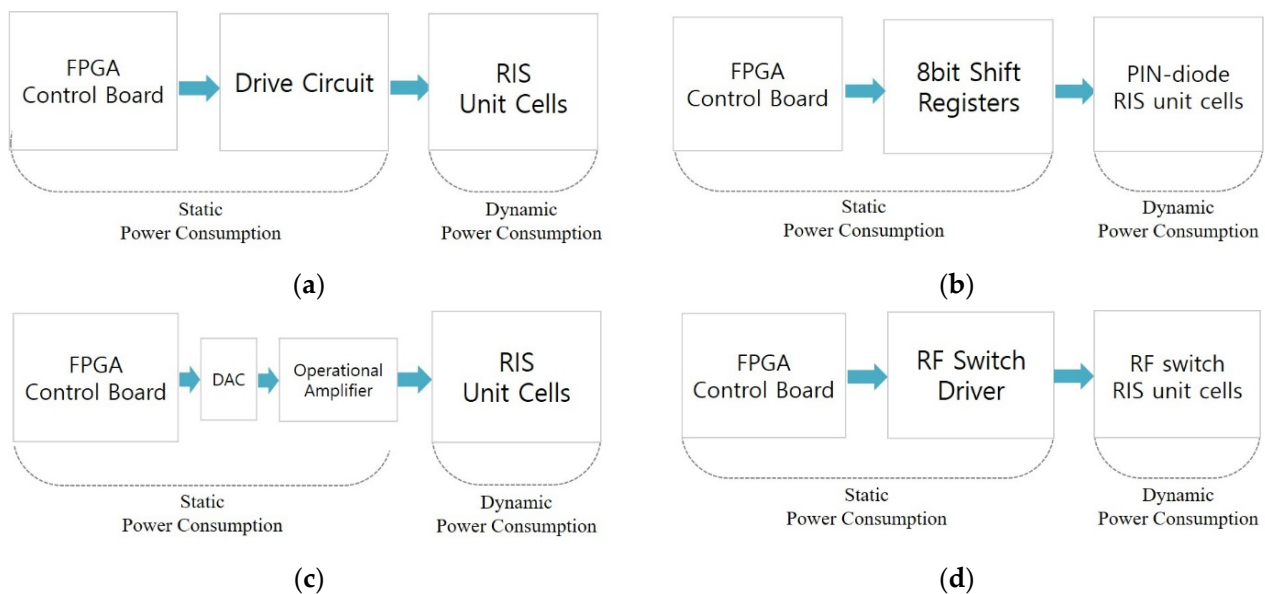


**Figure 36.** Power consumption of RIS [148]. (a) Typical RIS power consumption. (b) PIN diode-based RIS power consumption. (c) Varactor diode-based RIS power consumption. (d) RF switch-based RIS power consumption.

**Table 7.** Control circuit power consumption for each reconfiguration technique.

	PIN Diode [148]	Varactor Diode [149]	RF Switch [99]
Operating frequency	3.5 GHz	3.2 GHz	5.3 GHz
RIS size	16 × 16 (8 × 8 sub)	8 × 16	8 × 8
Control	FPGA + 8-bit shift register	DAC(DAC3484) + OP Amp (AD8021)	FPGA XC3S400AN
$P_c$	4.8 W	4.8 W	4.8 W
$P_d$	0.066 mW $V_{cc} = 3.3 \text{ V}, I_{cc} = 20 \text{ } \mu\text{A}$	430 mW (250 mW + 180 mW) $V_{cc} = \pm 12 \text{ V}, I_{cc} = 7.5 \text{ mA}$	240 mW $V_{cc} = 12 \text{ V}, I_{cc} = 20 \text{ mA}$
$P_{td}$	2.112 mW	1720 mW	240 mW
Parameters	$N_c = 256, N_g = 1,$ $N_s = 8, N_{dc} = 32$	$N_c = 256, N_g = 32,$ $N_s = 1, N_{dc} = 4$	$N_c = 64, N_g = 1,$ $N_s = 75, N_{dc} = 1$

### 3. RIS Field Trials

#### 3.1. RIS Performance Evaluation Parameters [28]

##### 3.1.1. Rate/Throughput

The first consideration in RIS performance evaluation is data throughput, which should be considered from the user and system perspectives. From the user perspective, user throughput is defined as the number of correctly received bits, i.e., the number of bits contained in the Service Data Unit (SDU) sent to Layer 3, and averaged over a period of time. In an RIS-enabled system, correctly received bits may be received directly from the BS/user in the case of DL/UL, or from RIS, or a combination thereof. If the total bandwidth is aggregated across multiple bands (one or more transmission and reception point (TRxPs) layers), the user throughput is summed across bands. From a system perspective, system throughput is the total throughput of all users.

##### 3.1.2. Spectral Efficiency

Spectral efficiency is the total throughput of all users divided by the channel bandwidth of a given band divided by the number of TRxPs and is measured in bit/s/Hz/TRxP. The channel bandwidth for this purpose is defined as the effective bandwidth multiplied by the frequency reuse factor, where the effective bandwidth is the operating bandwidth appropriately normalized to account for the uplink/downlink ratio.

##### 3.1.3. Coverage

Coverage is defined as the area where more than  $X\%$  of users can achieve user throughput  $R$ . For example, coverage is often defined as the area where at least 95% of users have a throughput of 1 Mbps or higher.

##### 3.1.4. Energy Efficiency

Network energy efficiency is the ability of an RIS-enabled system to minimize wireless access network energy consumption in relation to the amount of traffic served. Device energy efficiency is the ability of the RIS-enabled system to minimize the power consumed by the device modem in relation to the traffic characteristics. RIS energy efficiency is a measure of the RIS energy consumption associated with supporting the transmission of traffic from the transmitter to the receiver. The energy efficiency of a network, device, and RIS can be related to its support for two aspects, as follows:

- Efficient data transfer under load: Efficient data transfer under load is characterized by spectral efficiency as defined above.
- Low energy consumption in the absence of data: Low energy consumption in the absence of data can be estimated by the sleep ratio. The sleep ratio is the percentage of the time resource (in the case of a network) or sleep time (in the case of a device or RIS) that is unoccupied for a period corresponding to a control signal cycle (in the

case of a network) or a discontinuous receive cycle (in the case of a device or an RIS) when no user data transmission occurs.

### 3.1.5. Secrecy Rate

Secrecy rates play an important role in physical layer security. It is a metric that defines the rate at which a transmitted signal reaches a legitimate receiver without being intercepted by an eavesdropper. One definition of the secrecy rate is the non-negative difference between the capacity of the intended receiver and the capacity of the eavesdropper. Without precise knowledge of the eavesdropper's identity and channel, the secrecy rate for each receiver can be estimated by considering all legitimate but unintended terminals in the network as potential eavesdroppers.

Latency, reliability, and overhead can also be used as performance parameters for the RIS systems. In practice, there are several methods and techniques to measure or evaluate the performance metrics of RISs. The first is to use a System Level Simulator, a software tool that can model the behavior and performance of an RIS with different parameters and configurations in realistic scenarios such as urban or rural environments [149–151]. The second is to measure parameters that can characterize the characteristics and capabilities of the RIS, such as the reflection coefficient, phase shift, polarization, and scattering of the RIS. The third is to analyze the integration performance using a mathematical framework that can derive analytical expressions for the performance metrics of RISs in different channel models [152–155].

## 3.2. Field Test Reviews

In November 2021, NTT and NTT Docomo announced the world's first use of 5G base stations and RIS metasurface reflectors in the 28 GHz band to improve indoor communications by dynamically changing the direction of radio waves as mobile devices move in an indoor environment [156]. NTT's reflection control technology dynamically controls the direction of reflection based on the movement of the receiving device, and is applied to the millimeter-wave RIS reflector device developed by AGC Inc. (Tokyo, Japan) to create an indoor mobile environment that enables the use of high-frequency bands for 5G and next-generation mobile communications. The test was conducted at NTT Yokosuka R&D Center in Japan from October 8 to 22 with the measurement setup shown in Figure 37. Docomo designed the indoor network and operated the base station. The tests confirmed that the RIS reflector improves the strength of the signal received by the moving receiver. Radio waves from a remote base station entered the test room through a window, and the RIS was used to control the direction of reflection. From the measurements in Figure 38, the strength of the received 28 GHz signal was improved by up to 20 dB compared to the signal received without the RIS.

In China, China Mobile conducted the world's first field trial for RIS application in the urban area of Nanjing to investigate the practical performance of coverage improvement in 5G commercial mobile networks [157]. A  $32 \times 16$  (1.6 m  $\times$  0.8 m) RIS with a phase resolution of 1 bit in each unit cell and independently programmable was introduced and utilized in the field trial, as shown in Figure 39. In addition, three common under-coverage scenarios, known as under tower shadow zone, indoor shadow zone, and outdoor building shadow zone, were selected as test sites to verify the improvement capabilities of the RIS, as shown in Figure 40. The measurement results confirm that the application of the RIS can significantly improve the communication quality for users in current 5G commercial mobile networks. In the shadow zone under the building, deploying the RIS increased the reference signal receiving power (RSRP) of the user at the edge of the cell by 4.03 dB and the average RSRP by 3.8 dB, and the average throughput of the user increased from 91.50 Mbps to 109 Mbps, which is an improvement of about 19%. In indoor shadow zone, most test locations, including meeting rooms, offices, and supermarkets, showed significant improvements, with average gains of 9.9 dB in RSRP, 2.87 dB in signal-to-interference-plus-noise ratio (SINR), and 78.61 Mbps in throughput. However, testing in the studio

did not show any significant improvement with the deployment of the RIS, which may be due to the limited beamwidth of the RIS reflector beam not being able to reach the area, indicating that it may be necessary to deploy the RIS inside the building. With respect to the shaded area at the outdoor of the building, gains of 3.3 dB, 1.45 dB, and 79 Mbps in the RSRP, SINR, and throughput were observed, respectively, when the RIS was placed in the area where the RSRP was lower than  $-90$  dBm [157]. Figure 41 shows the comparative performance of the RSRP, SINR, and throughput with and without the RIS in the shadowed area under the building and the shadowed area behind the building. The significance of these experimental results is that the aRIS was tested using a working 5G base station. Since the RIS with a 1-bit phase resolution used in the experiment can generate non-negligible sidelobes when performing beamforming, causing electromagnetic pollution, signal interference, and energy consumption, higher performance improvements can be achieved through joint optimization of the BS, RIS, and UE.

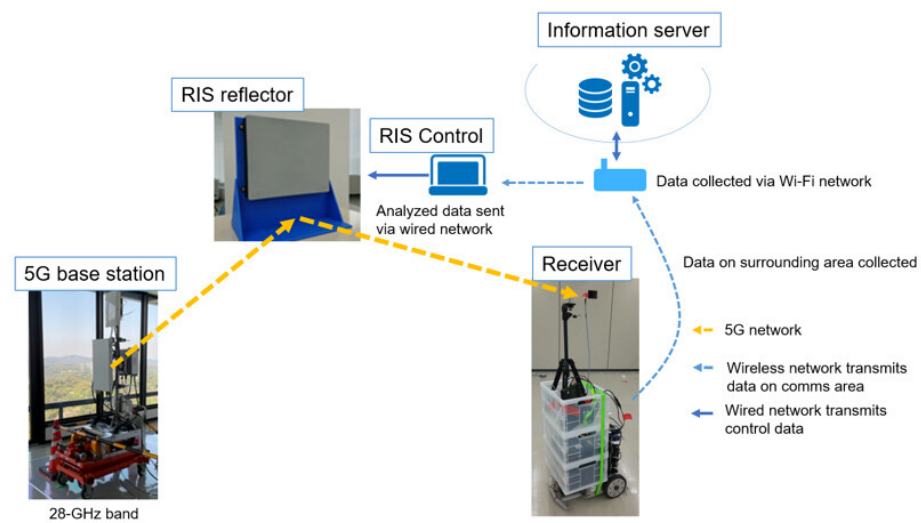


Figure 37. Testbeds for RIS system evaluation [156].

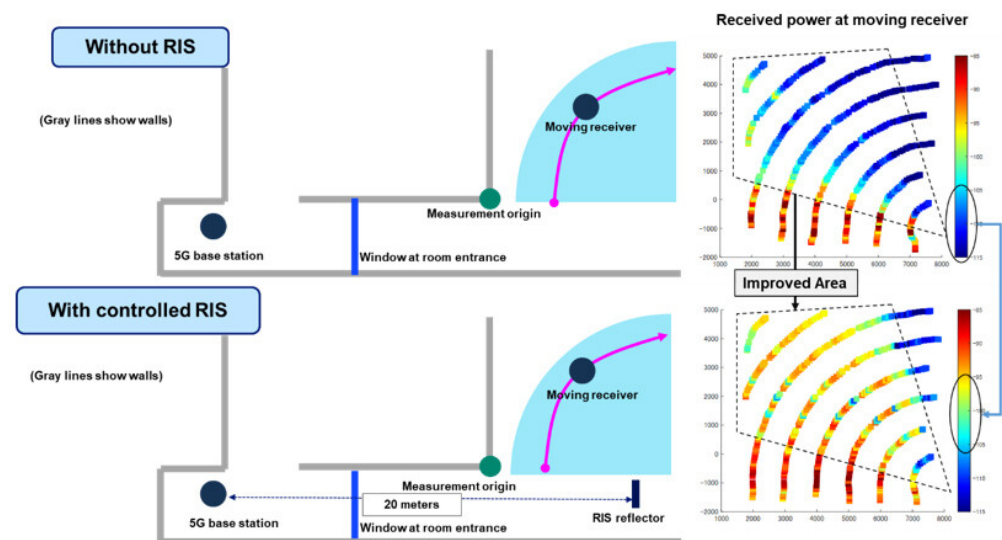


Figure 38. Received signal strength of the received 28 GHz signal with and without RIS [156].

In [158], various RIS prototypes were designed and fabricated, including 1-bit single-polarization, 1-bit dual-polarization, 1.5-bit single-polarization, 2-bit dual-polarization, and 4-bit dual-polarization panels (as shown in Figure 42) with dimensions of  $20 \times 20$ ,  $32 \times 32$ , or  $64 \times 64$  and operating at 2.6 GHz, 4.9 GHz, or 26 GHz. Using commercial 5G UEs, 5G BSs, and reference signals defined in the 3GPP 5G standard, they conducted 26 GHz indoor OTA tests, 26 GHz outdoor tests, 2.6 GHz outdoor/indoor tests, 4.9 GHz outdoor/indoor tests, and 26 GHz outdoor/indoor tests, as shown in Figure 43. RSRP was used as the performance evaluation parameter, and the test results show that the RIS can increase RSRP by about 15 dB to 35 dB in various reception scenarios, depending on the detailed test settings and the RIS implementation, as shown in Table 8.

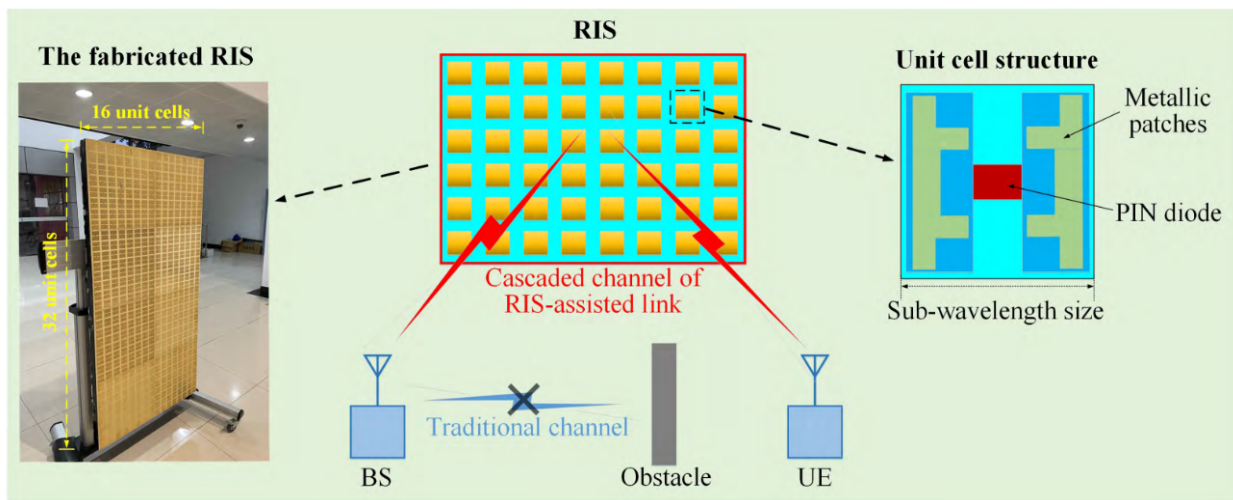


Figure 39. RIS used for testing. Adapted with permission from [157]. Copyright 2023 IEEE.

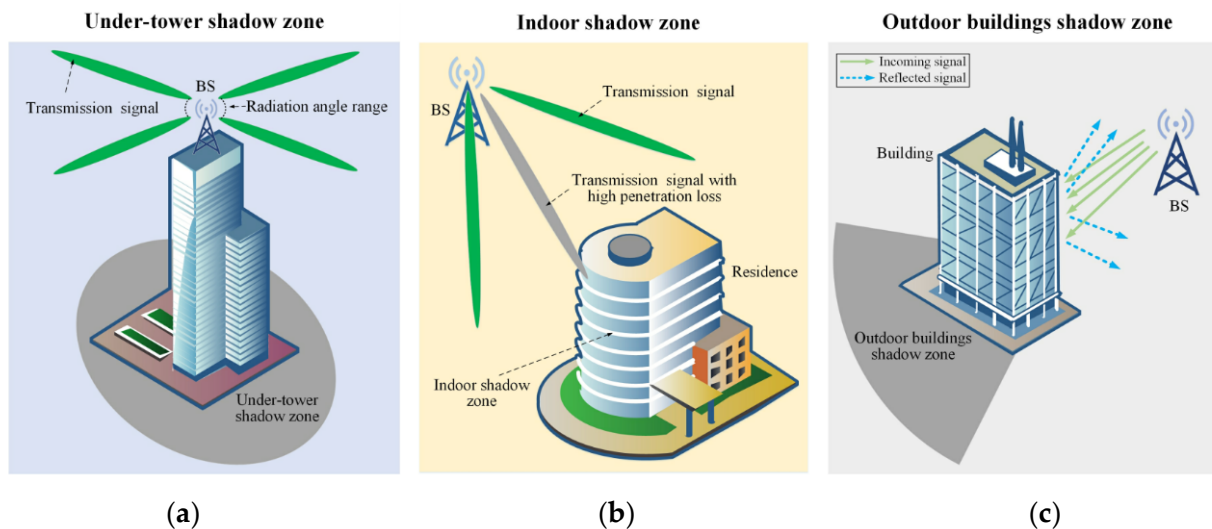
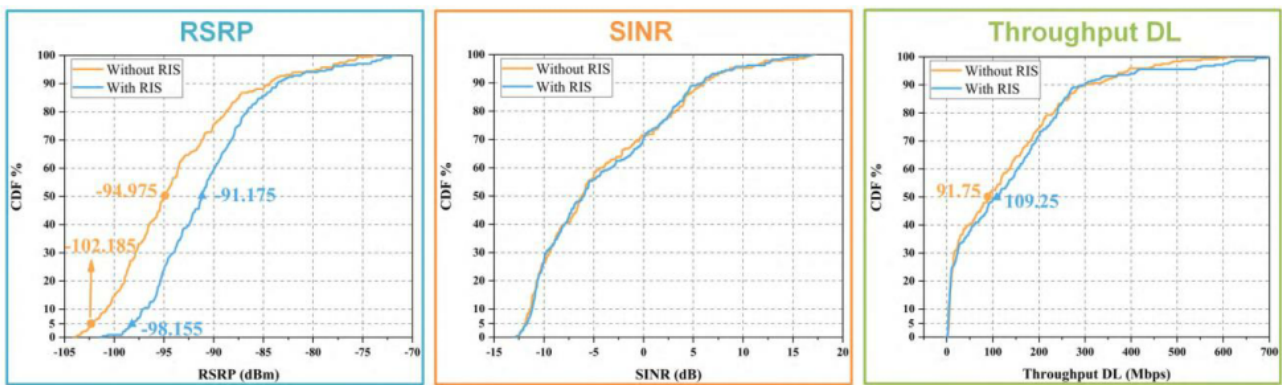
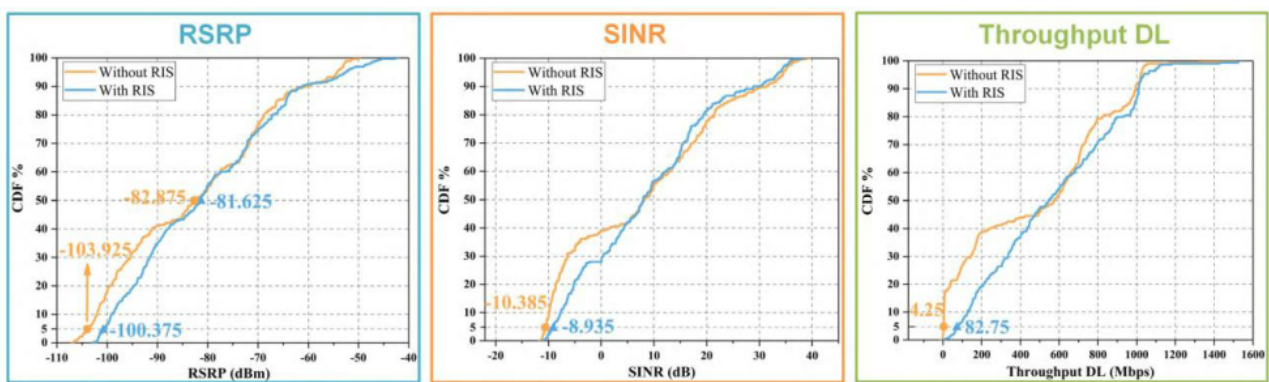


Figure 40. Three common under-coverage scenarios. (a) Under tower shadow zone. (b) Indoor shadow zone. (c) Outdoor building shadow zone. Adapted with permission from [157]. Copyright 2023 IEEE.



(a)



(b)

Figure 41. Communication performance in (a) shadow zone under tower shadow zone and (b) outdoor building shadow zone. Adapted with permission from [157]. Copyright 2023 IEEE.

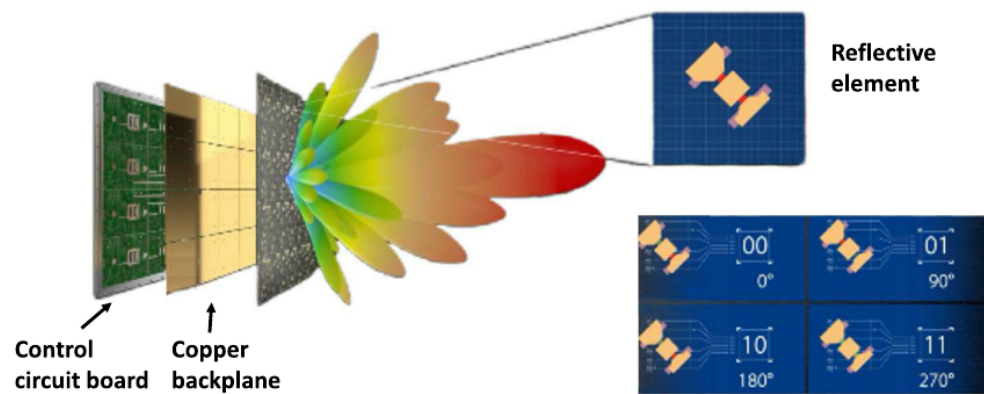


Figure 42. RIS used for testing [158].

Direct comparison with similar real-world RIS field trial work is difficult due to the large differences in operating environment, RIS size, and degrees of control freedom. As shown in Table 9, a common trend is the improvement in received signal strength as shown in each case.



(a)



(b)



(c)



(d)



(e)

**Figure 43.** (a) A 26 GHz indoor OTA test; (b) 26 GHz outdoor test; (c) 2.6 GHz outdoor/indoor test; (d) 4.9 GHz outdoor/indoor test; and (e) 26 GHz outdoor/indoor test. Adapted with permission from [158]. Copyright 2022 IEEE.

**Table 8.** Test results summary.

	Scenario #1	Scenario #2	Scenario #3	Scenario #4	Scenario #5
	Indoor	Outdoor	Outdoor/Indoor	Outdoor/Indoor	Outdoor/Indoor
Operation frequency	26 GHz	26 GHz	2.6 GHz (60 MHz)	4.9 GHz (100 MHz)	26 GHz (100 MHz)
RIS size	64 × 64	32 × 32	20 × 20 (1 m × 1 m)	32 × 32 (1 m × 1 m)	64 × 64
BS–RIS	20 m	120 m	206 m	145 m	45 m
RIS–UE	10 m	20 m	7 m	45 m	106 m
RSRP	1-bit single polarization 30 dB 4-bit double polarization	1-bit single polarization 30 dB	1.5-bit single polarization 15 dB	4-bit dual polarization 21 dB	1-bit dual polarization 12 dB
Data rate			DL: 275% UL: 200%	DL: 442% UL: 442%	

**Table 9.** Comparison of RIS field trial works at sub-6 GHz [159].

Ref.	Phase Resolution	Tuning Mechanism	Size No. of Elements	Frequency	Bandwidth	Scenarios	Effects on Channel Response
[79]	1-bit	Varactor	0.80 m × 0.31 m (15.5λ × 6λ) 1100 elements (55 × 20)	5.8 GHz	500 MHz	Indoor NLOS. Outdoor rooftops at 50 and 500 m.	27 dB@50 m. 14 dB@500 m. 26 dB@indoor via a thick concrete wall.
[160]	1-bit	PIN diodes	0.41 m × 0.26 m (7.9λ × 5λ) 160 elements (16 × 10)	5.8 GHz	150 MHz	Outdoor NLOS via large occlusion.	6 dB SNR improvement.
[77]	1-bit	RF switches	2.45 m × 2.45 m (19.6λ × 19.6λ) 3200 elements (64 × 50)	2.4 GHz	38 MHz	Indoor office environment with mixed LOS/NLOS.	Max 9.8 dB Doubling of channel capacity.
[161]	1-bit	PIN diodes	512 elements (16 × 32)	2.64 GHz	160 MHz	Indoor NLOS at a corridor junction.	10 dB/10 Mbps.
[68]	Continuous	Varactor	1.14 m × 1.16 m (13.3λ × 13.5λ) 2430 elements (30 × 81)	3.5 GHz	-	Indoor NLOS. Room to room wireless link.	15 dB.
[159]	3-bit	PIN diodes	1.02 m × 0.72 m (12.8λ × 9λ) 2304 elements (48 × 48)	3.75 GHz	1.5 GHz	Indoor mixed LOS/NLOS. Corridor junctions and multiple floors.	16 dB. Up to 40 dB in deep fading. Multi-floor 20 dB.

#### 4. Conclusions

It has been theoretically and experimentally studied that the RIS creates many potential opportunities and broad application prospects for improving the performance of communication shadow areas in B5G and future 6G networks. However, few studies have focused on the engineering aspects of the RIS-enabled wireless communication systems based on practical constraints and technical issues for real-world applications. Therefore, in this paper, the technical issues that need to be considered for the practical implementation of an RIS, such as the standardization of an RIS, types of RISs according to operation modes,

channel modeling, considerations for hardware implementation, differences with existing communication modules and the need to implement active RISs, noise and power characteristics to ensure the efficiency of RISs, etc. are discussed. In addition, the performance parameters of an RIS system and the results of field tests of an RIS in indoor and outdoor environments are presented.

The choice of which type of RIS to select depends on the requirements of the deployment scenario of the RIS. If the RIS is used outdoors, it seems that various types of configurations such as passive/active, reflective/transmissive, etc. are possible. However, in the case of a passive RIS, a review of the management entity is required because it is not an operator-oriented structure; in the case of an active RIS, the implementation of CSI on the service operator side will be essential. Therefore, a mixed RIS structure in which only some of the cells of the total unit cells comprising the RIS have sensor functions for CSI, or only some of the cells have an active structure, is expected to be the ultimate solution. In addition, since the RIS is located outdoors, it is necessary to consider securing publicity, such as an alliance between operators or government initiative to overcome the same problems of environmental pollution and duplicate investment that occurred in the existing individual base station installation by implementing a different RIS for each operator. In the case of O2I, where the base station of the RIS is located outdoors and the user is indoors, the RIS can be used as a transmissive type in the windows of buildings, etc. Therefore, an RIS structure with transmissive characteristics and a transparent RIS for the use in windows are required. Therefore, in this case, the RIS requires a reconfigurable structure with transparent unit cells. Among the current research results, the most favorable structure in terms of transparency is the reconstructed structure using VO2. In the case of the transparent RIS using metal mesh with a PIN, varactor, or RF switch, even though the overall light transmittance is high, the RIS is difficult to use due to the opacity of the lumped elements. If the RIS is located indoors, it should be used to improve performance against external electromagnetic signals from windows and other sources, so that the RIS can be used as a passive or active reflective structure. As mentioned earlier, the passive type has a fixed reflection angle and can only be used in certain scenarios, and the RIS must be constructed face-to-face for it to be effective. In the case of a passive RIS, the management entity will need to be a government, building owner, or a coalition of operators because it is operated independently of the operator. In the case of an active RIS used indoors, among the currently proposed technologies, a lumped device-based RIS with a PIN or varactor seems to be advantageous in terms of technical maturity. However, there are problems with it such as the price required for circuit configuration and the implementation of CSI technology for the RIS operation that is limited by the operator. Therefore, the recently researched liquid crystal-based RIS seems to be a promising alternative due to its price competitiveness and the use of TFT technology already perfected in the display industry; however, its disadvantage is that it is only available in millimeter-wave and higher frequency bands, and it is necessary to continue research on issues such as overcoming technical limitations on slow switching times.

The commercialization of the RIS to enable B5G/6G communications requires, first, the identification of killer applications to ensure commercial viability for a complex multi-panel RIS and/or multi-user scenarios and to identify industry verticals that show the greatest benefit in terms of return on investment. Second, it requires sensing and network transmission technologies, including those related to channel modeling, channel estimation, and feedback techniques to maintain and improve the quality of communication services. Third, there is a need for concerted standardization efforts and broad consensus to determine appropriate channel models, waveforms, control signals, and performance requirements, considering possible spectrum, technology, and test solutions. Finally, there is a need to improve unit cell designs that consider characteristics such as wideband and low loss, and fabrication techniques to make the RIS more reliable and affordable, considering manufacturing costs, power consumption, and network control protocol overhead.

**Funding:** This work was supported in part by the Basic Science Research Program under Grant 2020R111A3057142 and in part by the Priority Research Center Program through the National Research Foundation under Grant 2019R1A6A1A03032988.

**Data Availability Statement:** Not applicable.

**Conflicts of Interest:** The author declares no conflict of interest.

## References

- Liu, Y.; Liu, X.; Mu, X.; Hou, T.; Xu, J.; Di Renzo, M.; Al-Dhahir, N. Reconfigurable intelligent surfaces: Principles and opportunities. *IEEE Commun. Surv. Tutor.* **2021**, *23*, 1546–1577. [CrossRef]
- Wu, Q.; Zhang, R. Towards smart and reconfigurable environment: Intelligent reflecting surface aided wireless network. *IEEE Commun. Mag.* **2020**, *58*, 106–112. [CrossRef]
- Liaskos, C.; Nie, S.; Tsioliariidou, A.; Pitsillides, A.; Ioannidis, S.; Akyildiz, I. A new wireless communication paradigm through software-controlled metasurfaces. *IEEE Commun. Mag.* **2018**, *56*, 162–169. [CrossRef]
- Hu, S.; Rusek, F.; Edfors, O. Beyond massive MIMO: The potential of data transmission with large intelligent surfaces. *IEEE Trans. Signal Process.* **2018**, *66*, 2746–2758. [CrossRef]
- Glybovski, S.B.; Tretyakov, S.A.; Belov, P.A.; Kivshar, Y.S.; Simovski, C.R. Metasurfaces: From microwaves to visible. *Phys. Rep.* **2016**, *634*, 1–72. [CrossRef]
- Smith, D.R.; Pendry, J.B.; Wiltshire, M.C.K. Metamaterials and negative refractive index. *Science* **2004**, *305*, 788–792. [CrossRef]
- Hong, I.-P. Review of antenna technology using metasurfaces. *Electromagn. Tech. KIEES* **2022**, *33*, 20–53.
- Yu, N.F.; Genevet, P.; Kats, M.A.; Aieta, F.; Tetienne, J.P.; Capasso, F.; Gaburro, Z. Light propagation with phase discontinuities: Generalized laws of reflection and refraction. *Science* **2011**, *334*, 333–337. [CrossRef] [PubMed]
- Hu, J.; Bandyopadhyay, S.; Liu, Y.-h.; Shao, L.-y. A review on metasurface: From principle to smart metadevices. *Front. Phys.* **2021**, *8*, 586087. [CrossRef]
- Kamoda, H.; Iwasaki, T.; Tsumochi, J.; Kuki, T.; Hashimoto, O. 60-GHz electronically reconfigurable large reflectarray using single-bit phase shifters. *IEEE Trans. Antennas Propag.* **2011**, *59*, 2524–2531. [CrossRef]
- Cui, T.J.; Qi, M.Q.; Wan, X.; Zhao, J.; Cheng, Q. Coding metamaterials, digital metamaterials and programmable metamaterials. *Light Sci. Appl.* **2014**, *3*, e218. [CrossRef]
- Subrt, L.; Pechac, P. Controlling propagation environments using intelligent walls. In Proceedings of the 2012 6th European Conference on Antennas and Propagation (EUCAP), Prague, Czech Republic, 26–30 March 2012.
- Kaina, N.; Dupré, M.; Lerosey, G.; Fink, M. Shaping complex microwave fields in reverberating media with binary tunable metasurfaces. *Sci. Rep.* **2014**, *4*, 6693. [CrossRef]
- Yang, H.; Cao, X.; Yang, F.; Gao, J.; Xu, S.; Li, M.; Chen, X.; Zhao, Y.; Zheng, Y.; Li, S. A programmable metasurface with dynamic polarization, scattering and focusing control. *Sci. Rep.* **2016**, *6*, 35692. [CrossRef] [PubMed]
- Tan, X.; Sun, Z.; Jornet, J.M.; Pados, D. Increasing indoor spectrum sharing capacity using smart reflect-array. In Proceedings of the 2016 IEEE International Conference on Communications (ICC), Kuala Lumpur, Malaysia, 22–27 May 2016.
- Renzo, M.D.; Debbah, M.; Phan-Huy, D.-T.; Zappone, A.; Alouini, M.-S.; Yuen, C.; Sciancalepore, V.; Alexandropoulos, G.C.; Hoydis, J.; Gacanin, H.; et al. Smart radio environments empowered by reconfigurable ai meta-surfaces: An idea whose time has come. *EURASIP J. Wirel. Commun. Netw.* **2019**, *129*, 1–20. [CrossRef]
- Liu, R. Key use cases and latest progress in prototyping, testing & standardization of RIS. In Proceedings of the IEEE Global Communications Conference, Madrid, Spain, 7–11 December 2021.
- Jian, M.; Liu, R.; Chen, Y. Standardization for reconfigurable intelligent surfaces: Progresses, challenges and the road ahead. In Proceedings of the 2021 IEEE/CIC International Conference on Communications in China (ICCC Workshops), Xiamen, China, 28–30 July 2021.
- Jiang, M.; Cezanne, J.; Sampath, A.; Shental, O.; Wu, Q.; Koymen, O.; Bedewy, A.; Li, J. Wireless fronthaul for 5G and future radio access networks: Challenges and enabling technologies. *IEEE Wirel. Commun.* **2022**, *29*, 108–114. [CrossRef]
- Wu, Q.; Zhang, S.; Zheng, B.; You, C.; Zhang, R. Intelligent reflecting surface-aided wireless communications: A tutorial. *IEEE Trans. Commun.* **2021**, *69*, 3313–3351. [CrossRef]
- Björnson, E.; Özdoğan, Ö.; Larsson, E.G. Reconfigurable intelligent surfaces: Three myths and two critical questions. *IEEE Commun. Mag.* **2020**, *58*, 90–96. [CrossRef]
- Liu, R.; Alexandropoulos, G.C.; Wu, Q.; Jian, M.; Liu, Y. How can reconfigurable intelligent surfaces drive 5G-advanced wireless networks: A standardization perspective. In Proceedings of the 2022 IEEE/CIC International Conference on Communications in China (ICCC Workshops), Foshan, China, 11–13 August 2022.
- Liu, R.; Wu, Q.; Di Renzo, M.; Yuan, Y. A path to smart radio environments: An industrial viewpoint on reconfigurable intelligent surfaces. *IEEE Wirel. Commun.* **2022**, *29*, 202–208. [CrossRef]
- IEEE Communications Society Reconfigurable Intelligent Surfaces Emerging Technology Initiative—Reconfigurable Intelligent Surfaces Emerging Technology Initiative. Available online: <https://riseti.committees.comsoc.org/> (accessed on 8 October 2023).
- IEEE COMSOC WTC SIG RISE. Available online: <https://sites.google.com/view/ieee-comsoc-wtc-sig-rise> (accessed on 8 October 2023).

26. SIG on REconFigurabLE Intelligent Surfaces for Signal Processing and CommunicatiONS (REFLECTIONS)—IEEE Communications Society Signal Processing and Computing for Communications Technical Committee. Available online: <https://spcc.committees.comsoc.org/special-interest-groups/sig-reflections/> (accessed on 8 October 2023).
27. ETSI—Our Group Reconfigurable Intelligent Surface (RIS). Available online: <https://www.etsi.org/committee/1966-ris> (accessed on 8 October 2023).
28. ETSI GR RIS 003(V1.1.1). Reconfigurable Intelligent Surfaces (RIS); Communication Models, Channel Models, Channel Estimation and Evaluation Methodology. June 2023. Available online: [https://www.etsi.org/deliver/etsi\\_gr/RIS/001\\_099/003/01.01.01\\_60/gr\\_RIS003v010101p.pdf](https://www.etsi.org/deliver/etsi_gr/RIS/001_099/003/01.01.01_60/gr_RIS003v010101p.pdf) (accessed on 8 October 2023).
29. China Communications Standards Association. Meeting Detail of TC5 WG6 Meeting 55. September 2020. Available online: <https://www.ccsa.org.cn/meetingDetail/?id=91&title=TC5WG6%E7%AC%AC55%E6%AC%A1%E5%B7%A5%E4%BD%9C%E7%BB%84%E4%BC%9A%E8%AE%AE> (accessed on 8 October 2023).
30. FuTURE Forum | Home. Available online: <http://www.future-forum.org.cn/en/index.asp> (accessed on 8 October 2023).
31. Report ITU-R M.2516-0. Future Technology Trends of Terrestrial IMT Systems towards 2030 and beyond. November 2022; p. 93. Available online: [https://www.itu.int/dms\\_pub/itu-r/oth/0a/0e/R0A0E0000E80001PDFE.pdf](https://www.itu.int/dms_pub/itu-r/oth/0a/0e/R0A0E0000E80001PDFE.pdf) (accessed on 8 October 2023).
32. Yuan, Y.; Wu, D.; Huang, Y.; I, C.-L. Reconfigurable intelligent surface relay: Lessons of the past and strategies for its success. *IEEE Commun. Mag.* **2022**, *60*, 117–123. [[CrossRef](#)]
33. ZTE Corporation, Sanetchips. Support of Reconfigurable Intelligent Surface For 5G Advanced. March 2021. Available online: [https://www.3gpp.org/ftp/TSG\\_RAN/TSG\\_RAN/TSGR\\_91e/Docs/RP-210618.zip](https://www.3gpp.org/ftp/TSG_RAN/TSG_RAN/TSGR_91e/Docs/RP-210618.zip) (accessed on 8 October 2023).
34. ETSI GR RIS 001(V1.1.1). Reconfigurable Intelligent Surfaces (RIS); Use Cases, Deployment Scenarios and Requirements. April 2023. Available online: [https://etsi.org/deliver/etsi\\_gr/RIS/001\\_099/001/01.01.01\\_60/gr\\_RIS001v010101p.pdf](https://etsi.org/deliver/etsi_gr/RIS/001_099/001/01.01.01_60/gr_RIS001v010101p.pdf) (accessed on 8 October 2023).
35. Huang, J.; Wang, C.X.; Sun, Y.; Feng, R.; Huang, J.; Guo, B.; Zhong, Z.; Cui, T.J. Reconfigurable intelligent surfaces: Channel characterization and modeling. *Proc. IEEE* **2022**, *110*, 1290–1311. [[CrossRef](#)]
36. ETSI TR 138 901 (V16.1.0). 5G; Study on Channel Model for Frequencies from 0.5 to 100 GHz (3GPP TR 38.901 Version 16.1.0 Release 16). November 2022. Available online: [https://www.etsi.org/deliver/etsi\\_tr/138900\\_138999/138901/16.01.00\\_60/tr\\_138901v160100p.pdf](https://www.etsi.org/deliver/etsi_tr/138900_138999/138901/16.01.00_60/tr_138901v160100p.pdf) (accessed on 8 October 2023).
37. Yildirim, I.; Basar, E. Channel modelling in RIS-empowered wireless communications. In *Intelligent Reconfigurable Surfaces (IRS) for Prospective 6G Wireless Networks*; Wiley: Hoboken, NJ, USA, 2022; pp. 123–148. [[CrossRef](#)]
38. Di Renzo, M.; Danufane, F.H.; Xi, X.; De Rosny, J.; Tretyakov, S. Analytical modeling of the path-loss for reconfigurable intelligent surfaces—Anomalous mirror or scatterer? In *Proceedings of the 2020 IEEE 21st International Workshop on Signal Processing Advances in Wireless Communications (SPAWC)*, Atlanta, GA, USA, 26–29 May 2020.
39. Bartoli, G.; Abrardo, A.; Decarli, N.; Dardari, D.; Di Renzo, M. Spatial multiplexing in near field MIMO channels with reconfigurable intelligent surfaces. *IET Signal Process.* **2023**, *17*, e12195. [[CrossRef](#)]
40. Ellingson, S.W. Path loss in reconfigurable intelligent surface-enabled channels. In *Proceedings of the 2021 IEEE 32nd Annual International Symposium on Personal, Indoor and Mobile Radio Communications (PIMRC)*, Helsinki, Finland, 13–16 September 2021.
41. Özdoğan, Ö.; Björnson, E.; Larsson, E.G. Intelligent reflecting surfaces: Physics, propagation, and pathloss modeling. *IEEE Wirel. Commun. Lett.* **2019**, *9*, 581–585. [[CrossRef](#)]
42. Tang, W.; Chen, M.; Chen, X. Wireless communications with reconfigurable intelligent surface: Path loss modeling and experimental measurement. *IEEE Trans. Wirel. Commun.* **2021**, *20*, 421–439. [[CrossRef](#)]
43. Danufane, F.H.; Renzo, M.; de Rosny, J.; Tretyakov, S. On the path-loss of reconfigurable intelligent surfaces: An approach based on green’s theorem applied to vector fields. *IEEE Trans. Commun.* **2021**, *69*, 5573–5592. [[CrossRef](#)]
44. Björnson, E.; Sanguinetti, L. Power scaling laws and near-field behaviors of massive MIMO and intelligent reflecting surfaces. *IEEE Open J. Commun. Soc.* **2020**, *1*, 1306–1324. [[CrossRef](#)]
45. Zhi, K.; Pan, C.; Ren, H.; Wang, K. Power scaling law analysis and phase shift optimization of RIS-aided massive MIMO systems with statistical CSI. *IEEE Trans. Commun.* **2022**, *70*, 3558–3574. [[CrossRef](#)]
46. Gradoni, G.; Di Renzo, M. End-to-end mutual coupling aware communication model for reconfigurable intelligent surfaces: An electromagnetic-compliant approach based on mutual impedances. *IEEE Wirel. Commun. Lett.* **2021**, *10*, 938–942. [[CrossRef](#)]
47. Sun, Y.; Wang, C.; Huang, J.; Wang, J. A 3D non-stationary channel model for 6G wireless systems employing intelligent reflecting surfaces with practical phase shifts. *IEEE Trans. Cogn. Commun. Netw.* **2021**, *7*, 496–510. [[CrossRef](#)]
48. Jiang, H.; Ruan, C.; Zhang, Z.; Dang, J.; Wu, L.; Mukherjee, M.; da Costa, D.B. A general wideband non-stationary stochastic channel model for intelligent reflecting surface-assisted MIMO communications. *IEEE Trans. Wirel. Commun.* **2021**, *20*, 5314–5328. [[CrossRef](#)]
49. Basar, E.; Yildirim, I. Reconfigurable intelligent surfaces for future wireless networks: A channel modeling perspective. *IEEE Wirel. Commun.* **2021**, *28*, 108–114. [[CrossRef](#)]
50. Basar, E.; Yildirim, I.; Kilinc, F. Indoor and outdoor physical channel modeling and efficient positioning for reconfigurable intelligent surfaces in mmWave bands. *IEEE Trans. Commun.* **2021**, *69*, 8600–8611. [[CrossRef](#)]

51. Kilinc, F.; Yildirim, I.; Basar, E. Physical channel modeling for RIS-empowered wireless networks in sub-6 GHz bands. In Proceedings of the 2021 55th Asilomar Conference on Signals, Systems, and Computers, Pacific Grove, CA, USA, 31 October–3 November 2021.
52. Faqiri, R.; Saigre-Tardif, C.; Alexandropoulos, G.C.; Shlezinger, N.; Imani, M.F.; Del Hougne, P. PhysFad: Physics-based end-to-end channel modeling of RIS-parametrized environments with adjustable fading. *IEEE Trans. Wirel. Commun.* **2022**, *22*, 580–595. [[CrossRef](#)]
53. Van Tuan, P.; Hong, I.P. IRS-aided wireless communication: From physics to channel modeling and characterization. *IEEE Access* **2023**, *11*, 3184–3197. [[CrossRef](#)]
54. Gong, H.; Zhang, J.; Zhang, Y.; Zhou, Z.; Pan, J.; Liu, G. How to Extend 3D GBSM Model to RIS Cascade Channel with Non-ideal Phase Modulation? *arXiv* **2023**, arXiv:2302.07501.
55. Rana, B.; Cho, S.S.; Hong, I.P. Review paper on hardware of reconfigurable intelligent surfaces. *IEEE Access* **2023**, *11*, 29614–29634. [[CrossRef](#)]
56. Hum, S.V.; Perruisseau-Carrier, J. Reconfigurable reflectarrays and array lenses for dynamic antenna beam control: A review. *IEEE Trans. Antennas Propag.* **2014**, *62*, 183–198. [[CrossRef](#)]
57. Rodrigo, D.; Jofre, L.; Perruisseau-Carrier, J. Unit cell for frequency-tunable beamscanning reflectarrays. *IEEE Trans. Antennas Propag.* **2013**, *61*, 5992–5999. [[CrossRef](#)]
58. Saeed, T.; Soteriou, V.; Liaskos, C.; Pitsillides, A.; Lestas, M. Toward fault-tolerant deadlock-free routing in hypersurface-embedded controller networks. *IEEE Netw. Lett.* **2020**, *2*, 140–144. [[CrossRef](#)]
59. Rains, J.; Kazim, J.; Tukmanov, A.; Zhang, L.; Abbasi, Q.; Imran, M. Practical Design Considerations for Reconfigurable Intelligent Surfaces. In *Intelligent Reconfigurable Surfaces (IRS) for Prospective 6G Wireless Networks*; Wiley: Hoboken, NJ, USA, 2022; pp. 99–122. [[CrossRef](#)]
60. Elmossallamy, M.A.; Zhang, H.; Song, L.; Seddik, K.G.; Han, Z.; Li, G.Y. Reconfigurable intelligent surfaces for wireless communications: Principles, challenges, and opportunities. *IEEE Trans. Cogn. Commun. Netw.* **2020**, *6*, 990–1002. [[CrossRef](#)]
61. Jian, M.; Alexandropoulos, G.C.; Basar, E.; Huang, C.; Liu, R.; Liu, Y.; Yuen, C. Reconfigurable intelligent surfaces for wireless communications: Overview of hardware designs, channel models, and estimation techniques. *Intell. Conver. Netw.* **2022**, *3*, 1–32. [[CrossRef](#)]
62. Turpin, J.P.; Bossard, J.A.; Morgan, K.L.; Werner, D.H.; Werner, P.L. Reconfigurable and tunable metamaterials: A review of the theory and applications. *Int. J. Antennas Propag.* **2014**, *2014*, 429837. [[CrossRef](#)]
63. Hashemi, M.R.M.; Yang, S.H.; Wang, T.; Sepúlveda, N.; Jarrahi, M. Fully-integrated and electronically-controlled millimeter-wave beam-scanning. In Proceedings of the 2016 IEEE MTT-S International Microwave Symposium (IMS), San Francisco, CA, USA, 22–27 May 2016.
64. Wu, X.; Lan, F.; Shi, Z.; Yang, Z. Switchable terahertz polarization conversion via phase-change metasurface. In Proceedings of the 2017 Progress in Electromagnetics Research Symposium-Spring (PIERS), St. Petersburg, Russia, 22–25 May 2017.
65. Zhang, Y.; Wang, T.; Wang, X.; Kuhl, F.; Becker, M.; Polity, A.; Klar, P.J. Thermally switchable terahertz metasurface devices. In Proceedings of the 2019 44th International Conference on Infrared, Millimeter, and Terahertz Waves (IRMMW-THz), Paris, France, 1–6 September 2019.
66. Xue, W.; Han, J.; Qiao, C.; Li, L. Design of 1-bit digital coding reconfigurable reflectarray using aperture-coupled elements controlled by pin diodes. In Proceedings of the 2018 International Conference on Microwave and Millimeter Wave Technology (ICMMT), Chengdu, China, 7–11 May 2018.
67. Wu, Q.; Zhang, R. Beamforming optimization for wireless network aided by intelligent reflecting surface with discrete phase shifts. *IEEE Trans. Commun.* **2019**, *68*, 1838–1851. [[CrossRef](#)]
68. Araghi, A.; Khalily, M.; Safaei, M.; Bagheri, A.; Sing, V.; Wang, F.; Tafazolli, R. Reconfigurable intelligent surface (RIS) in the sub-6 GHz band: Design, implementation, and real-world demonstration. *IEEE Access* **2022**, *10*, 2646–2655. [[CrossRef](#)]
69. Rana, B.; Lee, I.G.; Hong, I.P. Digitally reconfigurable transmitarray with beam-steering and polarization switching capabilities. *IEEE Access* **2021**, *9*, 144140–144148. [[CrossRef](#)]
70. Rana, B.; Cho, S.S.; Hong, I.P. Parameters and measurement techniques of reconfigurable intelligent surfaces. *Micromachines* **2022**, *13*, 1841. [[CrossRef](#)]
71. Zhang, Z.; Dai, L.; Chen, X.; Liu, C.; Yang, F.; Schober, R.; Poor, H.V. Active RIS vs. passive RIS: Which will prevail in 6G? *IEEE Trans. Commun.* **2023**, *71*, 1707–1725. [[CrossRef](#)]
72. Zhang, X.G.; Jiang, W.X.; Jiang, H.L.; Wang, Q.; Tian, H.W.; Bai, L.; Luo, Z.J.; Sun, S.; Luo, Y.; Qiu, C.W.; et al. An Optically Driven Digital Metasurface for Programming Electromagnetic Functions. *Nat. Electron.* **2020**, *3*, 165–171. [[CrossRef](#)]
73. Kossifos, K.M.; Petrou, L.; Varnava, G.; Ptilakis, A.; Tsilipakos, O.; Liu, F.; Karousios, P.; Tasolamprou, A.C.; Seckel, M.; Manassis, D.; et al. Toward the realization of a programmable metasurface absorber enabled by custom integrated circuit technology. *IEEE Access* **2020**, *8*, 92986–92998. [[CrossRef](#)]
74. Artiga, X. Row-column beam steering control of reflectarray antennas: Benefits and drawbacks. *IEEE Antennas Wirel. Propag. Lett.* **2017**, *17*, 271–274. [[CrossRef](#)]
75. Petrou, L.; Karousios, P.; Georgiou, J. Asynchronous circuits as an enabler of scalable and programmable metasurfaces. In Proceedings of the 2018 IEEE International Symposium on Circuits and Systems (ISCAS), Florence, Italy, 27–30 May 2018.

76. Liaskos, C.; Tsioliariidou, A.; Pitsillides, A.; Ioannidis, S.; Akyildiz, I. Using any surface to realize a new paradigm for wireless communications. *Commun. ACM* **2018**, *61*, 30–33. [CrossRef]
77. Arun, V.; Balakrishnan, H. RFocus: Beamforming using thousands of passive antennas. In Proceedings of the 17th USENIX Symposium on Networked Systems Design and Implementation (NSDI 20), Santa Clara, CA, USA, 25–27 February 2020.
78. Dai, L.L.; Wang, B.C.; Wang, M. Reconfigurable intelligent surface-based wireless communications: Antenna design, prototyping, and experimental results. *IEEE Access* **2020**, *8*, 45913–45923. [CrossRef]
79. Pei, X.; Yin, H.; Tan, L.; Cao, L.; Li, Z.; Wang, K.; Björnson, E. RIS-aided wireless communications: Prototyping, adaptive beamforming, and indoor/outdoor field trials. *IEEE Trans. Commun.* **2021**, *69*, 8627–8640. [CrossRef]
80. Fara, R.; Ratajczak, P.; Phan-Huy, D.T.; Ourir, A.; Di Renzo, M.; De Rosny, J. A prototype of reconfigurable intelligent surface with continuous control of the reflection phase. *IEEE Wirel. Commun.* **2022**, *29*, 70–77. [CrossRef]
81. Gros, J.B.; Popov, V.; Odit, M.A.; Lenets, V.; Lerosey, G. A reconfigurable intelligent surface at mmWave based on a binary phase tunable metasurface. *IEEE Open J. Commun. Soc.* **2021**, *2*, 1055–1064. [CrossRef]
82. Shekhawat, A.S.; Kashyap, B.G.; Tjahjadi, B.; Trichopoulos, G.C. Beamforming characterization of a mmWave single-bit reflective metasurface. In Proceedings of the 2022 IEEE International Symposium on Antennas and Propagation and USNC-URSI Radio Science Meeting (AP-S/URSI), Denver, CO, USA, 10–15 July 2022.
83. Jeong, J.; Oh, J.H.; Lee, S.Y.; Park, Y.; Wi, S.H. An improved path-loss model for reconfigurable-intelligent-surface-aided wireless communications and experimental validation. *IEEE Access* **2022**, *10*, 98065–98078. [CrossRef]
84. Wang, R.; Yang, Y.; Makki, B.; Shamim, A. A wideband reconfigurable intelligent surface for 5G millimeter-wave applications. *arXiv* **2023**, arXiv:2304.11572.
85. Vassos, E.; Churm, J.; Feresidis, A. Ultra-low-loss tunable piezoelectric-actuated metasurfaces achieving 360 and 180 dynamic phase shift at millimeter-waves. *Sci. Rep.* **2020**, *10*, 15679. [CrossRef] [PubMed]
86. Yang, X.; Xu, S.; Yang, F.; Li, M.; Fang, H.; Hou, Y.; Jiang, S.; Liu, L. A mechanically reconfigurable reflectarray with slotted patches of tunable height. *IEEE Antennas Wirel. Propag. Lett.* **2018**, *17*, 555–558. [CrossRef]
87. Jeong, H.; Park, E.; Phon, R.; Lim, S. Mechatronic reconfigurable intelligent-surface-driven indoor fifth-generation wireless communication. *Adv. Intell. Syst.* **2022**, *4*, 2200185. [CrossRef]
88. Qu, K.; Chen, K.; Zhao, J.; Zhang, N.; Hu, Q.; Zhao, J.; Jiang, T.; Feng, Y. An electromechanically reconfigurable intelligent surface for enhancing Sub-6G wireless communication signal. *J. Inform. Intell.* **2023**, *1*, 207–216. [CrossRef]
89. Ruan, Y.; Nie, Q.F.; Chen, L.; Cui, H.Y. Optical transparent and reconfigurable metasurface with autonomous energy supply. *J. Phys. D Appl. Phys.* **2019**, *53*, 065301. [CrossRef]
90. Liang, J.C.; Gao, Y.; Cheng, Z.W.; Jiang, R.Z.; Dai, J.Y.; Zhang, L.; Cheng, Q.; Jin, S.; Cui, T.J. An optically transparent reconfigurable intelligent surface with low angular sensitivity. *Adv. Opt. Mater.* **2022**, 2202081. [CrossRef]
91. Lu, Z.; Xia, C.; Zhang, Y.; Tan, J. Metasurface with electrically tunable microwave transmission amplitude and broadband high optical transparency. *ACS Appl. Mater. Interfaces* **2023**, *15*, 29440–29448. [CrossRef]
92. Liang, J.C.; Zhang, P.; Cheng, Q.; Cui, T.J. Reconfigurable intelligent surface with high optical-transparency based on metal mesh. *J. Inf. Intell.* **2023**, in press. [CrossRef]
93. Kitayama, D.; Kurita, D.; Miyachi, K.; Kishiyama, Y.; Itoh, S.; Tachizawa, T. 5G radio access experiments on coverage expansion using metasurface reflector at 28 GHz. In Proceedings of the Asia-Pacific Microwave Conference Proceedings, Hong Kong, China, 8–11 December 2019.
94. Press Releases: DOCOMO Conducts World’s First Successful Trial of Transparent Dynamic Metasurface | News & Notices | NTT DOCOMO. Available online: [https://www.nttdocomo.co.jp/english/info/media\\_center/pr/2020/0117\\_00.html](https://www.nttdocomo.co.jp/english/info/media_center/pr/2020/0117_00.html) (accessed on 8 October 2023).
95. Kitayama, D.; Hama, Y.; Miyachi, K.; Kishiyama, Y. Research of transparent RIS technology toward 5G evolution & 6G. *NTT Tech. Rev.* **2021**, *23*, 14–23.
96. Greenerwave Unveils the Future Brick of 5G Network through its Reconfigurable Intelligent Surfaces | Microwave Journal. Available online: <https://www.microwavejournal.com/articles/39718-greenerwave-unveils-the-future-brick-of-5g-network-through-its-reconfigurable-intelligent-surfaces> (accessed on 8 October 2023).
97. Matsuno, H.; Ohto, T.; Hayashi, T.; Amano, Y.; Okita, M.; Suzuki, D.; Matsunaga, K.; Oka, S. Development of a dual-polarized direction-variable liquid-crystal meta-surface reflector for intelligent reflecting surface. *IEEE Access* **2023**, *11*, 95757–95767. [CrossRef]
98. Cheng, C.-C.; Abbaspour-Tamijani, A. Study of 2-bit antenna-filter-antenna elements for reconfigurable millimeter-wave lens arrays. *IEEE Trans. Microw. Theory Tech.* **2006**, *54*, 4498–4506. [CrossRef]
99. Ven katesh, S.; Saeidi, H.; Sengupta, K.; Lu, X. Active and Passive Reconfigurable Intelligent Surfaces at mm-Wave and THz bands enabled by CMOS Integrated Chips. In Proceedings of the 2023 IEEE Wireless and Microwave Technology Conference (WAMICON), Melbourne, FL, USA, 17–18 April 2023; pp. 113–116. [CrossRef]
100. Yang, Y.; Wang, R.; Vaseem, M.; Makki, B.; Shamim, A. A via-less fully screen-printed reconfigurable intelligent surface for 5G millimeter wave communication. In Proceedings of the 2023 IEEE International Symposium on Antennas and Propagation and USNC-URSI Radio Science Meeting (USNC-URSI), Portland, OR, USA, 23–28 July 2023; pp. 215–216. [CrossRef]
101. Björnson, E.; Özdogan, Ö.; Larsson, E.G. Intelligent reflecting surface versus decode-and-forward: How large surfaces are needed to beat relaying? *IEEE Wirel. Commun. Lett.* **2020**, *9*, 244–248. [CrossRef]

102. Lu, W.; Di Renzo, M. Stochastic geometry modeling and system-level analysis & optimization of relay-aided downlink cellular networks. *IEEE Trans. Commun.* **2015**, *63*, 4063–4085. [[CrossRef](#)]
103. Rappaport, T.S.; Xing, Y.; Kanhere, O.; Ju, S.; Madanayake, A.; Mandal, S.; Alkhateeb, A.; Trichopoulos, G.C. Wireless communications and applications above 100 GHz: Opportunities and challenges for 6G and beyond. *IEEE Access* **2019**, *7*, 78729–78757. [[CrossRef](#)]
104. Subrt, L.; Pechac, P. Intelligent walls as autonomous parts of smart indoor environments. *IET Commun.* **2012**, *6*, 1004–1010. [[CrossRef](#)]
105. Huang, C.; Zappone, A.; Alexandropoulos, G.C.; Debbah, M.; Yuen, C. Reconfigurable intelligent surfaces for energy efficiency in wireless communication. *IEEE Trans. Wirel. Commun.* **2019**, *18*, 4157–4170. [[CrossRef](#)]
106. Ntontin, K.; Di Renzo, M.; Lazarakis, F. On the rate and energy efficiency comparison of reconfigurable intelligent surfaces with relays. In Proceedings of the 2020 IEEE 21st International Workshop on Signal Processing Advances in Wireless Communications (SPAWC), Atlanta, GA, USA, 26–29 May 2020.
107. Zhou, S.; Xu, W.; Wang, K.; Di Renzo, M.; Alouini, M.S. Spectral and energy efficiency of IRS-assisted MISO communication with hardware impairments. *IEEE Wirel. Commun. Lett.* **2020**, *9*, 1366–1369. [[CrossRef](#)]
108. Qian, X.; Di Renzo, M.; Liu, J.; Kammoun, A.; Alouini, M.S. Beamforming through reconfigurable intelligent surfaces in single-user MIMO systems: SNR distribution and scaling laws in the presence of channel fading and phase noise. *IEEE Wirel. Commun. Lett.* **2020**, *10*, 77–81. [[CrossRef](#)]
109. Qian, X.; Di Renzo, M.; Liu, J.; Kammoun, A.; Alouini, M.S. Hybrid RIS-empowered reflection and decode-and-forward relaying for coverage extension. *IEEE Commun. Lett.* **2021**, *25*, 1692–1696. [[CrossRef](#)]
110. Obeed, M.; Chaaban, A. Relay-reconfigurable intelligent surface cooperation for energy-efficient multiuser systems. In Proceedings of the 2021 IEEE International Conference on Communications Workshops (ICC Workshops), Montreal, QC, Canada, 14–18 June 2021.
111. Wang, X.; Shu, F.; Shi, W.; Liang, X.; Dong, R.; Li, J.; Wang, J. Beamforming design for IRS-aided decode-and-forward relay wireless network. *IEEE Trans. Green Commun. Netw.* **2022**, *6*, 198–207. [[CrossRef](#)]
112. Zheng, B.; You, C.; Mei, W.; Zhang, R. A survey on channel estimation and practical passive beamforming design for intelligent reflecting surface aided wireless communications. *IEEE Commun. Surv. Tuts* **2022**, *24*, 1035–1071. [[CrossRef](#)]
113. Kan, T.Y.; Chang, R.Y.; Chien, F.T.; Chen, B.J.; Poor, H.V. Hybrid relay and reconfigurable intelligent surface assisted multiuser MISO systems. *IEEE Trans. Veh. Technol.* **2023**, *72*, 7653–7668. [[CrossRef](#)]
114. Zhang, H.; Di, B.; Bian, K.; Han, Z.; Poor, H.V.; Song, L. Toward ubiquitous sensing and localization with reconfigurable intelligent surfaces. *Proc. IEEE* **2022**, *110*, 1401–1422. [[CrossRef](#)]
115. Li, Y.B.; Li, L.L.; Xu, B.B.; Wu, W.; Wu, R.Y.; Wan, X.; Cheng, Q.; Cui, T.J. Transmission-type 2-bit programmable metasurface for single-sensor and single-frequency microwave imaging. *Sci. Rep.* **2016**, *6*, 23731. [[CrossRef](#)] [[PubMed](#)]
116. Wang, X.; Ding, J.; Zheng, B.; An, S.; Zhai, G.; Zhang, H. Simultaneous realization of anomalous reflection and transmission at two frequencies using bi-functional metasurfaces. *Sci. Rep.* **2018**, *8*, 1876. [[CrossRef](#)] [[PubMed](#)]
117. Xu, J.; Liu, Y.; Mu, X.; Zhou, J.T.; Song, L.; Poor, H.V.; Hanzo, L. Simultaneously transmitting and reflecting intelligent omni-surfaces: Modeling and implementation. *IEEE Veh. Technol. Mag.* **2022**, *17*, 46–54. [[CrossRef](#)]
118. Zhang, S.; Zhang, H.; Di, B.; Tan, Y.; Han, Z.; Song, L. Beyond intelligent reflecting surfaces: Reflective-transmissive metasurface aided communications for full-dimensional coverage extension. *IEEE Trans. Veh. Technol.* **2020**, *69*, 13905–13909. [[CrossRef](#)]
119. Zeng, S.; Zhang, H.; Di, B.; Tan, Y.; Han, Z.; Poor, H.V.; Song, L. Reconfigurable intelligent surfaces in 6G: Reflective, transmissive, or both? *IEEE Commun. Lett.* **2021**, *25*, 2063–2067. [[CrossRef](#)]
120. Tang, J.; Cui, M.; Xu, S.; Dai, L.; Yang, F.; Li, M. Transmissive RIS for B5G communications: Design, prototyping, and experimental demonstrations. *IEEE Trans. Commun.* **2023**, *in press*. [[CrossRef](#)]
121. Reis, J.R.; Caldeirinha, R.F.; Hammoudeh, A.; Copner, N. Electronically reconfigurable FSS-inspired transmitarray for 2-D beamsteering. *IEEE Trans. Antennas Propag.* **2017**, *65*, 4880–4885. [[CrossRef](#)]
122. Cho, K.W.; Mazaheri, M.H.; Gummeson, J.; Abari, O.; Jamieson, K. mmWall: A reconfigurable metamaterial surface for mmWave networks. In Proceedings of the 22nd International Workshop on Mobile Computing Systems and Applications (HotMobile), London, UK, 24–26 February 2021.
123. Zhang, S.; Zhang, H.; Di, B.; Tan, Y.; Di Renzo, M.; Han, Z.; Poor, H.V.; Song, L. Intelligent omni-surfaces: Ubiquitous wireless transmission by reflective-refractive metasurfaces. *IEEE Trans. Wirel. Commun.* **2022**, *21*, 219–233. [[CrossRef](#)]
124. Liu, Y.; Mu, X.; Xu, J.; Schober, R.; Hao, Y.; Poor, H.V.; Hanzo, L. STAR: Simultaneous transmission and reflection for 360° coverage by intelligent surfaces. *IEEE Wirel. Commun.* **2021**, *28*, 102–109. [[CrossRef](#)]
125. Ahmed, M.; Wahid, A.; Laique, S.S.; Khan, W.U.; Ihsan, A.; Xu, F.; Chatzinotas, S.; Han, Z. A survey on STAR-RIS: Use cases, recent advances, and future research challenges. *IEEE Internet Things J.* **2023**, *10*, 14689–14711. [[CrossRef](#)]
126. Wu, Q.; Zhang, R. Intelligent reflecting surface enhanced wireless network via joint active and passive beamforming. *IEEE Trans. Wirel. Commun.* **2019**, *18*, 5394–5409. [[CrossRef](#)]
127. Wang, P.; Fang, J.; Yuan, X.; Chen, Z.; Li, H. Intelligent reflecting surface-assisted millimeter wave communications: Joint active and passive precoding design. *IEEE Trans. Veh. Technol.* **2020**, *69*, 960–973. [[CrossRef](#)]
128. Wang, Y.; Peng, J. Energy efficiency fairness of active reconfigurable intelligent surfaces-aided cell-free network. *IEEE Access* **2023**, *11*, 5884–5893. [[CrossRef](#)]

129. Long, R.; Liang, Y.C.; Pei, Y.; Larsson, E.G. Active reconfigurable intelligent surface aided wireless communications. *IEEE Trans. Wirel. Commun.* **2021**, *20*, 4962–4975. [CrossRef]
130. Li, H.; Cai, W.; Liu, Y.; Li, M.; Liu, Q.; Wu, Q. Intelligent reflecting surface enhanced wideband MIMO-OFDM communications: From practical model to reflection optimization. *IEEE Trans. Commun.* **2021**, *69*, 4807–4820. [CrossRef]
131. Wu, L.; Lou, K.; Ke, J.; Liang, J.; Luo, Z.; Dai, J.Y.; Cheng, Q.; Cui, T.J. A wideband amplifying reconfigurable intelligent surface. *IEEE Trans. Antennas Propag.* **2022**, *70*, 623–631. [CrossRef]
132. Moore, C.M. Reconfigurable Frequency Selective Surfaces. Ph.D. Thesis, Loughborough University, Loughborough, UK, 1994.
133. Zhang, J.; Li, Z.; Zhang, Z. Wideband active RISs: Architecture, modeling, and beamforming design. *IEEE Commun. Lett.* **2023**, *27*, 1899–1903. [CrossRef]
134. Taha, A.; Alrabeiah, M.; Alkhateeb, A. Deep learning for large intelligent surfaces in millimeter wave and massive MIMO systems. In Proceedings of the IEEE Global Communications Conference (GLOBECOM), Waikoloa, HI, USA, 9–13 December 2019.
135. Alexandropoulos, G.C.; Vlachos, E. A hardware architecture for reconfigurable intelligent surfaces with minimal active elements for explicit channel estimation. In Proceedings of the IEEE International Conference on Acoustics, Speech, and Signal Processing, Barcelona, Spain, 4–8 May 2020.
136. Nguyen, N.T.; He, J.; Nguyen, V.D.; Wymeersch, H.; Ng, D.W.K.; Schober, R.; Chatzinotas, S.; Juntti, M. Hybrid relay-reflecting intelligent surface-aided wireless communications: Opportunities, challenges, and future perspectives. *arXiv* **2021**, arXiv:2104.02039.
137. Nguyen, N.T.; Vu, Q.D.; Lee, K.; Juntti, M. Spectral efficiency optimization for hybrid relay-reflecting intelligent surface. In Proceedings of the IEEE International Conference on Communications Workshops (ICC Workshops), Montreal, QC, Canada, 14–23 June 2021.
138. Ngo, K.H.; Nguyen, N.T.; Dinh, T.Q.; Hoang, T.M.; Juntti, M. Low-latency and secure computation offloading assisted by hybrid relay-reflecting intelligent surface. In Proceedings of the IEEE International Conference on Advanced Technologies for Communications (ATC), Ho Chi Minh City, Vietnam, 14–16 October 2021.
139. Ahmed, S.; Ahmed, E.K.; Mohamed, Y.S. Adding active elements to reconfigurable intelligent surfaces to enhance energy harvesting for IoT devices. In Proceedings of the IEEE Military Communications Conference (ATC), San Diego, CA, USA, 29 November–2 December 2021.
140. Yigit, Z.; Basar, E.; Wen, M.; Altunbas, I. Hybrid reflection modulation. *IEEE Trans. Wirel. Commun.* **2022**, *22*, 4106–4116. [CrossRef]
141. Nguyen, N.T.; Nguyen, V.D.; Wu, Q.; Tölli, A.; Chatzinotas, S.; Juntti, M. Hybrid active-passive reconfigurable intelligent surface-assisted multi-user MISO systems. In Proceedings of the 2022 IEEE 23rd International Workshop on Signal Processing Advances in Wireless Communication (SPAWC), Oulu, Finland, 4–6 July 2022.
142. Best, S.R. Realized noise figure of the general receiving antenna. *IEEE Antennas Wirel. Propag. Lett.* **2013**, *12*, 702–705. [CrossRef]
143. Kimionis, J.; Georgiadis, A.; Collado, A.; Tentzeris, M.M. Enhancement of RF tag backscatter efficiency with low-power reflection amplifiers. *IEEE Trans. Microw. Theory Tech.* **2014**, *62*, 3562–3571. [CrossRef]
144. Zhang, Z.; Dai, L. Reconfigurable intelligent surfaces for 6G: Nine fundamental issues and one critical problem. *Tsinghua Sci. Technol.* **2023**, *28*, 929–939. [CrossRef]
145. Yang, H.; Yang, F.; Cao, X.; Xu, S.; Gao, J.; Chen, X.; Li, M.; Li, T. A 1600-element dual-frequency electronically reconfigurable reflectarray at X/Ku-Band. *IEEE Trans. Antennas Propag.* **2017**, *65*, 3024–3032. [CrossRef]
146. Wang, J.; Tang, W.; Liang, J.C.; Zhang, L.; Dai, J.Y.; Li, X.; Jin, S.; Cheng, Q.; Cui, T.J. Reconfigurable intelligent surface: Power consumption modeling and practical measurement validation. *arXiv* **2022**, arXiv:2211.00323.
147. Zappone, A.; Di Renzo, M.; Shams, F.; Qian, X.; Debbah, M. Overhead-aware design of reconfigurable intelligent surfaces in smart radio environments. *IEEE Trans. Wirel. Commun.* **2020**, *20*, 126–141. [CrossRef]
148. Wang, J.; Tang, W.; Jin, S.; Li, X.; Matthaiou, M. Static power consumption modeling and measurement of reconfigurable intelligent surfaces. *arXiv* **2023**, arXiv:2303.00299.
149. Liang, J.C.; Cheng, Q.; Gao, Y.; Xiao, C.; Gao, S.; Zhang, L.; Jin, S.; Cui, T.J. An Angle-Insensitive 3-Bit Reconfigurable Intelligent Surface. *IEEE Trans. Antennas Propag.* **2022**, *70*, 8798–8808. [CrossRef]
150. Gu, Q.; Wu, D.; Su, X.; Wang, H.; Cui, J.; Yuan, Y. System-level simulation of reconfigurable intelligent surface assisted wireless communications system. *arXiv* **2022**, arXiv:2206.14777.
151. Sihlbom, B.; Poulakis, M.I.; Di Renzo, M. Reconfigurable intelligent surfaces: Performance assessment through a system-level simulator. *IEEE Wirel. Commun.* **2023**, *30*, 98–106. [CrossRef]
152. Hao, L.; Fastenbauer, A.; Schwarz, S.; Rupp, M. Towards system level simulation of reconfigurable intelligent surfaces. In Proceedings of the 2022 International Symposium ELMAR, Zadar, Croatia, 12–14 September 2022.
153. Raffique, A.; Hassan, N.U.; Naqvi, I.H.; Mehmood, M.Q.; Zubair, M. Benchmarking framework for reconfigurable intelligent surfaces. In Proceedings of the 2021 IEEE Global Communications Conference (GLOBECOM), Madrid, Spain, 7–11 December 2021.
154. Swindlehurst, A.L.; Zhou, G.; Liu, R.; Pan, C.; Li, M. Channel estimation with reconfigurable intelligent surfaces—A general framework. *Proc. IEEE* **2022**, *110*, 1312–1338. [CrossRef]
155. Di Renzo, M.; Danufane, F.H.; Tretyakov, S. Communication models for reconfigurable intelligent surfaces: From surface electromagnetics to wireless networks optimization. *Proc. IEEE* **2022**, *110*, 1164–1209. [CrossRef]
156. Press Releases: NTT and NTT DOCOMO Trial First Use of User-Tracking Metasurface Reflector for Extreme Mobile Coverage in Current 5G and Coming 6G Era | News & Notices | NTT DOCOMO. Available online: [https://www.docomo.ne.jp/english/info/media\\_center/pr/2021/1112\\_00.html](https://www.docomo.ne.jp/english/info/media_center/pr/2021/1112_00.html) (accessed on 8 October 2023).

157. Sang, J.; Yuan, Y.; Tang, W.; Li, Y.; Li, X.; Jin, S.; Cheng, Q.; Cui, T.J. Coverage enhancement by deploying RIS in 5G commercial mobile networks: Field trials. *IEEE Wirel. Commun.* 2023, *in press*. [[CrossRef](#)]
158. Liu, R.; Dou, J.; Li, P.; Wu, J.; Cui, Y. Simulation and field trial results of reconfigurable intelligent surfaces in 5G networks. *IEEE Access* 2022, 10, 122786–122795. [[CrossRef](#)]
159. Rains, J.; Tukmanov, A.; Cui, T.J.; Zhang, L.; Abbasi, Q.H.; Imran, M.A. High-Resolution Programmable Scattering for Wireless Coverage Enhancement: An Indoor Field Trial Campaign. *IEEE Trans. Antennas Propag.* 2023, 71, 518–530. [[CrossRef](#)]
160. Trichopoulos, G.C.; Theofanopoulos, P.; Kashyap, B.; Shekhawat, A.; Modi, A.; Osman, T.; Kumar, S.; Sengar, A.; Chang, A.; Alkhateeb, A. Design and evaluation of reconfigurable intelligent surfaces in real-world environment. *IEEE Open J. Commun. Soc.* 2022, 3, 462–474. [[CrossRef](#)]
161. Fei, D.; Chen, C.; Zheng, P.; You, M.; Ding, J.; Wang, W.; Zhan, J.; Ai, B.; Jin, S.; Cui, T.J. Research and experimental verification of reconfigurable intelligent surface in indoor coverage enhancement. *J. Electron. Inf. Technol.* 2022, 44, 2374–2381.

**Disclaimer/Publisher’s Note:** The statements, opinions and data contained in all publications are solely those of the individual author(s) and contributor(s) and not of MDPI and/or the editor(s). MDPI and/or the editor(s) disclaim responsibility for any injury to people or property resulting from any ideas, methods, instructions or products referred to in the content.